Russian Original Vol. 40, No. 5, May, 1976

November, 1976

SATEAZ 40(5) 445-538 (1976)

SOVIET ATOMIC ENERGY

АТОМНАЯ ЭНЕРГИЯ
(ATOMNAYA ÉNERGIYA)

TRANSLATED FROM RUSSIAN

CONSULTANTS BUREAU, NEW YORK

SOVIET ATOMIC ENERGY

Soviet Atomic Energy is a cover-to-cover translation of *Atomnaya Énergiya*, a publication of the Academy of Sciences of the USSR.

An agreement with the Copyright Agency of the USSR (VAAP) makes available both advance copies of the Russian journal and original glossy photographs and artwork. This serves to decrease the necessary time lag between publication of the original and publication of the translation and helps to improve the quality of the latter. The translation began with the first issue of the Russian journal.

Consultants Bureau journals appear about six months after the publication of the original Russian issue. For bibliographic accuracy, the English issue published by Consultants Bureau carries the same number and date as the original Russian from which it was translated. For example, a Russian issue published in December will appear in a Consultants Bureau English translation about the following June, but the translation issue will carry the December date. When ordering any volume or particular issue of a Consultants Bureau journal, please specify the date and, where applicable, the volume and issue numbers of the original Russian. The material you will receive will be a translation of that Russian volume or issue.

Subscription
$107.50 per volume (6 Issues)
2 volumes per year
Prices somewhat higher outside the United States.

Single Issue: $50
Single Article: $7.50

CONSULTANTS BUREAU, NEW YORK AND LONDON

227 West 17th Street
New York, New York 10011

Published monthly. Second-class postage paid at Jamaica, New York 11431.

Soviet Atomic Energy is abstracted or indexed in *Applied Mechanics Reviews, Chemical Abstracts, Engineering Index, INSPEC—Physics Abstracts and Electrical and Electronics Abstracts, Current Contents,* and *Nuclear Science Abstracts.*

SOVIET ATOMIC ENERGY

A translation of *Atomnaya Énergiya*

November, 1976

Volume 40, Number 5 May, 1976

CONTENTS

	Engl.	Russ.
From the Proceedings of the 25th Congress of the Communist Party of the Soviet Union	445	363
20 Years of the Journal "Atomnaya Énergiya"	448	367
ARTICLES		
Steam-Superheating Fuel Elements of the Reactors in the I. V. Kurchatov Beloyarsk Nuclear Power Station – A. G. Samoilov, A. V. Pozdnyakova, and V. S. Volkov	451	371
Some Physical Investigations in BFS-1 Fast Critical Assemblies – V. A. Dulin, Yu. A. Kazanskii, V. F. Mamontov, and G. I. Sidorov	457	377
Some Results of Postreactor Testing of Six-Element Thermionic Units Operating for 2670 h – G. A. Batyrbekov, E. S. Bekmukhambetov, V. I. Berzhatyi, S. E. Ermatov, Sh. Sh. Ibragimov, V. P. Kirienko, B. S. Kurmangaliev, M. V. Mel'nikov, V. V. Sinyavskii, Yu. A. Sobolev, and Yu. I. Sukhov	462	382
Effect of Heterogeneity on the Measurement of Integral Parameters in Subcritical Systems – L. N. Yurova, A. V. Bushuev, V. I. Naumov, V. M. Duvanov, N. N. Khrennikov, and V. N. Zubarev	465	384
Investigation of the Liberation of Helium from Construction Materials during Their Heating – D. M. Skorov, N. P. Agapova, A. I. Dashkovskii, Yu. N. Sokurskii, A. G. Zaluzhnyi, O. M. Storozhuk, V. D. Onufriev, and I. N. Afrikanov	468	387
The Evolution of Gas from Uranium Dioxide – B. V. Samsonov, Yu. G. Spridonov, V. Sh. Sulaberidze, and V. A. Tsykanov	472	390
Sputtering of Thin Films of Uranous–Uranic Oxide under the Influence of Fission Fragments at Low Irradiation Doses – V. A. Bessonov, G. P. Ivanov, N. A. Grinevich, and E. A. Borisov	477	395
REVIEWS		
Radiation Defects in Graphite – T. N. Shurshakova, Yu. S. Virgil'ev, and I. P. Kalyagina	481	399
DEPOSITED PAPERS		
Asymptotic Solution of a γ-Ray Transport Equation – L. D. Pleshakov	493	411
LETTERS TO THE EDITOR		
Correction for Time of Fall in Negative-Reactivity Determination by Rod-Drop – O. A. Elovskii	500	418
An Investigation of the Parameters of a Critical Assembly – É. Ya. Tomsons, V. V. Bute, V. V. Gavar, A. S. Dindun, U. A. Kruze, and É. Ya. Platatsis	503	420
Ampule Devices in the VVR-M Reactor for Irradiating Carbon-Based Materials – G. Ya. Vasil'ev, Yu. S. Virgil'ev, V. G. Makarchenko, and Yu. P. Semenov	506	423

CONTENTS

(continued)

	Engl.	Russ.
Neutron-Spectrum Structure near a Resonant Absorption Line – A. I. Dod', I. M. Kisil', and I. P. Markelov	509	425
Calorimeter Measurement of the Heat Released by Irradiated Nuclear Fuel – A. P. Kirillovich, P. S. Gordienko, and V. P. Buntushkin	511	427
Structural Changes in Irradiated Dysprosium Titanate – V. M. Kosenkov, T. M. Guseva, S. A. Alekseeva, and V. K. Nevorotin	513	428
Separation of Isotopic Mixtures of Hydrogen in the Hydrogen–Palladium System – B. M. Andreev, A. S. Polevoi, and O. V. Petrenik	516	431
Magnetic Susceptibilities of Beryllides – V. P. Gladkov, V. I. Petrov, A. V. Svetlov, D. M. Skorov, and V. I. Tenishev	519	433
CONFERENCES AND MEETINGS		
Radiochemistry and Nuclear Technology on the 11th Mendeleev Congress of General and Applied Chemistry – É. V. Renard	521	435
Use of Radioisotope Techniques and Instruments in Machine Construction – M. L. Gol'din	525	438
The Annual Conference of the Plasma Physics Division of the American Physical Society – A. A. Kalmykov	526	439
IN INSTITUTES AND DESIGN OFFICES		
Acceleration of ^{48}Ca Ions and New Possibilities of Synthetizing Superheavy Elements – A. A. Pleve	528	440
The Operator–Stereotelevision–Manipulator System in Nuclear Power Generation – Yu. A. Gerasimov, V. P. Ivanov, and D. P. Malyuzhonok	529	441
EXHIBITIONS		
New Exhibits in the Hall "Atomic Energy" the Exhibition of Achievements of the National Economy of the USSR – P. A. Sokolov	532	443
BOOK REVIEWS		
A. A. Glazkov, I. F. Malyshev, and G. L. Saksaganskii. Vacuum Systems for Electrophysical Apparatus – Reviewed by A. P. Kukushkin and L. N. Rozanov	534	445
V. I. Subbotin, M. Kh. Ibragimov, P. A. Ushakov, V. P. Bobkov, A. V. Zhukov, and Yu. S. Yur'ev. Hydrodynamics and Heat Exchange in Atomic-Power Installations – Reviewed by V. N. Smolin	535	445
B. V. Lysikov, V. K. Prozorov, V. V. Vasil'ev, D. N. Popov, L. F. Gromov, and Yu. V. Rybakov. Temperature Measurements in Nuclear Reactors – Reviewed by I. S. Kochenev	537	446

The Russian press date (podpisano k pechati) of this issue was 4/22/1976. Publication therefore did not occur prior to this date, but must be assumed to have taken place reasonably soon thereafter.

FROM THE PROCEEDINGS OF THE 25TH CONGRESS OF THE COMMUNIST PARTY OF THE SOVIET UNION

With regard to energy technology, during the past five years we have begun the creation of technology for atomic power stations. In years ahead atomic engineering will develop at an accelerated rate. Along with reactors of 10^3 MW, we will exploit the integral equipping of atomic energy units with $1.5 \cdot 10^3$ MW reactors. The energy-producing industry will turn out turbines and generators of 500, 800, and 1000-1200 MW, and steam-gas equipment of up to 250 MW.

From the address of the Chairman of the Council of Ministers of the USSR, Comrade A. N. Kosygin, "The Main Directions of Development of the National Economy of the USSR in 1976-1980."

We will ensure $1340-1380 \cdot 10^9$ kWh of electricity generated during 1980. Power-station capacity of the order of $67-70 \cdot 10^6$ kW will be commissioned, including $13-15 \cdot 10^6$ kW at atomic power stations. We will continue to construct $4-6 \cdot 10^6$-kW thermal power stations with energy units 500 and $800 \cdot 10^3$ kW each along with atomic power stations with reactors $1-1.5 \cdot 10^6$ kW each.

We envisage the rapid development of atomic energy in the European part of the USSR. We will accelerate the construction and commissioning of fast-neutron reactors. We will instigate preparatory work in order to use atomic energy for district heating.

We will organize mass production for atomic power stations of thermal-neutron reactors and associated turbosets each of at least $1 \cdot 10^6$ kW. We will exploit integral equipping for thermal-neutron units of capacities up to $1.5 \cdot 10^6$ kW.

In the European part of the RSFSR and in the Urals we will ensure the following.

The consolidation of electrical-energy resources through the construction and expansion of atomic and thermal power stations. We will raise the capacity of the Leningrad Atomic Power Station to $4 \cdot 10^6$ kW, of the Kostroma State Regional Power Station to $3.6 \cdot 10^6$ kW, and of the Reftinskii State Regional Power Station to $3.3 \cdot 10^6$ kW. We will commission into operation the Novovoronezh, Smolensk, and Kursk Atomic Power Stations, the Ryazan and Stavropol' State Regional Power Stations, and other power stations. We will expand the construction of the Perm' Thermal Power Station, and start the construction of two high-capacity atomic power stations and Irganaisk State Power Station.

In the Ukrainian SSR we will ensure the commissioning into operation of the Chernobyl', Roven'ki, and South Ukraine Atomic Power Stations and begin construction of two new atomic power stations.

In the Lithuanian SSR we will expand the construction of the Ignalina Atomic Power Station with reactors $1.5 \cdot 10^6$ kW each.

From the document "The Main Directions of Development of the National Economy of the USSR in 1976-1980."

The large program of atomic-power-station construction will be fulfilled in regard to Soviet plans and aid from the Soviet Union to countries that are members of the Council for Mutual Economic Aid, including the construction of a large atomic power station in geographically remote, but ideologically close, revolutionary Cuba. (Applause).

In the 10th Five-Year Plan we require the commissioning of at least $70 \cdot 10^6$ kW of new generating capacity, including at least $15 \cdot 10^6$ kW from atomic power stations, to ensure the output in 1980 of $1400 \cdot 10^9$ kWh. It should be noted that recently it has been necessary, in the electrical and thermal energy industry, to com-

Translated from Atomnaya Énergiya, Vol. 40, No. 5, pp. 363-366, May, 1976.

mission generating capacity ahead of schedule; this reduces the reliability of the energy supply in the national economy.

The 10th Five-Year Plan should serve as a beginning for further development of energy resources on a qualitatively new technical basis. We will begin the creation of large atomic power stations with a sustained capacity of $4-8 \cdot 10^6$ kW with thermal-neutron reactors of $1 \cdot 10^6$ kW, $1.5 \cdot 10^6$ kW, and $2.4 \cdot 10^6$ kW, with turbines for these reactors each of $750 \cdot 10^3$, $1 \cdot 10^6$, and $1.2 \cdot 10^6$ kW. In this period we will make the transition to fast-neutron reactors and continue scientific and industrial development directed to the subsequent creation of thermonuclear power stations. (Applause).

From the speech of the Minister for Energy and Electrification of the USSR, Comrade P. S. Neporozhnii.

Many specialists, engineers, and industrial workers sometimes wrongly assess the value of fundamental research. Sometimes they have said: Fundamental science is science for academics, but applied science is science for everyone else.

From a plethora of examples, I will cite only one that demonstrates the contribution of fundamental science. In 30 years at the Leningrad Physical and Technical Institute, I. V. Kurchatov and other scientists instigated studies of the physics of the atomic nucleus. A number of other institutes of the Academy began the development of these studies, which seemingly had no relevance to practical matters. Academician N. N. Semenov, in a completely different field, studying combustion and explosion phenomena, elucidated the mechanism of propagation of chemical reactions that were termed autocatalytic, i.e., those that proceed with transfer of the reaction from one atom to another.

By comparing all this and assessing new scientific data, I. V. Kurchatov showed as early as 1940 the necessity for extending work on atomic technology in our country, but the war began. At the height of the war we discovered that not only fascist Germany but also our own allies were clandestinely carrying out intensive work on the creation of a nuclear weapon; and then in 1943 we began this research. Many institutes of the Academy of Sciences, the biggest industrial organizations, and engineers were drawn to this type of work. Specialized branches of scientific and industrial organizations were set up. Unimpeded contact and the concerted work of scientists of various specializations, of industrial workers, and constant supervision and assistance by the Central Committee of the Party led within only five years to the solution of a problem of immense complexity. Our country was saved from the nuclear threat. (Applause). This was fundamental work, but its practical results were needed for the very survival of our country.

And what is to be the future destiny of this fundamental line of research? Comrade delegates! You know that on the basis of the resolutions of the 24th Congress of the Communist Party of the Soviet Union we have developed atomic energy technology and in the Ninth Five-Year Plan we commissioned two more units at the Novovoronezh Atomic Power Station, viz., the Kol'sk and Leningrad Atomic Power Stations, and assisted in the construction of atomic power stations in the German Democratic Republic, Bulgaria, etc. The Leningrad Atomic Power Station consists of units each of $1 \cdot 10^6$ kW capacity, i.e., they are among the most powerful reactors in the world. We have constructed a new, powerful atomic icebreaker, the "Arktika," and launched the icebreaker "Sibir'." In the current five-year plan we intend to introduce atomic power stations of $12-15 \cdot 10^6$ kW with units each of at least $1 \cdot 10^6$ kW.

Atomic technology is used today in thousands of plants to test manufactured goods by various methods; during geological exploration for analyses of commercial minerals; and is widely used in medicine for the diagnosis and treatment of a number of diseases...

Biology and agriculture use radiation to accelerate the selection of microorganisms and plants. For example, the Institute of Cytology and Genetics of the Siberian Branch of the Academy of Sciences in conjunction with the Institute of Husbandry of the V. I. Lenin All-Union Academy of Agricultural Sciences created by means of radiation mutation a new variety of spring corn, "Novosibirskaya-67." The variety is zoned, and by 1978 it is proposed to sow it over $2 \cdot 10^6$ ha of land; this will give an additional $600 \cdot 10^6$ kg of grain from the same land since its cropping capacity is 1000-1500 kg above that attained up to this time.

Scientists continue to work successfully so that thermonuclear energy will not be used as bombs but in controlled form for the production of energy. I am pleased to be able to inform the Congress that we have made great advances here. (Applause).

We have the Tokamak-10 which Grigorii Vasil'evich Romanov neglected to mention although he was greatly involved in its construction at the Leningrad plants. With this installation at the Institute of Atomic Energy we already have an advanced thermonuclear reaction in the laboratory. (Applause).

Comrades! In the area of thermonuclear energy technology we have made good progress not only in the laboratories of the Institute of Atomic Energy but also in Leningrad, at the Physics Institute of the Academy of Sciences. We now are confident that these enormous thermonuclear resources will be devoted to the service of the people. (Applause).

The generation of energy in lower forms, exploration for and production of natural energy resources for this, and a system of converting the energy into a lower form for consumption demand more than 50% of the country's total budget. The structure of the thermal-energy balance must gradually change. This will also be affected by the need for economy in the use of petroleum and gas so that they are used more efficiently, the broadening of the range of uses of atomic energy, and the inclusion in energy production by the close of the century of thermonuclear sources, magnetohydrodynamic generators, and new methods of energy transmission, as well as new trends in energy use. Enlargement of units at power stations to a few million kilowatts and the needs of energy transmission and of thermonuclear energy technology require the use of superconductors, etc., in electrical engineering. The involvement of many areas of science is needed for this.

The developments will also be long-term, e.g., the transition from the laboratory carrying out the thermonuclear reaction, which we visited today, to an operationally profitable power station will take place, just as in atomic energy technology in the last 15 years, and thermonuclear power stations will probably have capacities of not less than $10 \cdot 10^6$ kW, thus requiring study of the problems of distribution to consumers and transmission of the energy in the optimum form.

Plainly we should not equate this long-term program with the concrete plan for the development of science in the five-year plan – it must contain long-term technicoeconomic forecasts. This state program has scientific, technical, political, and economic aspects and must be constantly adjusted and refined. Economists, geologists, energy technologists, atomic technologists, and specialists in systems analysis in the Academy of Sciences are united in the solution of this problem.

From the speech of the President of the Academy of Sciences, Academician A. P. Aleksandrov.

20 YEARS OF THE JOURNAL "ATOMNAYA ÉNERGIYA"

The first issue of the journal appeared in May 1956. The world's first atomic power station at Obninsk was opened in its second year. Our physicists and engineers had already delivered lectures at the Sessions of the Academy of Sciences of the USSR and at the 1st Geneva Conference. Atomic energy began to be used for peaceful purposes and large reserves of information had accumulated at that time. To accelerate scientific progress this information would have to be made available to a wide circle of researchers and engineers. This task was assigned to our journal.

Naturally in the first issue of the journal an article was published on the world's first atomic power station [1,2]. Its history and significance and the subsequent development of Soviet atomic energy technology are not difficult to follow in the pages of the journal right up to the anniversary session, convened in Obninsk in June 1974 [3]. At present, atomic energy technology, starting from a 5-MW reactor, has already commissioned the 50th Anniversary of the USSR Novovoronezh Atomic Power Station (1455 MW) [4] and the V. I. Lenin Leningrad Atomic Power Station (2000 MW) [5], not to mention several large stations in the construction and planning stages [6]. High-capacity fast breeder reactors [7] are in industrial operation; these seem likely to make an important contribution to the further development of energy technology. The 25th Congress of the Communist Party of the Soviet Union took the decision to construct atomic power stations to a total capacity of $13\text{-}15 \cdot 10^3$ MW during the 10th Five-Year Plan.

In the first issue of the journal we published information on an exhibition where a model was demonstrated of an atomic-powered icebreaker that was then under construction [8]. The two atomic icebreakers "Lenin" and "Arktika" are now operating successfully in northern waters; they have greatly expanded the possibility of polar navigation [9] and a third, "Sibir'," has been launched.

Studies of the controlled thermonuclear reaction were from the very start one of the main concerns of contributors to the journal. In the third issue we published Academican I. V. Kurchatov's widely noted lecture, "On the possibility of producing thermonuclear reactions in a gas discharge," which was delivered on April 25, 1956 at the British research center at Harwell [10]. This reported for the first time the researches of Soviet physicists, who observed the appearance of neutrons as a result of pulsed pinching of a deuterium plasma. After this, publication of research into controlled thermonuclear synthesis began and the internation exchange of information started at conferences, seminars, and symposia. I. V. Kurchatov greatly expanded thermonuclear studies and attracted to them many physics laboratories in the country. The first advances in this area were also reflected in the pages of "Atomnaya Énergiya." Later, however, our journals proved inadequate for the publication of all the material, and so the new journal "Fizika Plazmy" (Plasma Physics) was created. Studies have now reached the stage where there is a definite possibility not only of the actual construction of a thermonuclear reactor but also of elucidating the many important characteristics of its equipment and of preparing for trials and operation installations capable according to calculations of giving an actual yield from thermonuclear synthesis. Great progress in this was made at the I. V. Kurchatov Institute of Atomic Energy with the creation of installations of the tokamak type [11]. The Tokamak-10, completed in autumn of 1975, is one of the most perfect modern thermonuclear installations. The state of research now urgently requires studies of ways of developing thermonuclear energy technology and its efficient combination with nuclear-fission energy technology [12].

The peaceful use of nuclear explosions is beginning to acquire practical significance [13, 14, 15]. In the large hydraulic-engineering plan to divert part of the flow of northern rivers to the south into the Volga basin, nuclear explosions were considered a highly effective means of constructing channels [16].

The pages of the journal have reflected the progress of fundamental scientific researches. The first issue carried an article [17] describing the then largest heavy-particle synchrotron, the 10-GeV machine at Dubna. Later large electron accelerators were built at Khar'kov, Erevan, and Tomsk, a heavy-ion accelerator at Dubna,

Translated from Atomnaya Énergiya, Vol. 40, No. 5, pp. 367-369, May, 1976.

a proton accelerator at Moscow, and one of the largest proton accelerators in the world, the 70-GeV machine at Serpukhov [18]. It is equipped with large-scale research installations of Soviet ("Lyudmila") and foreign ("Mirabelle") manufacture [19-21]. The use of the accelerators promoted the discovery of new phenomena in the interactions of particles and nuclei and manifestly expanded and consolidated international scientific collaborations. Some methods of research developed in our laboratories have been used in the subsequently constructed giant accelerator at Batavia (USA) by a group of Soviet physicists working there in collaboration with the Americans.

Together with the principal lines of energy research other areas of science and technology were also developed, united under the concept of atomic energy and by the subject matter of our journal. The industrial use of research methods developed in physical and chemical laboratories has grown and spread; radioactive isotopes as well as technical devices and materials created in the atomic industry have been assimilated in the practice of many areas of the national economy. Information on the main advances in these diverse fields has constituted one of the aims of the journal, and its pages have reflected many achievements of a practical nature, such as nuclear instrumentation [22], activation analysis [23], nuclear geophysics, radiation chemistry [24], dosimetry and radiation protection [25, 26], radioecology [27], and the presowing irradiation of agricultural crops [28].

The flow of scientific information sent to the journal is vast; consequently, in 1965 we introduced a method for the deposition of papers that later was adopted by many other journals. The founding of new journals ("Yadernaya Fizika," "Fizika Plazmy," "Khimiya Vysokikh Énergii," etc.) and of the collection "Voprosy Atomnoi Nauki i Tekhniki" has lightened the portfolio of the journal, but the deposition of papers has been retained and remains highly advisable.

Atomic science and technology in the Soviet Union has made profound advances in the last 20 years, both in important and subsidiary directions in energy research, and the editorial board and staff hope that the journal "Atomnaya Énergiya" has contributed to these achievements.

The quality and timeliness of the scientific information published in the journal depend on its numerous authors and reviewers. The editorial board and staff acknowledge their services and share with them the satisfaction of 20 years' activities on behalf of Soviet science and technology.

LITERATURE CITED

1. D. I. Blokhintsev, N. A. Dollezhal', and A. K. Krasin, "The reactor at the atomic power station of the Academy of Sciences of the USSR," At. Énerg., No.1, 10 (1956).
2. D. I. Blokhintsev, M. E. Minashin, and Yu. A. Sergeev, "Physical and thermal calculations for the reactor at the atomic power station of the Academy of Sciences of the USSR," At. Énerg., No. 1, 24 (1956).
3. D. I. Blokhintsev, N. A. Dollezhal', and A. K. Krasin, "Some conclusions from the operation of the world's first atomic power station," At. Énerg., 36, No. 6, 423 (1974).
4. A. N. Grigor'yants et al., "Ten years of operation of the 50th Anniversary of the USSR Novovoronezh Atomic Power Station," At. Énerg., 38, No. 1, 3 (1975).
5. N. A. Dollezhal' and I. Ya. Emel'yanov, "Experience in the creation of high-capacity reactors in the USSR," At. Énerg., 40, No. 2, 117 (1976).
6. L. M. Voronin and E. Yu. Zharkovskii, "Atomic energy in the USSR in the Ninth Five-Year Plan," At. Énerg., 40, No. 2, 167 (1976).
7. O. D. Kazachkovskii, "Development of work on fast reactors in the USSR," At. Énerg., 36, No. 6, 444 (1974).
8. I. I. Novikov, "Exhibition on the peaceful use of atomic energy," At. Énerg., No. 1, 102 (1956).
9. F. M. Mitenkov et al., "The icebreaker 'Arktika,' a new achievement of Soviet atomic shipbuilding," At. Énerg., 39, No. 3, 163 (1975).
10. I. V. Kurchatov, "On the possibility of producing thermonuclear reactions in a gas discharge," At. Énerg., No. 3, 65 (1956).
11. L. A. Artsimovich, "Studies of controlled thermonuclear synthesis in the USSR," At. Énerg., 31, No. 4, 365 (1971).
12. I. N. Golovin, "On the place of hybrid reactors in the world energy system," At. Énerg., 39, No. 6, 379 (1975).
13. I. D. Morokhov et al., "Third International Conference on the Peaceful Use of Underground Nuclear Explosions," At. Énerg., 34, No. 5, 407 (1973).
14. I. D. Morokhov et al., "Fourth International Conference on the Peaceful Use of Underground Nuclear Explosions," At. Énerg., 39, No. 2, 148 (1975).

15. I. D. Morokhov et al., "The peaceful use of atomic energy and the problem of restricting the spread of nuclear weapons," At. Énerg., 40, No. 2, 99 (1976).
16. A. K. Kruglov, "Atomic science and technology in the national economy of the USSR," At. Énerg., 40, 2, 103 (1976).
17. V. I. Veksler, "Principles of charged-particle accelerators," At. Énerg., No. 1, 75 (1956).
18. Yu. M. Ado et al., "Some results of bringing into operation the 70-GeV proton synchrotron at the Institute of High-Energy Physics," At. Énerg., 28, No. 2, 132 (1970).
19. V. A. Vasil'ev, "The Lyudmila liquid hydrogen bubble chamber," At. Énerg., 32, No. 3, 262 (1972).
20. "Inauguration of the French liquid hydrogen bubble chamber Mirabelle at the Institute of High-Energy Physics," At. Énerg., 31, No. 6, 641 (1971).
21. A. Berthelot and R. M. Sulyaev, "The Mirabelle bubble chamber for the Serpukhov accelerator," At. Énerg., 32, No. 5, 371 (1972).
22. L. M. Isakov and V. V. Matveev, "On the use of nuclear instrumentation in the control of environmental pollution," At. Énerg., 35, No. 6, 417 (1973).
23. A. S. Shtan', "Instrumental basis of activation analysis in the USSR," At. Énerg., 33, No. 4, 858 (1972).
24. V. I. Gol'danskii, "Radiation photochemistry as the possible basis for efficient use of dual-purpose reactors," At. Énerg., 39, No. 4, 243 (1975).
25. Yu. A. Izrael', "Peaceful use of atomic energy and the environment," At. Énerg., 32, No. 4, 273 (1972).
26. A. I. Burnazyan, "Radiation protection in the operation of atomic power stations," At. Énerg., 39, No. 3, 167 (1975).
27. M. Zaduban, "Problems of radioecology associated with the development of nuclear energy technology," At. Énerg., 34, No. 5, 376 (1973).
28. N. M. Berezina et al., "On the introduction of presowing gamma irradiation of seeds in 'Kolos' equipment into agricultural practice," At. Énerg., 37, No. 1, 43 (1974).

ARTICLES

STEAM-SUPERHEATING FUEL ELEMENTS OF THE REACTORS IN THE I. V. KURCHATOV BELOYARSK NUCLEAR POWER STATION

A. G. Samoilov, A. V. Pozdnyakova, and V. S. Volkov

UDC 621.039.54:621.311.2:621.039

One of the most promising directions in nuclear power development is that of high-temperature thermal-neutron reactors; the high efficiency of these reactors enables nuclear power stations to compete with thermal power stations using organic fuels.

One of these is the high-pressure steam-superheating uranium–graphite reactor, which underwent its initial development in the Soviet Union at the end of the fifties [1]. This reactor is one of the channel class, in which the coolant pressure is taken up by individual, small-diameter channels. The reactor uses slightly enriched uranium, the moderator is graphite, the number of fuel channels 998, of which 730 evaporating channels are provided for the preheating and partial evaporation of the water of the first circuit ($P \sim 150$ atm, $T \sim 340°C$, mass content of steam at the outlet ~ 30%) and 268 superheating channels are used for superheating the steam of the second circuit ($P \sim 90$ atm, $T \sim 500^0$ C) [1, 2]. The superheated steam is passed directly, without any intermediate heat exchanger, from the superheating channels to the turbine of the electrical generator. The active zone of the reactor (7.2 m in diameter and 6 m high) is surrounded by a graphite reflector 0.8 m thick. The thermal power of the reactor is 285 MW, the rated period of a campaign 730 days, and the amount of ^{235}U consumed during the campaign 243/198 kg (the denominator indicates the amount of fissile isotopes).

We see from the specification and parameters of the reactor that the fuel elements of the superheating channels are expected to endure severe working conditions. Since this reactor constitutes a further development of the reactor used in the world's first nuclear power station, it retains the basic structural concept of a tubular fuel element, withstanding the coolant pressure during normal operation and preventing contamination of the circuit and turbine by fission activity should the fuel element lose its hermetic properties. The designed operating conditions of the fuel elements are indicated in Table 1.

For the evaporating channels it is quite possible to use fuel elements similar to those of the first nuclear power station, with the same fuel composition but slightly greater dimensions of the central and outer cans. The question of using the same fuel elements in the superheating channels raised serious doubts and it was considered essential to develop a more reliable fuel element. In creating a fuel element producing steam at a temperature of ~ 500°C and a pressure of ~ 100 atm and working under fairly severe thermal loads lay one

TABLE 1. Operating Conditions of the Reactor Fuel Elements [1]

Characteristic	Channel of max. power	
	EC*	SC†
Thermal flux, kcal/(m^2 · h)	$525 \cdot 10^3$	$480 \cdot 10^3$
Max. coolant velocity, m/sec	0.0	57.0
Max. temperature, °C:		
inner fuel-element can	355	530
fuel composite	400	550
graphite	660	725

* Evaporating channel.
† Superheating channel.

Translated from Atomnaya Énergiya, Vol. 40, No. 5, pp. 371-377, May, 1976. Original article submitted July 9, 1975.

TABLE 2. Design Characteristics and Working Conditions of the Superheating Channels [6]

Characteristic	Initial form for reactor of first unit	U-shaped channel with six fuel elements for reactor of second unit	
		down-going fuel elements	up-coming fuel elements
Max. channel power kW	368	767	
Min. channel power kW	202	548	
Steam flow through max.-power channel, kg/h	1900	3600	
Steam flow through min.-power channel, kg/h	1040	2570	
Press. at channel entrance, atm	110	132	124
Press. at channel outlet, atm	100	125	110
Steam temp. at channel entrance, °C	316	328	397
Steam temp. at channel outlet, °C	510	399	508
Max. thermal loading, kcal/(m²·h)	$480 \cdot 10^3$	$820 \cdot 10^3$	$680 \cdot 10^3$
Max. steam velocity, m/sec	57	76	112
Max. temp., °C:			
inner can of fuel element	530	426	531
fuel composite	550	482	565
graphite	725	735	

of the chief scientific and technical problems besetting the development of reactors with nuclear steam superheating.

The main requirements imposed upon the fuel elements of the superheating channls are: good radiation resistance over long periods, compatibility between the fuel-element materials, and between the fuel-element can, the graphite stack, and the superheated water vapor, a reasonably high thermal conductivity of the fuel composite (so as to avoid large temperature drops in the fuel element, thermal stresses, and the possibility of exceeding the temperature limit of compatibility of the fuel-element materials), good heat resistance and hot strength in order to ensure the mechanical wholeness of the fuel element during the entire operating period, and corrosion and erosion resistance of the fuel composite in superheated steam so as to avoid loss of material on dehermetizing the fuel element.

In designing the fuel elements, certain mutually exclusive requirements were encountered, and these had to be met with a compromise solution. Thus, e.g., the requirement of a high mechanical strength in order to ensure the wholeness of the fuel element, insignificant radiation damage, containment of the fission products, etc., contradicted the requirement that rapid mechanical breakdown of the fuel element should occur after damage to the central tube so as to ensure the rapid transfer of radioactive fission products into the reactor stack together with the stream of coolant, and hence prevent radioactive contamination in the circulation circuit and the power equipment of the power-station machine room.

In the initial analysis of possible methods of developing the steam-superheating fuel element, a number of solutions characteristic of other reactors were rejected. In particular it was found unacceptable to consider such heat-resistant materials as graphite-based dispersion-type fuel composites, or composites of uranium dioxide and stainless steel as used in certain foreign developments ("Pathfinder" superheated-steam reactor [3], the high-temperature gas reactors HTGR [4], "Dragon" [5], and others). The basis of our rejection of these materials was as follows. It was impossible to use graphite as a construction material in a tubular fuel element sustaining a high water-vapor pressure. The UO_2–stainless steel composite was unacceptable owing to its inadequate thermal conductivity, since for a heavy loading of the reactor with uranium a fairly thick active layer would be required and this would involve extremely high temperature drops. In addition to this, in view of the mechanical characteristics of this fuel composite, it would be impossible to use a high volumetric proportion of uranium dioxide, so that a high proportion of stainless steel would have to be employed and highly enriched uranium would be required.

The development of the steam-superheating fuel element proceeded in several directions. After preliminary tests on the technology of making and checking the serviceability of fuel elements constructed in various ways with various materials, a tubular fuel element with a stainless steel can and a uranium dioxide-base composite fuel was chosen for more extensive development.

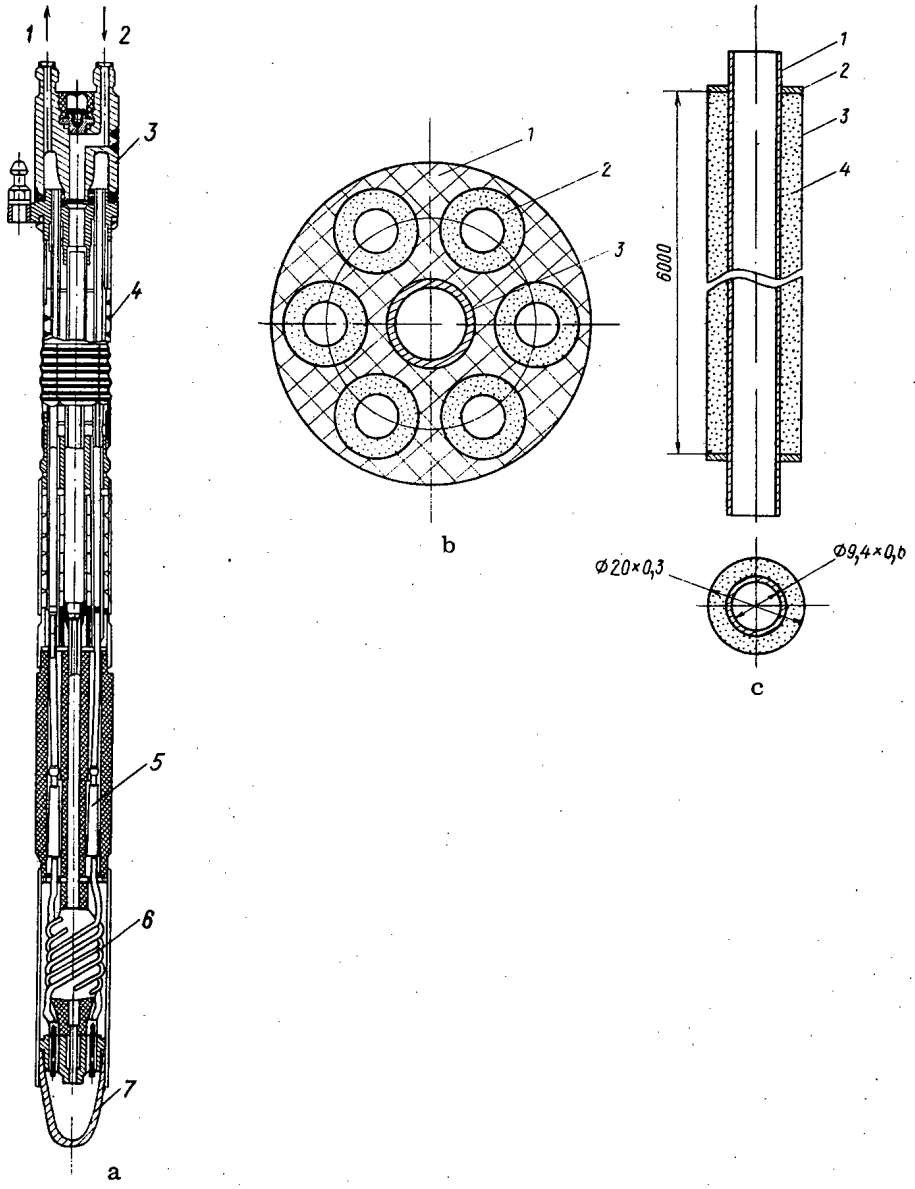

Fig. 1. Basic construction of the steam-superheating channel and the fuel element. a) Channel: 1) release of steam from the channel; 2) entry of steam into the channel; 3) upper head; 4) sealing rings; 5) fuel element; 6) linear-expansion compensator; 7) lower head. b) Channel cross section: 1) graphite collar; 2) fuel element; 3) steam tube. c) Fuel element: 1) inner tube; 2) end cap; 3) outer can; 4) fuel composite.

In its initial form the fuel element was of tubular construction, formed by two coaxial cylindrical stainless-steel cans having dimensions of $\phi 9.4 \times 0.6$ and $\phi 20 \times 0.3$ mm, containing spaces distributed along the annular gap and connected at the ends of welding on end caps. In the annular gap between the inner and outer cans, a fuel composite consisting of UO_2 fragments dispersed in a matrix alloy was placed.

The steam-heating channels containing fuel elements of this kind were similar in construction to the evaporating channels, i.e., they consisted of six fuel elements arranged in a graphite collar around the central steam-carrying tube. Passing along this tube the steam enters the central tubes of the fuel elements and is superheated as it moves along them [6]. The construction of the steam-superheating fuel element and channel is illustrated in Fig. 1, and the designed working conditions are given in Table 2.

Later a U-shaped construction of the steam-superheating channels was developed; this was distinguished by the fact that the central steam tube was eliminated and the steam was superheated by successively passing first through three fuel elements in a downward direction and then through three fuel elements in an upward

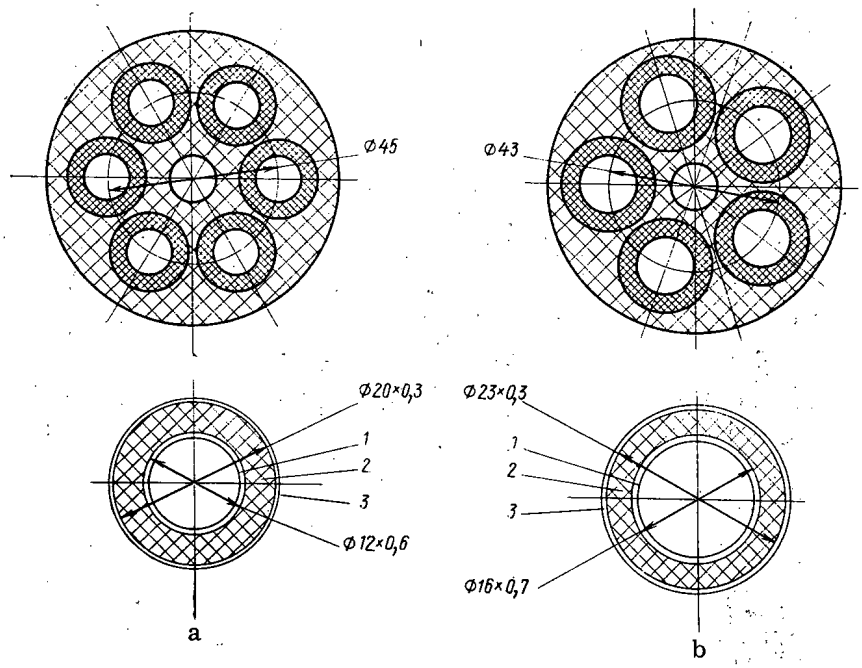

Fig. 2. Cross section of the U-shaped channel and the fuel element: Six-element channel (a); five-element channel (b); 1) inner tube of the fuel element; 2) fuel composite; 3) outer can of the fuel element.

direction. In the place of the former central tube was a soft-regulation absorbing rod enabling the power of the fuel channels to be to a certain extent equalized. This construction eases the operation of three of the fuel elements in the channel because of the lower temperature, and reduces the temperature of the graphite stack (~ 100°C for a channel power of 360 kW), which favorably influences the working conditions of the graphite and the physical characteristics of the reactor. The construction of the fuel elements was slighly altered in this kind of superheating channel: instead of the central tube 9.4 × 0.6 mm in size we used a tube of 12 × 0.6 mm, although leaving the can material and fuel composite as before. As a result of these constructional changes to the fuel element and channel the hydraulic resistance of the channel was reduced, while the reduction in the thickness of the active layer led to a reduction in the nonproductive absorption of neutrons and to an improvement in the physical characteristics of the reactor [2, 6]. Channels of such a construction were used in the reactors of the first and second units of the power station. The design characteristics of these channels and the working conditions of the fuel elements are shown in Table 2 and the construction in Fig. 2.

Efforts to improve the physical and thermotechnical characteristics of the reactor led to the further modernization of the channel and a change of fuel elements. One of the fuel elements in the channel was removed; the steam was then superheated in the five fuel elements (three down-coming and two rising). The inner tube of the fuel element was increased to a size of $\phi 16 \times 0.7$, the outer to $\phi 23 \times 0.3$ mm. Following this reconstruction the physical and thermotechnical characteristics improved sharply as a result of a reduction in the volume of matrix material in the fuel element and an increase in the open cross section of the channel. Superheating channels of this construction are being placed in the reactor of the second unit of the power station whenever the existing six-element U-shaped channels are exhausted and require renewal [7]. The basic construction of the channel and fuel element is presented in Fig. 2.

As can material of the steam-superheating fuel element we use stainless steel, which has a considerable corrosion and erosion resistance in high-pressure superheated water vapor, excellent mechanical characteristics, and an acceptable thermal conductivity, and is technologically convenient in the manufacture of the fuel elements (production of long, thin-walled tubes, welding, deformation, and so on).

As fuel composite for the steam-superheating fuel elements we use UO_2 fragments dispersed in a matrix alloy. Uranium dioxide has a number of favorable properties leading to its choice as fissile component: It is inert with respect to high-temperature water and steam, compatible with many construction materials (including the stainless steel used for the cans), has a fairly high radiation resistance, and contains a great deal of uranium. A serious disadvantage of uranium dioxide is its low thermal conductivity, which prevents its use in pure form as a nuclear fuel in a tubular fuel element with unilateral heat take-off. The temperature at the

TABLE 3. Average Characteristics of the First Unit of the Beloyarsk Nuclear Power Station before and after Installing Standard Superheating Channels [8]

Characteristic	Before use of steam-superheating elements	After introducing superheating elements
Electrical power of unit, MW	60-70	100-105
Steam press. in front of turbine, atm	60-64	80-85
Steam temp. in front of turbine, °C	395-405	490-505
Press. of exhausted steam, atm	0.09-0.11	0.035-0.04
Water flow in 1st circuit, tons/h	1400	2300-2400
Press. in separators, atm	95-100	120-130
Gross efficiency,%	29-32	35-36
Specific flow of steam, kg/(kW·h)	4.6-4.9	3.8-4.0
Expenditure of electric power on internal requirements, %	10-12	7-9

surface of the fuel element should never exceed 630-650°C, the temperature of the steam being ~ 500°C; hence the total temperature drop in the fuel element, including the temperature drops in the outer and inner cans, in the fuel layer, in the core-can contact resistance, and in the coolant layer close to the walls should not exceed 100-120°C. Thus uranium dioxide may only be used subject to its dispersion in a matrix with a high thermal conductivity.

The matrix alloy developed for this purpose has a high thermal conductivity, so ensuring a high thermal conductivity of the whole composite and satisfying the condition that the overall temperature drop in the fuel element should lie below 100-120°C. The alloy is compatible with UO_2 and stainless steel, its melting point is well above the maximum fuel-element working temperature, it is corrosion and erosion resistant in water vapor, its thermal-expansion coefficients ensure the absence of serious thermal stresses during the heating and cooling of the fuel element, the mechanical characteristics satisfy the demands made regarding the adequate strength of the fuel element, while providing for its breakdown by the pressure of the coolant if the inner tube should rupture. A shortcoming of the matrix alloy is its relatively high neutron capture cross section. However, this disadvantage is compensated by the fact that the number of superheating channels in the reactor is only ~ 27% and the volume of the alloy in the composite is relatively small. Hence the use of steam-superheating fuel elements with the foregoing fuel composite has no serious effects on the physical characteristics of the reactor.

A great complication in the fuel-element manufacturing technology was the size of the element (active length 6 m) and the necessity of ensuring fault-free thermal contact between the fuel composite and the inner can, as well as the requirement that the uranium distribution should be very uniform. Considerable difficulties also arose in developing methods of testing the quality of the fuel elements. The technology eventually developed overcame these difficulties, was adopted by industry, and ensured the production of good-quality fuel elements. Before placing the fuel elements in the reactor their characteristics were analyzed comprehensively in various test systems and their efficiency was verified by tests in the loop of the First Nuclear Power Station reactor.

The reactor in the first unit of the Beloyarsk Nuclear Power Station started operations in April 1964, and evaporating channels were initially used for superheating the steam. At this time the steam temperature was no greater than 400-410°C and the electrical power 60-70 MW. In November 1966, 20 experimental superheating channels were installed in the reactor, and in July-August 1967 all the heating channels used for superheating the steam were replaced by standard superheating channels. The use of the superheating fuel elements greatly improved the thermotechnical and economic indices of the NPS: The reactor was raised to its rated power, the efficiency of the unit and the power production were increased, and the expenses were lowered [8]. The average service characteristics of the first unit before and after installing the standard superheating channels are shown in Table 3.

The reactor of the second unit was furnished with standard superheating elements from the very beginning. On initial operation in 1967 the charging of the fuel channels was incomplete: 452 evaporating and 138

superheating channels. Complete charging (732 items) was effected in 1968 and complete charging with superheating channels (266 items) in 1969. The thermal power of the reactor was twice that of the first unit and amounted to 560 MW. Hence the specific power of the fuel and the mean thermal loading in the fuel elements of this reactor were also twice those of the first unit. The reactor of the second unit also differs from that of the first unit in having a one-circuit cooling system; the water in the evaporating channels is preheated and partly evaporated, while the steam separated from the water in drum separators passes into the superheating channels and is superheated in the fuel elements of these.

At the present time the fuel elements of the evaporating and superheating channels have operated for quite a long period in the reactors of the first and second units, and it has become possible to assess their true efficiency under full-scale conditions, as well as the technicoeconomic indices of the NPS, and also future prospects. Details were presented in earlier papers [7, 9]; in the present article we present only information relating directly to the steam-superheating fuel elements.

Since 1967, 300 superheating elements have been installed in the reactor of the first unit and about 30 have been taken out for various reasons (failure due to errors of the service personnel, damage in the coolant tract, and manufacturing faults, as well as for test inspections and monitoring). The remaining superheating channels continue satisfactory operation, none having failed as a result of radiation damage to the fuel elements or the incompatibility of their materials; premature extractions of the channels have been reduced to individual cases in each year. In view of the low burn-up intensity, the fuel elements have not yet reached the rated energy development of 720 MW·days per channel, and in order to exhaust the rated reserve they will have to operate in the reactor for another three years, when their total operation in the reactor will amount to about 10 years.

Over 450 superheating elements have been installed in the reactor of the second unit since 1967. In this time about 200 channels have been extracted for partial recharging and replaced by fresh six- and five-element superheating channels. The mean energy development of the discharged channels is 600-850 MW·days per channel, or 18-26 MW·days/kg U; their service life in the reactor has been five to six years, with over 200 complete cooling and heating cycles. Some of the discharged (incompletely used) channels have been installed in the reactor of the first unit for further burn-up. Over the period indicated only eight channels were prematurely extracted from the reactor of the second unit because of the breakdown of service conditions or for test inspections and monitoring.

The maximum energy development of the superheating channels working in the reactor of the second unit is 950 MW·days per channel.* Since the frequency of the premature extractions of the channels is apparently not increasing with time, it has been decided to increase the energy development of a considerable group of channels to 1200-1300 MW·days per channel (37-40 MW·days/kg U). Failure of the five-element channels has never yet been encountered; the energy development achieved is 275 MW·days per channel (the rated energy development is 980 MW·days).

Accounting for channels failing for constructional-technological reasons (experimental channels and channels failing because of a breakdown in service conditions not being taken into consideration), the probability of the fault-free operation of the superheating channels up to the rated energy development of 720 MW·days per channel is over 0.96, which is a very high value. Analysis of the operation of the superheating channels indicates that these have still not reached their limiting energy evolution.

During the operation of the superheating channels, considerable adjustments have been made to their temperature conditions. Initially the maximum temperature of the steam at the outlet of the superheating channel was limited to 510°C. However, the good results achieved in the use of steam-superheating fuel elements enabled this to be raised to 535°C in 1967 and 545°C in 1969. Prolonged service (more than four years) under these conditions has in no way reduced the efficiency of the fuel elements, so that in 1973 it was decided to raise the temperature at the outlet from individual channels to 560-565°C.

The high reliability of the steam-superheating fuel elements has ensured stable operation of the reactor in the nuclear-superheating mode of operation, and has constituted one of the main factors in ensuring a high efficiency and relatively low net cost in electrical power production. In the period 1970-1973 the mean net cost of electrical power in the Beloyarsk NPS was 1.15-1.16 for the first and 0.92-0.93 kopecks/(kW·h) for the second unit. The net cost of electrical power in the second unit equals the mean net cost of electrical

*As at the end of 1975 the energy development of the superheating channels was 1150 MW·days – Editor.

power in thermal power stations in the Ural region; this makes the second unit competitive with ordinary thermal power stations [7,9].

LITERATURE CITED

1. N. A. Dollezhal' et al., in: Transactions of the 2nd Geneva Conference 1958, Papers of Soviet Scientists [in Russian], Vol. 2 Atomizdat, Moscow (1959), p. 36.
2. P. I. Aleshchenkov et al., At. Énerg., 16, 489 (1964).
3. M. Novick et al., in: Proc. 3rd Intern. Conf. Geneva, Vol. 6 (1965), p. 225.
4. F. Hoffmann and C. Rickard, ibid., Vol. 5, p. 101.
5. C. A. Rennie et al., ibid., Vol. 1, p. 318.
6. N. A. Dollezhal' et al., in: 3rd Geneva Conference, Paper No. 309 [in Russian] (1964).
7. N. A. Dollezhal' et al., in: Experience in the Use of Nuclear Power Stations and Ways of Developing Nuclear Power Further [in Russian], Vol. 1, Obninsk (1974), p. 149.
8. N. A. Dollezhal' et al., At. Énerg., 27, No. 5, 379 (1969).
9. N. A. Dollezhal' et al., At. Énerg., 36, No. 6, 432 (1974).

SOME PHYSICAL INVESTIGATIONS IN BFS-1 FAST CRITICAL ASSEMBLIES

V. A. Dulin, Yu. A. Kazanskii,
V. F. Mamontov, and G. I. Sidorov

UDC 621.039.526:621.039.519.4

The accuracy with which the fundamental physical characteristics of prospective fast reactors may be predicted is as yet far from adequate. Systems of nuclear-physical constants and computing methods are therefore usually checked by reference to integrated (macroscopic) experiments in fast critical assemblies [1-4].

TABLE 1. Tablets of the BFS-1 Critical Assembly

Material	Index	Thickness, mm
^{235}U	1 2	0,3 5
UO_2^*	3	9,5
$^{239}Pu^\dagger$	4	2,4
$Na^\dagger$	5	10
C	6	10
Steel	7 8	10 5
Al	9 0	10 5

*In an aluminum can 0.3 mm thick.
†In a stainless steel can 0.3 mm thick.

Translated from Atomnaya Énergiya, Vol. 40, No. 5, pp. 377-381, May, 1976. Original article submitted November 27, 1974.

TABLE 2. Composition of the Unit Cell

Assembly	Cell	Indices of materials*
BFS -22	A	3525355353525353253523 5
BFS -23	A	5354353534535345353543 53
BFS -26	A	6967692676967
	B	161018161018161018160181610118161018
	B	608608608111111111111111111608608608
BFS -27	A	5656526565
	B	115116115116115116115116115
	B	565651111111111111111116565
BFS -28	A	9392393
	B	111911131119111311191113
BFS -30	A	5352353
	B	111511131115111311151113
	B	555111111111111111111333

* Table 1, column 2.

TABLE 3. Homogeneous Nuclear Concentrations of the Central Insertions $\cdot 10^{21}$, nuclei/cm^3

Assembly	Cell	^{235}U	^{238}U	^{239}Pu	^{23}Na	^{12}C	^{16}O	Al	Steel IKh18N9T
BFS -22	A	1,44	7,76	—	7,29	—	10,5	2,48	14,5
BFS -23	A	—	6,47	1,07	7,29	—	13,0	1,93	16,9
BFS -26	B	1,21	0,14	—	—	28,8	—	12,5	20.9
BFS -27	B	1,57	0,18	—	7,67	24	—	6,57	3,95
BFS -28	B	2,32	6,34	—	—	—	12,3	29,4	—
BFS -30	B	2,30	6,30	—	6,63	—	12,12	9,3	3,14

Note. The critical assemblies contained traces of hydrogen owing to the presence of glue in the sheaths of the sodium and 5 mm uranium tablets (Table 1, index 2). The maximum possible H concentration, referred to the concentration of ^{235}U, was 3% in BFS-22, 1% in BFS-23 (referred to ^{239}Pu), 0% in BFS-26, 1% in BFS-27, 0% in BFS-28, and 1% in BFS-30.

The accuracy of calculations relating to a number of characteristics has been studied on various occasions using the latest critical assemblies (BFS-22; 23; 26; 27; 28; 30) [5-7]. Measurements have included the central reactivity coefficients of the main fissile elements (^{235}U, ^{238}U, ^{239}Pu), as well as elements with well-known cross sections, including those of the absorbing (^{10}B, ^{197}Au, ^{6}Li) and scattering (^{1}H, ^{12}C, ^{23}Na, Pb) classes. The ratio of the cost of the generated neutrons to the cost of the absorbed neutrons and the ratio of the reaction rates of a number of fissile and absorbing elements have been measured. The neutron spectra have been determined in the critical assemblies BFS-26, 27, 28, and 30 [8, 9]. The results presented in this paper constitute a refinement of the data presented in [7].

The results of the experiments were compared with calculations using the 26-group BNAB-70 system of constants [2, 3]. Corrections chiefly associated with the finite dimensions of the samples and the heterogeneous structure of the critical assemblies had to be introduced into the experimental data. The values of these corrections were determined experimentally and also by calculation. An analysis of the estimated experimental data revealed the principal reasons for the differences between experiment and calculations. The character of the discrepancies demanded some specific changes in the macroscopic constants.

In this paper we shall briefly describe the critical BFS assemblies and the experimental techniques, verify the methods of introducing the corrections, and present the principal experimental results together with the results of homogeneous calculations.

A detailed description of the BFS-1 installation was presented earlier [10]. The critical assemblies were made up of tubes containing tablets of construction and fissile materials 46 mm in diameter. The thickness of the tablets was varied from fractions of a millimeter to 10 mm (Table 1). The existence of thin ^{235}U tablets enabled us to create critical assemblies with different degrees of heterogeneity in the center of the active zone ("homogeneous" insertion pieces). The homogeneous insertion pieces were situated in the center of the active zone and comprised 57 cells (in 19 central tubes with three cells in each).

Table 2 shows the composition of the elementary (unit) cells of the critical assemblies. A represents a cell of the active zone and B a cell of homogeneous insertion. The concentrations of ^{235}U and ^{238}U in the A and B cells are well known (error no worse than 0.5%) and differ from one another by no more than 3%. Table 3 shows the homogeneous nuclear concentrations of the central parts of the active zones. The remaining zones and the reflector of the critical assemblies were described in more detail in [11].

The reactivity introduced by the sample was determined by measuring two asymptotic periods of the reactor (with and without the sample). The mean square error of the measurement was $(1-3)\cdot 10^{-7}\ \Delta K/K$ for a mean scatter of $5\cdot 10^{-7}\ \Delta K/K$ in an individual measurement.

For measuring the spectral ratios of the indices of the fissile elements we used fission chambers containing ^{235}U and ^{239}Pu and chambers containing natural uranium. The captures in ^{197}Au were recorded by reference to the residual γ activity. We used the method of calibration in a thermal column.

The $\langle\sigma_c^{197}\rangle/\langle\sigma_f^{239}\rangle$ ratio was also measured by an absolute method. The absolute rate of captures in gold was determined by the $\beta-\gamma$ coincidence method and also by determining the total number of interactions in an

TABLE 4. Central Reactivity Coefficients

Assembly	Cell	^{235}U	^{239}Pu	^{6}Li	^{10}B	^{197}Au	^{1}H	^{12}C	^{23}Na	^{208}Pb
BFS -22	A	4,48±0,03	6,50±0,06	—	—4,93±0,10	—1,22±0,018	—	—	—0,0046±0,0020	—
BFS -23	A	6,05±0,06	8,1±0,13	—	—6,83±0,3	—1,8±0,02	—	—	—	—
BFS -26	B_{het}	8,47±0,14	11,8±0,25	—10,6±0,25	—	—11,3	1,5±0,03	0,156±0,003	—	—
	B_{hom}	7,66±0,08	10,35±0,16	—8,45±0,2	—28,0±0,4	—8,88±0,3	2,1±0,07	0,174±0,006	—	—
BFS -27	B_{het}	6,27±0,10	—	—6,45±0,15	—18,5±0,6	—6,22±0,16	2,22±0,06	—	—	—
	B_{hom}	6,2±0,1	9,30±0,16	—5,77±0,15	—16,8±0,6	—5,54±0,14	2,24±0,06	0,168±0,003	—	—
BFS -28	B_{hom}	8,15±0,04	12,9±0,1	—3,75±0,06	—7,90±0,19	—1,645±0,018	1,73±0,03	0,047±0,001	—	—0,056±0,005
BFS -30	B_{het}	7,3±0,09	—	—3,76±0,08	—7,59±0,08	—	1,83±0,03	0,0703±0,004	—	—0,05±0,01
	B_{hom}	7,24±0,08	11,6±0,16	—3,69±0,09	—7,54±0,08	1,70±0,04	1,89±0,03	0,071±0,0015	0,0472±0,002	—0,056±0,005

TABLE 5. Ratio of the Average Cross Sections to the Fission Cross Section of ^{239}Pu and the $\langle\Phi_x^+\rangle/\langle\Phi_c^+\rangle$ Ratio

Assembly	Cell	^{235}U	^{197}Au	^{238}U	$\langle\Phi_x^+\rangle/\langle\Phi_c^+\rangle$
BFS-22	A	1,00±0,02	0,30±0,01	—	0,97±0,03
BFS-23	A	1,03±0,02	0,37±0,01	0,0240±0,0005	—
BFS-26	B_{het}	—	0,69±0,02	—	—
BFS-26	B_{hom}	1,03±0,02	0,60±0,02	0,0227±0,0005	0,765±0,025
BFS-27	B_{het}	0,99±0,02	0,51±0,01	0,0300±0,0006	0,80±0,02
BFS-27	B_{hom}	0,98±0,02	0,49±0,01	0,0322±0,0006	0,80±0,02
BFS-28	B_{hom}	0,915±0,020	(0,50±0,01) * 0,207±0,005 (0,212±0,003) *	0,0341±0,0008	1,01±0,019
BFS-30	B_{het}	0,91±0,02	0,220±0,005	0,0365±0,0008	—
BFS-30	B_{hom}	0,92±0,02	0,218±0,005 (0,222±0,003) *	0,0369±0,0007	0,88±0,015

* The ratio was measured by determining the absolute capture rates in gold and the fission rates in plutonium.

NaI(Tl) crystal. The absolute number of fissions was measured with a chamber containing a known number of ^{239}Pu nuclei and an experimentally determined fission-recording efficiency [12].

The ratio of the cost of the fission neutrons to the cost of the neutrons absorbed in the gold (Φ_x^+ Φ_c^+) was determined by measuring the reactivity ρ_c, introduced by the absorbing sample (gold) and the absolute rate of absorption in gold N_c, as well as the pseudoreactivity ρ_{cf}^+ of a ^{252}Cf spontaneous-fission source of known absolute activity [13]. The activity of the ^{252}Cf was determined by several methods, the error being ~ 0.6%.

One of the aims of these experiments was to study the influence of the heterogeneity of the critical assemblies on the measured functionals. For this purpose we introduced homogeneous insertion pieces into the BFS-26, 27, 28, and 30 critical assemblies, which enabled us, on the one hand, greatly to reduce the influence of heterogeneity, and on the other to measure effects due to the heterogenization of the insertion pieces (Table 2). Tables 4 and 5 give the results of measurements in homogeneous and heterogeneous insertions. We see from Tables 4 and 5 that in certain cases homogeneous insertions change the measured functionals very substantially. Estimates regarding the influence of the finite dimensions of the homogeneous insertions and the magnitudes of the heterogeneous effects in the BFS-22 and 23 critical assemblies will be given later. Another aim of the experiments was to allow for the finite dimensions of the samples.

There are several ways of describing the calculated dependences of the effects under consideration on the sample dimensions; these are based on the fact that the neutron spectrum in the sample differs from the spectrum obtained before introducing the sample. In order to find the average flux pertubation in the sample we must allow for the resonance and nonresonance neutron absorption, the slowing down of the neutrons in the sample, and also their multiplication (breeding) in fissile samples. The resonance absorption was

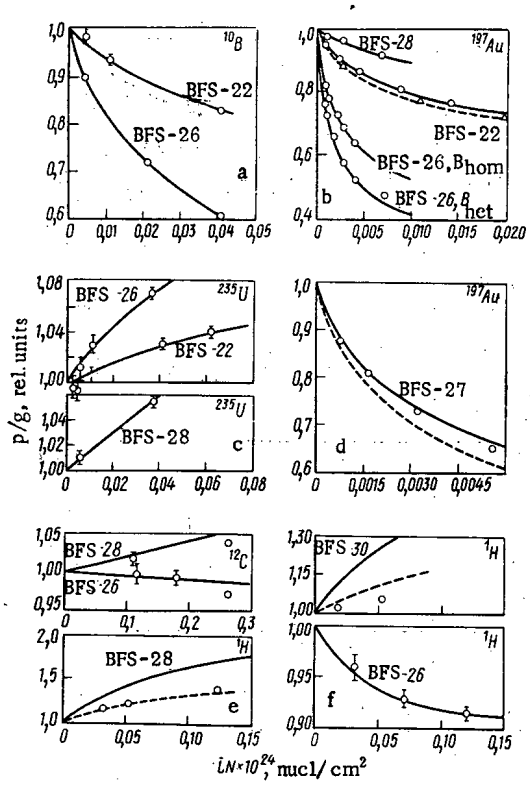

Fig. 1. Specific reactivity (per unit mass) and activation of the samples as functions of their dimensions: a) ——, ○) calculated and experimental reactivity; b) ——, ○) calculated and experimental activation – – –, Δ) calculated and experimental reactivity; c) ——, ○) calculated and experimental reactivity; d) ——, ○) calculated and experimental activation – – –), calculation of activation with an increased sodium concentration in the critical assembly; e, f) ——, ○) calculated and experimental reactivity, – – –) calculation of the reactivity based on the altered system of constants.

TABLE 6. Comparison between Certain Computed and Experimental Results

Material	Assembly, cell					
	BFS-22	BFS-23	BFS-26	BFS-27	BFS-28	BFS-30
	A		B_{hom}			
	$(\rho_i/\rho^{235})_{exp}/(\rho_i/\rho^{235})_{calc}$					
^{239}Pu	1,03	1,035	1,015	1,00	1,05	1,02
^{197}Au	1,27	1,37	1,25	1,43	1,14	1,22
^{10}B	1,27	1,38	1,20	1,20	1,21	1,32
^{6}Li	—	—	1,16	1,12	1,00	1,01
^{1}H	—	—	1,03	1,12	1,64	1,49
^{12}C	—	—	1,11	1,08	4,7	1,85
^{208}Pb	—	—	—	—	—	1,0
^{23}Na	0,33	—	—	—	—	3,8
^{238}U	—	1,08	—	—	—	0,82
	$(\langle\sigma_i\rangle/\langle\sigma_f^{235}\rangle)_{exp}/(\langle\sigma_i\rangle/\langle\sigma_f^{235}\rangle)_{calc}$					
^{239}Pu	1,02	1,03	1,12	1,09	1,06	1,03
^{197}Au	1,17	1,15	1,18	1,29	1,10	1,17
^{238}U	—	0,99	1,03	0,85	0,94	0,89
	$(\langle\Phi_x^+\rangle/\langle\Phi_c^+\rangle)_{exp}/(\langle\Phi_x^+\rangle/\langle\Phi_c^+\rangle)_{calc}$					
—	0,915	—	1,02	1,01	1,01	0,97

accounted for on the Wigner approximation [14], using the theorem of equivalence and the coefficients of resonance self-screening employed in the BNAB system [2, 3].

The perturbed group neutron flux in the samples may be defined [15] as

$$\Phi_j' = \Phi_j \frac{[f_c^j(\sigma_0)\,\sigma_c^j + f_f^j(\sigma_0)\,\sigma_f^j]\,(\sigma_p^j+\sigma_0)}{(\sigma_c^j+\sigma_f^j)\,[f_f^j(\sigma_0)\,\sigma_f^j + f_c^j(\sigma_0)\,\sigma_c^j + f_e^j(\sigma_0)\,\sigma_e^j+\sigma_0]},$$

where σ_c^j, σ_f^j, σ_e^j are the average group cross sections for capture, fission, and elastic scattering; f_c^j, f_f^j, f_e^j are the corresponding resonance self-screening coefficients; σ_p are the potential scattering cross sections of the sample; N is the density of the nuclei in the sample; $\sigma_0 = (lN)^{-1}$; l is the mean size of the sample. Allowance was also made for neutron breeding [15]. The depression of the neutron flux close to the sample was allowed for by the method described in [16].

Figure 1 illustrates the measured and calculated reactivity and activation of various elements. The accuracy achieved in calculating the dependence on sample size was governed by a large number of factors: the accuracy to which the group fluxes and cost of the neutrons in the critical assembly (as well as the cross sections and coefficients of resonance self-screening) were known, the validity of the method of description, and so on. Hence a formal approach (without knowing the experimental relationship) may lead to extrapolation errors. Thus we see from Fig. 1e and f that for the BFS-26 the calculated description of the relationship is excellent, while for BFS-28 and 30 there is a considerable discrepancy. As we shall subsequently show, the reactivity of hydrogen in BFS-28 and 30 is poorly predicted by calculation. Changes in the cross sections leading to such changes in the flux and cost function of the neutrons as will reduce the discrepancy between the experimental measurements and the calculation of the actual reactivity coefficients of hydrogen tend to produce a better description of the relationship for this sample (broken lines in Fig. 1e and f) [7].

Thus an iterative process is required in order to give a valid description of the influence of sample dimensions. The results obtained by extrapolation are, in our own opinion, reliable from the point of view of interpreting the difference between experiment and calculation.

Table 4 gives the experimental central reactivity coefficients of fissile, absorbing, and scattering elements (in β_{eff}/mole of the principal isotope), extrapolated to zero sample dimensions in accordance with the method presented. The errors indicated include statistical errors and those due to the extrapolation. The mean square measuring errors are shown in Fig. 1. For the smallest samples these are usually no greater than 1-1.5%.

In the ratios of the cross sections (Table 5) the statistical errors were no greater than 0.5%, the errors of the reference constants 0.5%, the errors in the isotopic composition of the natural uranium 0.5%, and the errors in integrating over the cell 1-1.5%.*

The errors in $\langle\Phi_x^+\rangle/\langle\Phi_c^+\rangle$ comprise errors in the central reactivity coefficient of gold referred to the pseudoreactivity of the californium source, and errors in determining the absolute rate of absorption in the gold sample (used when measuring the central reactivity coefficient of gold) and the absolute activity of the californium neutron source.

Table 6 compares experiment with the homogeneous calculation for the central reactivity ratios and the ratios of the mean cross sections at the center of the reactor. The calculation was carried out in the p_1 approximation. The differences between the calculated and experimental data usually exceed the experimental error by a factor of several times. It is reasonable to assume that these discrepancies are largely due to indeterminacies in the system of group constants. In order to discover the constant component of the error it is essential to allow for the limited dimensions of the homogeneous insertions, the residual heterogeneity, the influence of errors associated with the averaging of the cross sections, and so on. An analysis of the reasons for the observed discrepancies will be presented in the second part of this paper.

LITERATURE CITED

1. M. Drake, Data Formats and Procedure for the ENDF Neutron Cross Section Library, BNL-5027 (1970).
2. L. P. Abagyan et al., Group Constants for Calculating Nuclear Reactors [in Russian], Atomizdat, Moscow (1964).
3. L. Abagyan et al., in: Proc. IAEA Symp. "Nuclear Data for Reactors – 1970," Helsinki (June 15-19, 1970), Vol. 2, p. 667.
4. J. Rowlands et al., in: Proc. Intern. Symp. Physics of Fast Reactors, Tokyo (October 16-19, 1973), Rep. A-30, A-33, B-2.
5. A. I. Voropaev et al., Preprint FÉI-247 [in Russian], Obninsk (1971).
6. V. A. Dulin et al., Preprint FÉI-313 [in Russian], Obninsk (1972).
7. V. Dulin et al., [4], Rep. A-26.
8. Yu. Kazanskii et al., [4], Rep. B-19.
9. A. I. Leipunskii et al., At. Énerg., 36, No. 1, 3 (1974).
10. V. V. Bondarenko et al., At. Énerg., 24, No. 1, 82 (1968).
11. V. V. Orlov et al., Preprint FÉI-306 [in Russian], Obninsk (1972).
12. V. Dulin and V. Mozhaev, Nucl. Instrum. and Methods, 105, 277 (1972).

*Integration was carried out either by placing samples with a length equal to the length of the cell in the intertube gap (or moving shorter samples), or else by using disks with a diameter equal to the diameter of the BFS tablets.

13. V. A. Dulin et al., Preprint FÉI-422 [in Russian], Obninsk (1973).
14. L. Dresner, Resonance Absorption in Nuclear Reactors [Russian translation], Gosatomizdat, Moscow (1962), pp. 67 and 77.
15. V. A. Dulin and V. F. Mamontov, Preprint FÉI-392 [in Russian], Obninsk (1973).
16. K. H. Beckurtz and K. Wirtz, Neutron Physics, Springer-Verlag (1964).

SOME RESULTS OF POSTREACTOR TESTING OF SIX-ELEMENT THERMIONIC UNITS OPERATING FOR 2670 h

G. A. Batyrbekov, E. S. Bekmukhambetov,
V. I. Berzhatyi, S. E. Ermatov,
Sh. Sh. Ibragimov, V. P. Kirienko
B. S. Kurmangaliev, M. V. Mel'nikov,
V. V. Sinyavskii, Yu. A. Sobolev,
and Yu. I. Sukhov

UDC 621.362:621.039.577

The basic results of tests conducted in the channel of a reactor on the long-term performance of an ÉS-6-3 six-element thermionic unit were reported in [1]; the electrogenerating elements of the unit had hermetic emitter points. The elements had the following parameters: The emitter material was a tungsten–rhenium alloy (27% Re); the collector was niobium; the collector insulation was alumina; the distance-piece was beryllium oxide; the fissile material was uranium dioxide homogeneously diluted with 20% tungsten; emitter diameter 10 mm; interelectrode gap 0.3 mm. The unit operated in the reactor for 2670 h under thermal radiation ensuring a mean electric-power output of ~ 7 W/cm^2. For constant test conditions, the electrical power remained constant but, after any interruption of reactor operation, the return to the previous thermal power period produced a somewhat reduced value of the electrical power. The main cause of this discrete reduction in power [1] is short-circuiting of the elements and increase in the collector temperature considerably above the optimum on account of cleavage of the multilayer collector assembly during the thermal fluctuations, while other factors may be the increase in heat loss from the emitter as a result of embedding of the distance-piece in the electrode material and the increase in heat loss through the cesium vapor and gaseous fission products due to decrease in the interelectrode gap as a result of swelling processes.

In order to confirm experimentally the proposed explanation of the reduction in electric power, the thermionic unit was subjected to postreactor investigation in a hot cell. The present paper gives a brief account of the main results for the emitter points and the collector assembly.

Emitter Points. The surfaces of all the emitters were clean and bright, although strongly recrystallized along the whole length; only the area of the emitter adjacent to the distance-piece remained unrecrystallized. The diameter of all the emitters was increased; of the elements investigated (one was not investigated), all but one had a maximum diameter larger than 10.5 mm. The central emitter was the most strongly deformed,

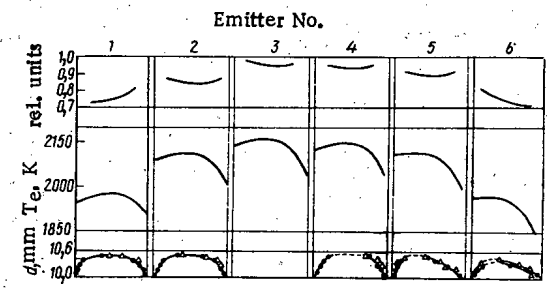

Fig. 1. Change over the height of the unit of the thermal-energy density, temperature, and emitter diameter: ●, Δ) change in diameter of calibrated disk of height 3 and 15 mm, respectively.

Translated from Atomnaya Énergiya, Vol. 40, No. 5, pp. 382-384, May, 1976. Original article submitted April 23, 1975.

and its hotter end was convex. The smallest increase in diameter was that of one of the outer elements (No. 6), which had a maximum diameter of 10.3-10.4 mm; however, this element had a depression of depth 0.05-0.07 mm. The increase in diameter was not uniform along the length of the elements, the diameter at the ends of the elements being close to its initial value. The change observed in the emitter diameter along its length is shown in Fig. 1. All the emitters were observed to have an indentation caused by the distance piece with a maximum depth of up to 0.2 mm.

Collector Assembly. The inside surface of the niobium collector was bright in its initial state, but after the test it had a gray coloration with spots of tarnish. The alumina insulation was strongly joined to the collector; it did not peel when cut, nor crack when the assembly was deformed. The outside surface of the insulation had lost its initial pure white coloration, and was light gray. The nickel substrate between the insulation and the supporting tube was also firmly joined to the supporting tube and the insulation in its initial state, but was easily separated from them at the end of the experiment; in the gap between the substrate and the supporting tube cesium compounds were observed. This confirms the assumption that there is cleavage of the collector assembly in the course of testing and that cesium vapor penetrates under the supporting tube (through a nonhermetic intercollector ceramic casing) because the contact between the substrate and the supporting tube is not gas-tight and evidently changes in the course of testing.

On the inside surface of all the collectors there were single defects in the form of dark spots (indentations), ~ 1 mm or less in size, or groups of smaller spots with aureoles of a different color. The reason for the appearance of these spots is not yet known.

The indentations in the collectors caused by distance-pieces increased in depth and width during testing. For a distance-piece diameter of 0.7 mm [2] and an indentation in the collector beneath the distance-piece of initial width 0.8 mm, the width of the indentation after testing was up to 3 mm. All the indentations were rounded at the edges. However, none of the distance pieces themselves were destroyed during testing, nor was the intercollector ceramic casing.

Discussion. Postreactor investigation of the ÉS-6-3 thermionic unit confirmed the basic hypotheses as to the causes of the reduction in power of the unit during long-term testing. It was confirmed experimentally that there is cleavage of the collector assembly, which must lead inevitably to a sharp increase in the thermal resistance of the assembly, and a corresponding rise in the collector temperature above the optimum; this in turn leads to a reduction in the electrical power for approximately parallel shifts in the volt–ampere characteristic. The high collector temperature is also indicated by the spots of tarnish on its inner surface.

The experiment also confirmed that there is a decrease in the interelectrode gap due to swelling. This leads to a short circuit of some elements and increases the heat losses from the emitter to the collector due to the increase in the effective thermal conductivity of the interelectrode gap and the region around the distance-piece, resulting in a corresponding reduction in power.

The thermionic unit tested had hermetic emitters. When the unit was irradiated, gaseous fission products collected in a central cavity of the core formed as a result of the transfer of uranium dioxide at the working temperature and temperature gradient. The creep of the emitter shell under the action of the gaseous fission products should be calculated according to one of the basic mechanisms of deformation of the emitter points. Calculations by the method of [3] showed that, for a mean emitter temperature of 1800°C for the ÉS-6-3 unit, the time in which the diameter of the tungsten–rhenium emitters increased by 0.5 mm was ~1000 h. In fact, it is possible that the operating characteristics of the elements also show the effect of other factors which may lead to improvement or deterioration in the performance. Thus, e.g., when the unit was tested, loss of hermeticity of the emitter shell was observed for several elements, associated with the periodic release of gaseous fission products [1]. This loss of hermeticity, evidently connected with the formation and subsequent mending of microcracks in the hermetic emitter shell, should lead to improvement in the performance of the element. Some improvement also should result from the gradual decrease in the emitter temperature on account of the increase in heat losses from the emitter with decrease in the interelectrode gap.

The performance of the unit may be worse than calculated as a result of the following effects: In the initial stages of testing (at least up to the first loss of hermeticity of the emitter shell), the emitter deformation is increased by the pressure of the residual gas in the porous uranium dioxide; displacement and misalignment of the emitters with respect to the collectors may lead to a decrease at certain points in the width of the interelectrode gap, which decreases the time of locking of the electrodes; similarly, the interelectrode gap is reduced as a result of plastic deformation (compression) of the collectors rigidly connected to the graphite bush of the heat-regulation system.

The results of the experiment showed that that there is relatively good correlation between the change in diameter and the distribution of the thermal-energy density and temperature of the emitter over the height of the element in the unit (see Fig. 1).

The distribution of the heat emitted was measured up to the beginning of testing on a physical model of the unit in the form of a steel shell inside which, in a graphite seal, were mounted models of the elements: six small tungsten tubes containing a uranium dioxide pellet. The heat emitted was measured by two independent methods: by autoradiography, using a detector giving a spatial picture of the distribution of the heat emission over the volume of the core, and by the calorimetric method, using a thermal-radiation heat-flux divider. The measurements showed significant nonuniformity of the heat emission over the height of the unit: The mean taken over the core volume of the relative density of the heat emission is larger by a factor of 1.37 in the central elements than in the outermost elements, and larger by a factor of 1.28 overall than in the outermost elements. Nonuniformity of heat emission is also observed over the height of individual elements, especially the outer elements (see Fig. 1).

Using the data obtained on the distribution of heat emission, the method of [4] gives the temperature distribution for the emitters of the tested unit in conditions corresponding to the beginning of testing. The results of these calculations are also shown in Fig. 1.

CONCLUSIONS

The results of postreactor investigation of a thermionic unit with hermetic emitters operating in the reactor for 2670 h confirmed the proposed explanations of the decrease in electrical power of the unit during testing. In order to improve the performance of similar units, it is necessary to develop a collector assembly with stable thermophysical properties and to arrange for the continuous removal of gaseous fission products from the emitter points.

LITERATURE CITED

1. E. S. Bekmukhambetov et al., At. Énerg., 35, No. 6, 387 (1973).
2. V. I. Berzhatyi et al., At. Énerg., 31, No. 6, 585 (1971).
3. Yu. I. Likhachev and V. A. Vakhrameeva, in: Proceedings of SÉV Conference on Recent and Future Developments in the Design of Nuclear-Power Stations Using Fast-Neutron Reactors [in Russian], Izd. FÉI, Obninsk (1967), paper 4, p. 7.
4. Yu. A. Broval'skii et al., in: Papers by Soviet Scientists at the Second International Conference on the Thermoemissive Transformation of Energy [in Russian], Izd. VNIIT, Moscow (1969), p. 281.

EFFECT OF HETEROGENEITY ON THE MEASUREMENT OF INTEGRAL PARAMETERS IN SUBCRITICAL SYSTEMS

L. N. Yurova, A. V. Bushuev,
V. I. Naumov, V. M. Duvanov,
N. N. Khrennikov, and V. N. Zubarev

UDC 621.039.519.4

Integral experiments associated with the measurement of relative reaction rates have an important place in reactor physics. Among the basic parameters that characterize physical processes in thermal reactors are the effective resonance integrals, the ratios $\langle\sigma_c^{28}\rangle/\langle\sigma_f^{25}\rangle$; $\langle\sigma_f^{25}\rangle/\langle\sigma_f^{49}\rangle$; ρ^{28}; δ^{28}; δ^{25}. The accuracy of these parameters that is required at present is 2-3%.

By using a reactor as a neutron source, it is possible to measure basic integral parameters in subcritical systems of relatively small dimensions [1]. Measurements in heterogeneous subcritical systems present the problem of creating conditions such that the neutron spectrum in the experimental system is comparable to the spectrum in a critical system of analogous structure.

Interpretation of the results of experiments on subcritical systems is usually based on the theory of a physical parameter [2] and, more precisely, on the possibility of separating the energy and space variables in the region in which the neutron spectrum is set up. By separating the variables, it is possible, in particular, to obtain the value of the physical parameter

$$\varkappa^2 = \alpha_\perp^2 - \beta^2 \tag{1}$$

from the measured axial distribution of neutrons, characterized by the parameter β^2, and the known eigenvalue $\alpha_\perp^2$ associated with the transverse dimensions of the system. The theory of a physical parameter can be successfully applied to heterogeneous systems with a sufficient number of cells which can be considered as quasi-homogeneous. However, in those cases where the subcritical heterogeneous system contains relatively few cells, the energy and space variables cannot be entirely separated. This means that the distribution of fast and thermal neutrons in the transverse section cannot be characterized by a single eigenvalue $\alpha_\perp^2$, and the neutron spectrum may differ for individual blocks of the system and change with change in its size. As a result there is a need to establish a basis for the choice of the system size such that acceptable accuracy of the measurements is ensured.

In order to determine the scale of the effect and the possibility of using the theory of a physical parameter for the analysis of results obtained on heterogeneous subcritical systems, analytical and experimental in-

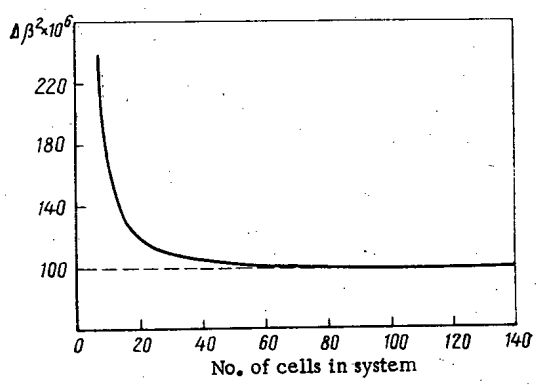

Fig. 1. Dependence of correction $\Delta\beta^2$ on number of cells in system.

Translated from Atomnaya Énergiya, Vol. 40, No. 5, pp. 384-386, May, 1976. Original article submitted July 16, 1975.

TABLE 1. Calculated Values of $(\Phi_r/\Phi_t)_{rel}$ for Systems with Different Numbers of Cells

System characteristic	(Φ_r/Φ_t) rel	No. of cells				
		9	16	25	36	49
$a/\sqrt{\tau} = 0{,}825$	Center	1,078	1,032	1,013	1,002	1,000
$\gamma/2\Pi D = 0{,}141$	Periphery	1,051	1,022	1,008	1,000	1,000
$a/\sqrt{\tau} = 1{,}11$	Center	1,112	1,056	1,021	1,003	1,000
$\gamma/2\Pi D = 0{,}249$	Periphery	1,072	1,041	1,012	1,001	1,000
$a/\sqrt{\tau} = 1{,}37$	Center	1,131	1,074	1,034	1,004	1,001
$\gamma/2\Pi D = 0{,}386$	Periphery	1,085	1,053	1,019	1,002	1,000

TABLE 2. Dependence of Relative Values of R^{28}_{Cd} and $\langle\sigma_f^{25}\rangle/\langle\sigma_f^{49}\rangle$ on the Number of Cells

No. of cells	$(R^{28}_{Cd})_{rel}$	$\langle\sigma_f^{25}\rangle/\langle\sigma_f^{49}\rangle_{rel}$
9	0,899±0,018	0,971±0,007
25	1,004±0,020	0,989±0,008
49	0,989±0,015	0,989±0,010
81	1,000±0,012	1,000±0,016

vestigations of the physical parameters of uranium–graphite systems with different numbers of cells were carried out. For the theoretical analysis of the effects of heterogeneity, the Galanin–Feinberg method was used [3].

The height of the system was assumed to be large so that, considering neutrons lying in planes perpendicular to the axes of the block, their distribution far away from the source is exponential, with decay constant β; the space–energy distribution of the neutrons can then be written in the form

$$\Phi(x, y, z, E) = \Phi_1(x, y, E)\exp(-\beta z), \tag{2}$$

where the energy and space variables characterizing the distribution of the neutrons in the transverse section cannot be separated. If Eq. (2) is substituted into the heterogeneous equation, the problem is then to determine the parameters depending on the space–energy distribution of the neutrons in the transverse section. A similar problem was solved for the homogeneous system with equivalent properties, permitting complete separation of variables. In the calculation, the aging model of deceleration was used, neglecting anisotropy of the neutron diffusion.

The basic parameters chosen to characterize the heterogeneity of the propagating system with lattice spacing a were the parameter $a/\sqrt{\tau}$ and the thermal constant γ, the ratio of the number of neutrons absorbed by the block in unit time to the density of neutrons at its surface.

Calculations were carried out for the uranium–graphite system with different numbers of cells for different values of the characteristic parameters. In Fig. 1 results are shown for the calculation of the correction $\Delta\beta^2 = \beta^2_{hom} - \beta^2_{het}$ caused by the heterogeneity of the system with $a/\sqrt{\tau} = 1.11$ and $\gamma/2\pi D = 0.249$ for a ratio of volumes of graphite and uranium $V_C/V_U = 38$. As seen from Fig. 1, the correction $\Delta\beta^2$ rises markedly as the number of cells decreases. In particular, for a lattice with natural uranium having a physical parameter $\varkappa^2 \approx 100 \cdot 10^{-6}\,cm^{-2}$ in a system of 20 cells, $\Delta\beta^2 \approx 15 \cdot 10^{-6}\,cm^{-2}$, i.e., the relative shift in the determined value of the physical parameter is about 15%. If $\varkappa^2$ increases, the critical size predicted on the basis of the data of the exponential experiment becomes too low. The results obtained are in qualitative agreement with the known calculations of the value of the critical load for a system with a small number of blocks [4].

In order to understand how the heterogeneity affects the neutron spectrum in the system, the ratio of the fluxes of resonance and thermal neutrons Φ_r/Φ_t was calculated for systems with different lattice spacings as a function of the number of cells. The thermal constants were chosen in such a way that the square of the migration length of the lattice, calculated from the relation

$$M^2 = L^2(1-\theta) + \tau, \tag{3}$$

was retained unchanged in all cases.

In Table 1, calculated values of $(\Phi_r/\Phi_t)_{rel}$ are shown for central and peripheral blocks. From these data it is evident that Φ_r/Φ_t depends on the number of cells and is not constant for all blocks of the system. With increase in the number of cells, Φ_r/Φ_t tends for all blocks to an asymptotic value; the more strongly

expressed the heterogeneity of the block, the more slowly does Φ_r/Φ_t tend to the asymptotic value.

If we take, e.g., 2% as an acceptable deviation of Φ_r/Φ_t from the asymptotic value, then for the uranium–graphite lattice in the range $a/\sqrt{\tau} = 0.8$–1.4 (which is sufficiently characteristic for the system with natural and slightly enriched uranium) the minium size of the subcritical system that ensures an acceptable divergence of the neutron spectrum is found to be 20–40 cells, depending on the degree of heterogeneity. Analogous results are obtained for other systems.

Experiments on the effect of the number of cells on the measurable parameters were conducted on subcritical uranium–graphite systems with natural uranium using an IRT reactor as the source of the neutron beam. The number of cells in the investigated lattice with $a/\sqrt{\tau} = 1.11$ for $V_C/V_U = 38$ was changed from 9 to 81. The height of the system was not changed: in all experiments it was 270 cm. Measurements were made in the central channel of the system at a distance of 135 cm from the lower end, known to be in the region of the asymptotic neutron spectrum. The cadmium ratio R^{28}_{Cd} and the ratio $\langle\sigma_f^{25}\rangle/\langle\sigma_f^{49}\rangle$ were measured. The measurements were made by the activation method, using a Ge(Li) spectrometer. The rate of the reaction $^{238}U(n,\gamma)$ was determined from the intensity of ^{239}Np γ radiation of energy 277 keV, and the rate of fission from the intensity of ^{143}Ce γ radiation at 283 keV. The procedures for the measurements and the treatment of the data were described in [1]. The results for the parameters of the system with n = 81 cells are shown in Table 2.

From Table 2 it is evident that the dependence of both R^{28}_{Cd} and $\langle\sigma_f^{25}\rangle/\langle\sigma_f^{49}\rangle$ on the number of cells is significant only in passing from 25 to 9 cells, when R^{28}_{Cd} reduces by 10% and $\langle\sigma_f^{25}\rangle/\langle\sigma_f^{49}\rangle$ by 3%.

Thus in the given case, R^{28}_{Cd} is the parameter most sensitive to change in size of the system. For 25 cells and more, the physical parameters are unchanged within the limits of experimental error. If we take into account that the value of δ^{28} in these lattices scarcely depends on the size of the system, we may conclude that, when the number of cells is varied, the value of R^{28}_{Cd} serves as a sufficiently objective criterion for the choice of a system size ensuring that the set of integral physical parameters characterizing the neutron spectrum in the lattice can be measured. Here the height of the system should be such as to ensure that the characteristic spectrum is established and that the flux can be represented in the form given in Eq. (2).

The results of relative measurements of R^{28}_{Cd} are in satisfactory agreement with heterogeneous calculations of Φ_r/Φ_t. It may be assumed that for a heterogeneous system of thermal neutrons the acceptable size satisfying the required level of accuracy may be determined on the basis of calculations using the Galanin–Feinberg method.

LITERATURE CITED

1. L. N. Yurova et al., At. Énerg., 38, No. 4, 245 (1975).
2. A. M. Weinberg and E. P. Wigner, Physical Theory of Neutron Chain Reactors, University of Chicago Press, Chicago (1958).
3. S. M. Feinberg, in: Reactor Construction and the Theory of Reactors [in Russian], Izd. Akad. Nauk SSSR, Moscow (1956), p. 152.
4. A. D. Galanin, ibid. p. 191.

INVESTIGATION OF THE LIBERATION OF HELIUM FROM CONSTRUCTION MATERIALS DURING THEIR HEATING

D. M. Skorov, N. P. Agapova,
A. I. Dashkovskii, Yu. N. Sokurskii,
A. G. Zaluzhnyi, O. M. Storozhuk,
V. D. Onufriev, and I. N. Afrikanov

UDC 621.039.546:541.183.5:546.291

It is a well-known fact that neutron irradiation generates helium and hydrogen in construction materials during the (n, α) and (n, p) reactions where the materials are composed of certain isotopes. The formation of these gases implies changes in the mechanical and physical properties of the materials, particularly in their radiation-dependent high-temperature embrittlement and swelling.

The present paper is concerned with investigations of the behavior of helium in nickel and OKh16N15M3B steel during tempering.

The nickel (99.99%) and OKh16N15M3B steel (~100-μ-thick foil with 30-50 μ recrystallized grains) samples were saturated with helium on the ILU-100 magnetic mass separator of the Physics Power Institute by bombarding the samples of the materials under inspection with 70-keV α particles to a dose of $\sim 3 \cdot 10^{16}$ particles/cm^2 (flux density 1 μA/cm^2). The sample temperature did not exceed 100°C during the irradiation process. The helium distribution over the thickness of samples treated on the magnetic mass separator corresponded to a Gaussian distribution [1]. According to calculations, the layer saturated with helium extends from the surface to a distance which is much smaller than the grain size in the samples of the materials under inspection.

Samples were saturated with helium by bombarding foils of OKh16N15M3B steel with α particles having energies of up to 40 MeV in the cyclotron of the I. V. Kurchatov Institute of Atomic Energy. In order to obtain samples of the alloy which were uniformly saturated with helium, a rotating disk with appropriate filters was inserted between the ion source and the foils to be saturated. The sample temperature did not exceed 70°C in the course of the irradiation. The calculated helium concentration in the irradiated samples was $\sim 10^{-2}$ at. %.

The liberation of helium from nickel and OKh16N15M3B steel was studied with the aid of a special setup [2] whose operation is based on the mass spectrometric determination of the partial pressure of an inert gas which has been liberated at some instant of time from the sample annealed in vacuum. However, in contrast to the previously described method of investigating the liberation of gases during isothermal annealing [2], the present work was based on investigations of the kinetics of helium liberation from construction materials heated at a constant rate. The uniform heating was ensured by changing the voltage applied to the heater in accordance with a preset program. In order to maintain the required vacuum in the annealing chamber, a getter-ion pump and an electrical discharge pump were simultaneously used during the experiments. The helium

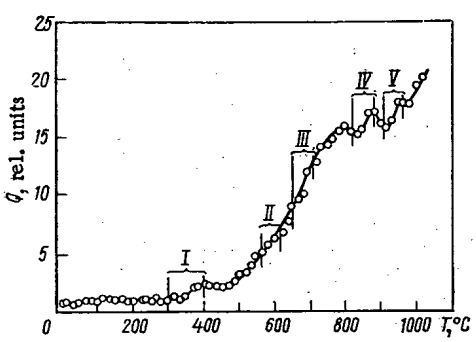

Fig. 1. Kinetics of helium liberation from a sample of OKh16N15M3B steel.

Translated from Atomnaya Énergiya, Vol. 40, No. 5, pp. 387-390, May, 1976. Original article submitted November 14, 1974.

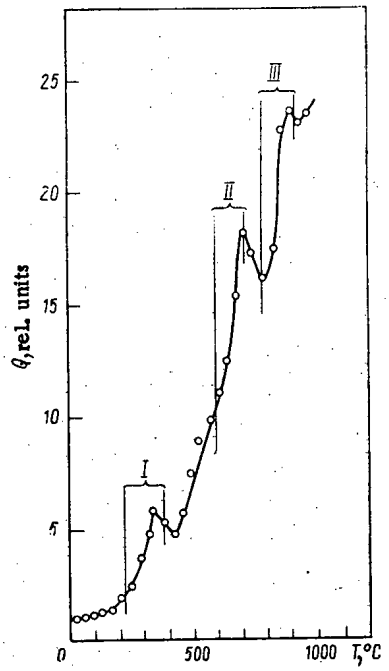

Fig. 2. Kinetics of helium liberation from a nickel sample.

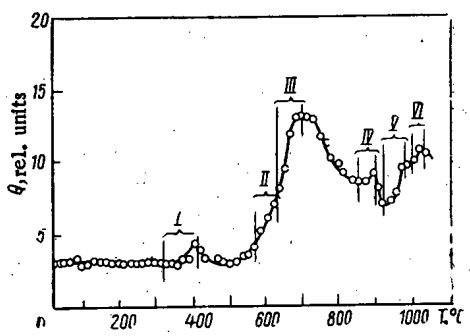

Fig. 3. Kinetics of the liberation of helium from an OKh16N15M3B steel sample saturated with gas in cyclotron (~ 0.01 at. % He).

liberated in the pressure interval of the experiments was therefore pumped off at a practically constant rate; the kinetic curves of gas liberation which were obtained logically characterize only the rate of helium liberation from the material: An ascending part of the curve indicates that the rate of liberation exceeds the rate of pumping; a descending part means that the rate of pumping exceeds the rate of gas liberation. Three experiments were made with each material heated at a rate of 7 and 15 deg C/min to establish the reproducibility of the results.

Figure 1 shows the liberation of helium from an OKh16N15M3B steel sample which had been saturated with the inert gas on the ILU-100 apparatus; the sample was heated at a rate of 7 deg C/min.

One can distinguish five peaks in the rate of helium liberation. The characteristic temperatures of the peaks differ in the experiments by less than 20-25°C. Figure 1 shows that the first peak (I) of the rate of gas liberation appears in the low-temperature region between 300 and 400°C. The other peaks (II-V) are observed at temperatures in excess of 600°C.

The curves representing the liberation of helium were obtained when nickel samples saturated with the inert gas on the ILU-100 apparatus were uniformly heated (at a rate of 7 deg C/min). The curves representing the rate of helium liberation from OKh16N15M3B steel and nickel are identical. The only difference is that the second peak is stronger in nickel than in steel and slightly shifted on the temperature scale: In the case of steel, the peak is observed at temperatures between 580 and 620°C, whereas the peak appears at temperatures between 600 and 700°C in the case of nickel.

Figure 2 shows the liberation of helium from a nickel sample which had been saturated with the inert gas on the ILU-100 magnetic mass separator and which was heated at a rate of 15 deg C/min. A similar curve was obtained from an OKh16N15M3B steel sample which had been saturated with the inert gas on the above apparatus and which was heated at the same rate. By contrast to the curves representing the separation of helium

from steel and nickel samples at a heating rate of 7 deg C/min, the latter curves have only three peaks. As far as the form is concerned, the curves coincide with the curves representing the helium liberation from the corresponding materials heated at a rate of 20 deg C/min [3]: Three peaks of the rate of gas liberation are observed (one in the low-temperature region of ~ 300°C, and two peaks at temperatures in excess of 600°C). This could be expected because in both the present work and in [3] the materials under consideration were uniformly heated at almost the same rate. Selection of the optimum heating rate of the samples under inspection is a rather difficult experimental problem, because in the case of a low rate, the peaks are smeared on the temperature scale, whereas in the case of a high rate, a superposition of neighboring peaks is observed.

The liberation of helium from OKh16N15M3B steel samples which had been uniformly saturated with the inert gas on a cyclotron was also studied. Figure 3 depicts the liberation of helium from such a steel sample during its uniform heating at a rate of 7 deg C/min. The liberation of helium from that sample took place in the same fashion as in the uniform heating of similar steel samples which had been saturated by the gas upon bombardment with low-energy helium ions in the ILU-100 apparatus: One peak (I) of the rate of helium liberation is clearly visible in the low-temperature range (280-380°C), whereas the other peaks appear at high temperatures (II-VI). In the case under consideration, one more peak is observed in the high-temperature range. The appearance of peak VI can be explained by the influence of boundaries upon the distribution of the gas in the material, because when steel is irradiated in the cyclotron, the entire sample volume rather than a narrow layer near the surface was saturated with helium ions (provided that the magnetic mass separator was used for irradiation).

An analysis of the results of [3-7] leads to the conclusion that the liberation of helium from the materials under inspection during their uniform heating takes place in several stages.

Investigations which were made with an EM-300 electron microscope on similar nickel and OKh16N15M3B steel samples annealed at 300, 400, and 500°C after irradiation with low-energy helium ions have shown that the helium does not cause porosity in the materials under these conditions. According to the results of electron microscopy, in nickel and steel saturated with helium ions, the black spots and small dislocation loops which are observed in the initial stage are converted into clearly distinguishable large dislocation loops when the temperature is increased to 500°C; the large dislocation loops are loops of interstitial atoms, as put into evidence by the work of [8]. The size of the loops increases at increasing annealing temperature and their concentration decreases (Fig. 4). One must assume that, after irradiation, most of the helium induced in the sample is in a metastable solid solution or forms complexes with a size of ~ 10 Å, as indicated by the results of electron microscopy. It is possible that some of the helium atoms remain in the form of the atoms introduced, which are characterized by increased mobility and which may leave the sample while they generate the first peak of gas liberation (see Figs. 1 and 3). It is also possible that a certain fraction of the induced helium atoms form a Cottrell atmosphere near the dislocation loops. This conclusion is corroborated by the fact that the first bubbles usually appear on dislocation lines. A sharp growth of the loops and the reduction of their concentration imply a reduction of the total length of loop dislocations and a decrease in the concentration of points at which helium atoms are adsorbed. The helium atoms which are liberated in this process leave the sample and cause the first peak of gas liberation in the corresponding temperature interval (according to the results shown in Fig. 4).

The results which the electron microscope helped to obtain in regard to the onset of helium-induced porosity in nickel at 600°C and in steel at 700°C indirectly confirm that the helium atoms in these materials have a significant diffusion-induced mobility. The second peaks of the rate of helium liberation in this temperature interval (600-700°C; see Figs. 1 and 3) indicate that vacancies are involved in the diffusion mechanism of the gas atoms.

If the liberation of a gas from a material which is heated at a constant rate is given by the volume diffusion of the gas atoms, one can determine the activation energy of the diffusion of the gas atoms in the material from the temperature T_m of the corresponding maximum [4, 5, 9]; the relation

$$\frac{Q}{T_m} \approx 69.5 + 4.6 \lg \frac{T_m}{p^2\beta} + 4.6 \lg \frac{K_0}{10^{15}},$$

is used, in which p denotes the number of atomic layers between the layer saturated with gas and the sample surface; and K_0 denotes the oscillation frequency of the diffusing atoms; a value of 10^{15} sec^{-1} can be assumed for the oscillation frequency of many metals [6]. In this manner one can obtain only tentative values of the activation energy, because the p and K_0 values which are employed are results of calculations. Calculations have shown that the activation energies which were calculated for the diffusion of helium in the materials under

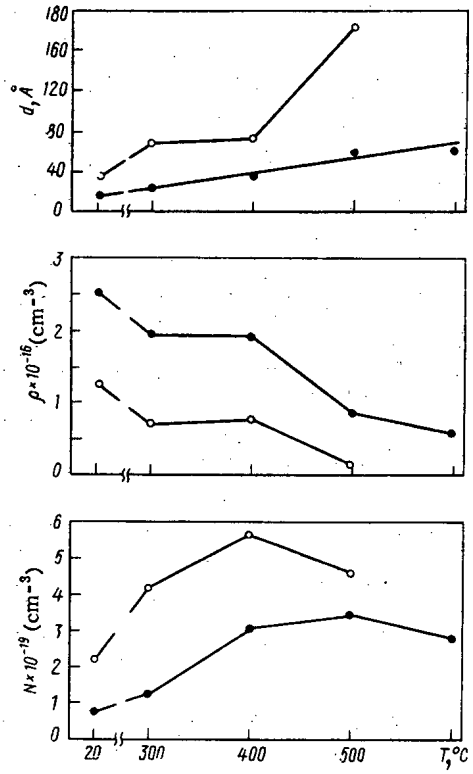

Fig. 4. Dependence of the average diameter $\bar{d}$, of the concentration ρ of loops, and of the number N of displaced atoms in dislocation loops upon the temperature of isochronous annealing cycles with a duration of 0.5 h each: ○) nickel; ●) OKh16N15M3B steel.

inspection on the basis of the temperature of the second peak on the inert-gas liberation curves are approximately the same for nickel and OKh16N15M3B steel: The activation energies amount to 45–50 kcal/(g·atom) because the temperatures of the peaks are practically identical (the difference is within the spread of the experimental data). The activation energies of the diffusion of helium in nickel and steel coincide with the results of [3]. The activation energy of the diffusion of helium in nickel corresponds to the activation energy of the self-diffusion of nickel [10]. This attests to a helium-diffusion mechanism in nickel involving vacancies at temperatures between 600 and 700°C.

Electron microscopical investigations of the gas bubbles which develop in the materials at the temperature of the third stage of gas liberation (800–900°C) have shown that almost all the introduced helium is enclosed in the bubbles. Therefore at temperatures of 900°C or more helium can be liberated from the material only by nondirectional migration of gas bubbles to the sample surface. It is unlikely that redissolved helium appears in the pores without neutron irradiation, because the solubility of this gas in metals and alloys is extremely low.

LITERATURE CITED

1. H. Glyde and K. Mayne, Phil. Mag., 12, 919 (1965).
2. D. M. Skorov et al., At. Énerg., 35, No. 4, 269 (1973).
3. D. Whitmell and R. Nelson, Radiation Effects, 14, 249 (1972).
4. R. Kelly and H. Matzke, J. Nucl. Mater., 20, 171 (1966).
5. E. Ruedl and R. Kelly, J. Nucl. Mater., 16, 89 (1965).
6. R. Kelly and F. Brown, Acta Met., 13, 169 (1965).
7. K. Willertz and P. Shewmon, Met. Trans., 1, 2217 (1970).
8. N. P. Agapova et al., Izv. Akad. Nauk SSSR, Ser. Fiz., 38, No. 11, 23 (1974).
9. J. Farrell et al., Vacuum, 16, No. 6, 295 (1966).
10. R. Rantanen et al., J. Vacuum Sci. Technol., 7, No. 1, 18 (1969).

THE EVOLUTION OF GAS FROM URANIUM DIOXIDE

B. V. Samsonov, Yu. G. Spiridonov,
V. Sh. Sulaberidze, and V. A. Tsykanov

UDC 621.039.343

Characteristic features of the macrostructure cross section of highly stressed container-type fuel elements with uranium dioxide cores (Fig. 1) are the zones of equiaxial grains and columnar crystals separated by ring-shaped cracks (in the majority of cases) and sometimes by radial cracks, which arise after irradiation due to a number of causes [1].

Fig. 1. Cross section of GD-122-type fuel element (after irradiation).

Translated from Atomnaya Énergiya, Vol. 40, No. 5, pp. 390-395, May, 1976. Original article submitted January 15, 1975; revision submitted November 25, 1975.

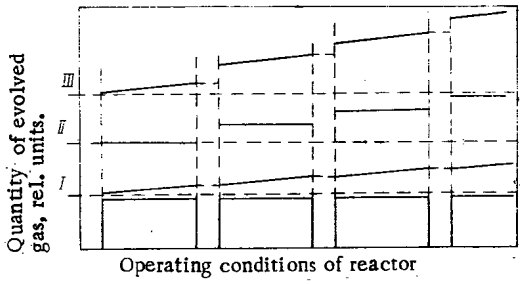

Fig. 2. Nature of gas evolution from the various structural zones of a fuel element: I) the equiaxial grain zone only; II) the columnar crystal zone only; III) the equiaxial grain and columnar crystal zones.

TABLE 1. Parameters of Fuel Elements

Fuel element*	External and internal diams. of can, mm	Fuel-briquet diam., mm	Fuel-column ht., mm	Uranium dioxide wt., g	Absorption by ^{235}U%	Initial filling of fuel element, atm.
D-6	6; 5,4	5,2	201	36	21	He;4
D-7	6; 5,4	5,2	200	36	21	He;4
GD-122	9,1; 8,2	8,15	350	182	21	Air; 1
GD-125	9,1; 8,2	8,15	349	182	21	He; 3,5
GD-115	9,1; 8,2	8,15	351	182	36	Air; 1

*Fuel density for all fuel elements ≥ 10.2 g/cm^3

TABLE 2. Thermal and Physical Parameters of Fuel Elements Tested

Fuel element	Fuel-element power, kW	Thermal power per unit length, W/cm	Surface temp. of fuel, °C	Max. temp. of fuel, °C	Radius of columnar crystal zone, cm	Rel. radius of columnar crystal zone, %
D-6	2,6	128	1300	1600	—	—
D-6	3,7	185	1300	1700	—	—
GD-115	22	630	1000	1800	0,1	25
GD-122	26	740	1000	2400	0,3	73
GD-125	27	770	1000	2460	0,32	76

In fuel which is run with a large temperature gradient, there is a transport of mass connected with the displacement of pores into hotter regions. The cause of this process during the first rise in fuel-element power is the initial porosity of the fuel, while in the following rises it may be due to the porosity of the fuel in the boundary region between the columnar crystal zone and the zone of equiaxial grains or the ring crack separating these two zones. The mechanism of pore migration is connected with the vaporization of uranium dioxide at the hotter wall of a pore and its condensation on the colder wall. The time needed to form the structure depends on thermal and physical conditions of operation of the fuel element and does not exceed some tens of minutes. The growing columnar crystals are formed under temperature gradient conditions; therefore a temperature stress does not arise in them during operation. In the case of the crystals within the equiaxial granular zone, the appearance of a temperature gradient does give rise to a temperature stress. When the fuel element ceases to operate, the stress is relieved in the equiaxial grain zone whereas it appears in the columnar crystal zone. The zones tend to break apart under the effect of these stresses. As the fuel element is run again, the process of forming these structures is repeated. The boundary of the zones lies along the 1700°C isotherm.

Consequently, above 1700°C the dioxide forms its original structure consisting of elongated columnar crystals lying adjacent to each other and having an almost theoretical density. The gaseous fission products from such crystalline structures are not released into the free volume in practice, but are fixed at their boundaries. It is as though all the gaseous fission products accumulated during the operation of the fuel element are cleared out of the columnar crystal zone at the same time as the structure of the transient pores is reformed.

Bearing in mind the variation in structure we have described, the kinetics of gas evolution from uranium dioxide can be represented in the following manner (Fig. 2). The gaseous fission products leave the equiaxial grain zone by thermal activation diffusion, complicated by the presence within the uranium dioxide crystal structure of pore-trap vacancies, which capture atoms of the gaseous fission products and so prevent them from leaving the fuel. The mechanism of this process is investigated in [2, 3]. If there is no columnar crystal zone in the fuel element, then gas evolution must be constant (curve 1). Gas evolution in fuel elements having only a columnar crystal zone must change suddenly at the instant the reactor comes on load and thereafter remains constant (curve II). If both characteristic zones are present in the fuel element, then gas evolution will show the features of both the extreme cases (curve III).

In order to test the proposed model experimentally, a method of direct measurement of the quantity of

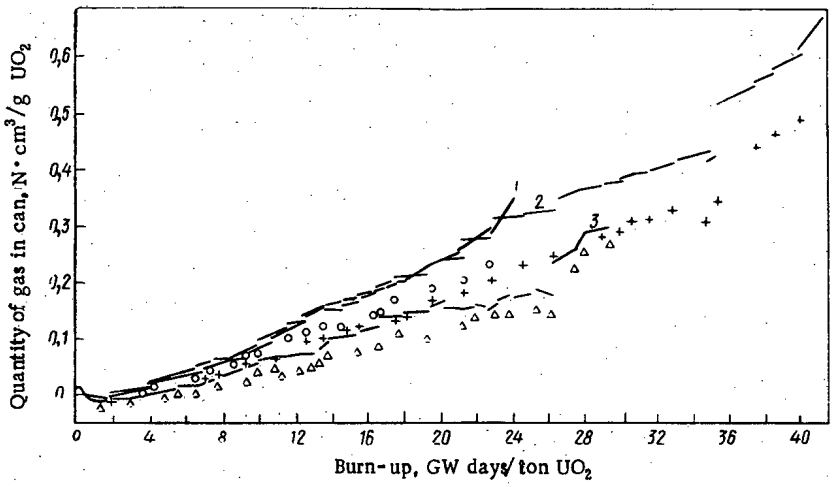

Fig. 3. Characteristics of gas evolution in fuel elements type GD: 1-3) pressure in can, measured at rated power; ○, +, Δ) ditto, at no load for fuel elements types GD-122, 125, and 115, respectively.

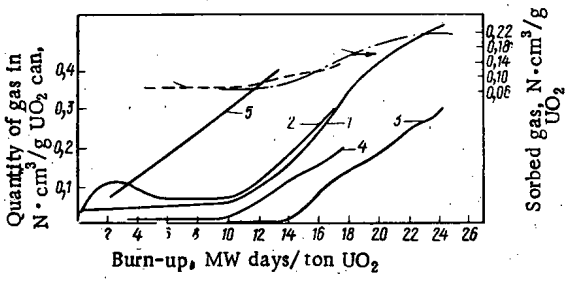

Fig.4

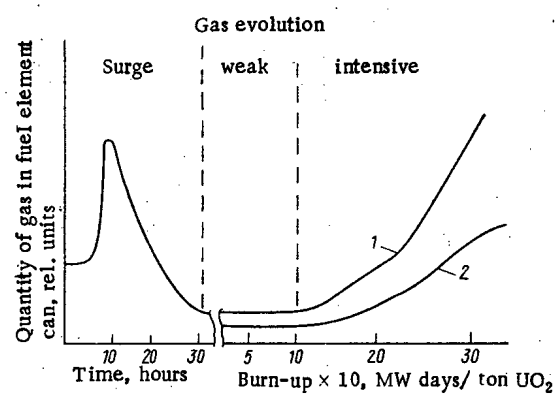

Fig.5

Fig. 4. Characteristics of gas evolution in fuel elements type D: 1, 2) pressure in can measured at rated load for fuel elements types D-7 and 6 respectively; 3, 4) ditto, at no load; 5) evolution of gaseous fission products in dioxide; —·—·—, - - - -) quantity of gas sorbed in fuel elements types D-7 and 6, respectively.

Fig. 5. Variation of the quantity of gaseous fission products in a fuel element can during irradiation: 1) with the fuel element in operation; 2) with the reactor shut down.

gaseous fission products during irradiation of the fuel elements was developed. This enables us not only to verify in general terms the picture of the gas evolution mechanism that is at work, but also to detect some new features of the process, such as an initial surge of gas evolution, absorption of gaseous fission products in uranium dioxide, and sorption of the gaseous fission products when the reactor is shut down.

Arrangement of Experiments. The kinetics of gas evolution were studied on two series of fuel elements: one having a columnar crystal zone (series GD) and one without it (series D).

The fuel elements of series GD were irradiated in a water loop of a type SM-2 reactor; the series D elements were irradiated in an ampoule channel [4] (Table 1). The thermal and physical parameters of the fuel elements did not remain constant from run to run; therefore, Table 2 gives the characteristics of the most typical conditions.

All the fuel elements were equipped with means for measuring the quantity of gaseous fission products evolved from the fuel, the results of the measurements being little affected by the temperature of the fuel in the element [4, 5]. The summation error in determining the quantity of gas did not exceed ± 8% over all the experiments.

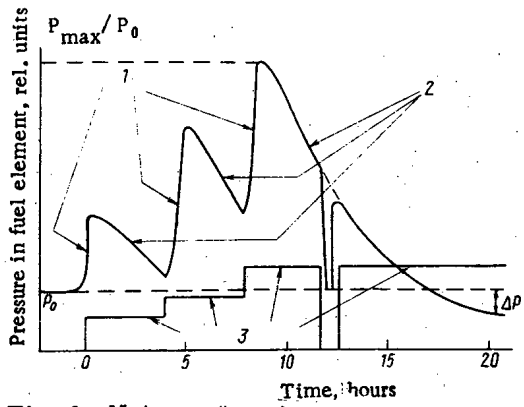

Fig. 6. Nature of variation of pressure within a fuel element during a surge: 1) leading front; 2) trailing front; 3) reactor power.

Experimental Results. Figures 3 and 4 show the variation in the amount of gaseous fission products in fuel elements series GD and D for various durations of irradiation. A fuel-element type GD-122 was removed from the reactor after 165 effective days so that the structure of its cross section could be examined (see Fig. 1). Figure 3 shows the pressure measured with the reactor shut down. It was considerably lower than when the reactor was operating, a fact which cannot be fully explained by the lower gas temperature. A reduction occurred in the quantity of gas inside the can, linked, in our opinion, with absorption by cooled uranium dioxide.

A sudden increase in the pressure within the can during increases in reactor load after a shut-down is characteristic of series-GD fuel elements having a columnar crystal zone (see fig. 3). In the case of series-D fuel elements, which do not have a columnar crystal zone, a uniform pressure in the can prior to shut-down and after start-up of the reactor is characteristic (see Fig. 4).

Discussion of Results. Analysis of the evolution of gaseous fission products from uranium dioxide during irradiation can best be carried out on the basis of a generalized curve of the kinetics of gas evolution (Fig. 5), in which it is possible to identify the sections of initial surge evolution, weak evolution, and intensive evolution. The evolution of gaseous fission products averaged over the series of runs is used in the case of fuel elements of series GD.

It is characteristic of all fuel elements that a sharp surge in pressure accompanies the first increase in power (Fig. 6). The duration of the reduction in pressure depends on a number of factors, but the surge does not usually appear on the scale of the abscissas of Figs. 3 and 4, as it lasts for some hours.

The difference between the pressures before and after the surge ($\Delta P = P_{init} - P_{fin}$) is basically determined by the initial gas medium in the fuel element. If the fuel element was filled with air at atmospheric pressure, then a vacuum of the order of 10 to 20 mm Hg is formed at the end of the surge. If the fuel element is filled with helium at 1 to 3 atm, ΔP will be less than it would be if the filling was air. If the fuel element is filled with argon, ΔP will be less, but the duration of the pressure surge will be greater.

When the fuel element is filled with an inert gas at a pressure of not less than 5 atm, the pressures before and after the surge will be practically the same.

The variation in the quantity of the gases within the can due to the pressure surge is caused by desorption at the surfaces of the heated uranium dioxide of gases that have accumulated during the processing and storage of the fuel. This is confirmed by the fact that the curve of pressure growth during the surge can be satisfactorily described by the relationship $P - P_{init} = P_{max} \exp(-E/RT)$ ($E = 5000$ to 8000 cal/mole). The subsequent absorption of these gases apparently follows from chemical interactions between the evolved gases and the incandescent uranium dioxide.

The boundary of the section of weak gas evolution for fuel elements which do not have a columnar crystal zone (see Fig. 5) corresponds to a burn-up of 10 GW·days/ton UO_2. For fuel elements having columnar crystal zones, gas evolution commences after the first period of continuous operation of the reactor at shut-down and during subsequent load shedding. However, in these fuel elements, as calculations show, the gasses are not evolved from the equiaxial grain zone over a period of time. Gas evolution only commences in this zone at a particular time.

We have calculated the accumulation of gaseous fission products in the equiaxial zone on the basis of experimental data, up to the moment when intensive evolution commences. In the case of fuel elements without a columnar crystal zone, the accumulation comprises ~ 0.3 $N \cdot cm^3/g\ UO_2$.

It is difficult to calculate the accumulation of gaseous fission products in fuel elements with columnar crystal zones as there is an appreciable nonuniformity of specific energy evolution with respect to the radius of the fuel element, which varies with enrichment, as this has an effect on the temperature distribution throughout the fuel, on the magnitude of the equiaxial grain zone, and on the quantity of gaseous fission products evolved. However, by estimating the accumulation of gaseous fission products in fuel elements with columnar crystal zones, we find that this will again be in the vicinity of 0.3 $N \cdot cm^3/g\ UO_2$. Consequently, the evolution of gases from the equiaxial zone remains significant after the accumulation of gaseous fission products to a level of ~ 0.3 $N \cdot cm^3/g\ UO_2$. We should note that over the section of curve with low gas evolution, the quantity of gases within the can is determined basically by quantity of gases that remain after the end of surge. Therefore, rarification can occur within the fuel element in a number of cases.

Intensive gas evolution in fuel elements without columnar crystal zones is linked with evolution of gaseous fission products from the equiaxial grain zone, while for fuel elements that do have columnar crystal zones, it is linked with the structural reformation process (provided the accumulation of gaseous fission products in the equiaxial grain zone is less than ~ 0.3 $N \cdot cm^3/g\ UO_2$) or with the combined action of reformation and evolution of gaseous fission products from the equiaxial grain zone (if the accumulation in this zone has reached a level of ~ 0.3 $N \cdot cm^3/g\ UO_2$). Data about the evolution of gaseous fission products from the equiaxial grain zone is in satisfactory accord with calculations carried out according to the following scheme. Every zone is divided by radius into an annular volume of thickness $2a$, where a is the radius of an equivalent sphere which depends upon the initial density [6]. The fuel temperature and specific density of energy evolution are taken to be constant for each annular volume. The quantity of stable gaseous fission products evolved from the fuel during a period of irradiation τ can be calculated by solving the diffusion equation for the sphere.

$$\partial N/\partial\tau = D\,\Delta N + fY, \tag{1}$$

where N is the number of atoms of gaseous fission products in the solid body, atoms/cm^3; D is the diffusion coefficient, cm^2/sec; f is the rate of fission of ^{235}U, nuclei/($cm^3 \cdot$ sec); Y is the summation evolution of stable gaseous fission products for each fission event.

The solution of this equation for initial condition [N(r, 0) = 0] and boundary condition [N(a, τ) = 0] for the number of gaseous fission product atoms found in the solid body (N') and volume V takes the form

$$N' = fY\tau VF, \tag{2}$$

where F characterizes that portion of the final concentration of atoms evolved from the sphere:

$$F = 1 - \frac{6a^2}{90D\tau} + \frac{6a^2}{\pi^4 D\tau}\sum_{n=1}^{\infty}\frac{1}{n^4}\exp\left(-\frac{n^2\pi^2 D\tau}{a^2}\right). \tag{3}$$

The coefficient can be determined from the expression

$$D = 1.65\cdot 10^{-6}\exp\left(-\frac{70000}{RT}\right). \tag{4}$$

The referred diffusion coefficient $D' = D/a^2$ increases with increase in burn-up, due to the reduction in a. The relative radius of the equivalent sphere (a/a_{init}) is 1.0, 0.45, 0.31, and 0.22 at burn-ups of 10, 20, 30, and 40 GW·days/ton UO_2, respectively.

This variation in a can be calculated from the increase in the surface of the fuel accompanying the increase in sorption of gaseous fission products due to the increase in burn-up, this being observed in experiments when the reactor is shut down (see Figs. 3 and 4). The quantity of sorbed gases can be determined from the difference between the quantity of gaseous fission products inside the can, measured when the reactor is operating and when it is shut down. It is clear from Figs. 3 and 4 that the quantity of sorbed gases varies little at first, and then rises considerably. This indicates an increase in the sorption surface of the fuel in the equiaxial grain and columnar crystal zones when the reactor is shut down.

CONCLUSIONS

We have examined the basic laws governing the character of gas evolution and the behavior of uranium dioxide during the operation of a fuel element prior to thorough burn-up. The behavior of the uranium dioxide

and the evolution of gases depend directly on the distributions of energy evolution and temperature with respect to radius in the fuel element, and on the process of structure formation and burn-up in the different zones of the fuel. The evolution of gases from uranium dioxide during irradiation can be estimated on the assumption that all the gaseous fission products evolve from the columnar crystal zone and that evolution of gases from the equiaxial grain zone takes place by a mechanism of thermally activated diffusion.

Sorption of gaseous fission products at the surface of the fuel can lead to errors in determining the quantity of gaseous fission products evolved from the uranium dioxide during postreactor determination by the fuel-can puncture method.

LITERATURE CITED

1. B. V. Samsonov et al., preprint NIIAR II-177, Dimitrovgrad (1972).
2. B. V. Samsonov and A. K. Frei, At. Énerg., 30, No. 4, 358 (1971).
3. B. V. Samsonov and A. K. Frei, At. Énerg., 31, No. 2, 136 (1971).
4. V. A. Tsykanov and B. V. Samsonov, The Technique of Irradiating Materials in Reactors at High Neutron Fluxes [in Russian], Atomizdat, Moscow (1973).
5. B. V. Samsonov, G. P. Lobanov, and V. V. Sidorov, Byull. Izobret. i Tov. Zn., No. 41, 48 (1974).
6. B. Lastman, Radiation Phenomena in Uranium Dioxide [in Russian], Atomizdat, Moscow (1964).

SPUTTERING OF THIN FILMS OF URANOUS – URANIC OXIDE UNDER THE INFLUENCE OF FISSION FRAGMENTS AT LOW IRRADIATION DOSES

V. A. Bessonov, G. P. Ivanov,
N. A. Grinevich, and E. A. Borisov

UDC 539.211:546.79

It is generally accepted that thin uranium-containing layers are sputtered in a neutron flux by tearing pieces of the material from a surface [1-4]. At a temperature of 10^4°C on the track and a density of 11 g/cm^3 of the material, the torn-off conglomerates can reach a length of 40 Å [5].

Observations made with an electron microscope have shown that by sputtering irradiated thin, 40–400-Å-thick UO_2 films and samples of metallic uranium in neutron fluxes exceeding 10^{14} neutrons/cm^2, particles in the form of "islands" or spots with linear dimensions of up to 400 Å can be precipitated on a collector. These "islands" of material contain about 10^4 uranium atoms [1, 3].

When accumulations of sputtered material were analyzed with the track detector technique [4], pieces of material appearing on the track detector as "stars" were detected. The authors assumed that the "stars" were formed by secondary irradiation of the pieces of the material which were observed under the electron microscope [1]. Sputtered thin films of uranium oxides had the form of conglomerates of large size (up to 10^9 atoms in a piece) [6].

Kaminsky and Das [7] have observed the sputtering of a niobium surface; large conglomerates containing as many as 10^{11} atoms were formed under the influence of 14-MeV neutrons. But other authors [8] could not detect a sputtering of the surface of certain metals under the influence of fission fragments nor the formation of conglomerates with a size greater than 1000 Å. It is possible that the formation of the conglomerates in the experiments made by Rogers results from the irradiation-induced redistribution of the sputtered material on the collector surface [9]. Furthermore, it is unclear how the sputtering of conglomerates depends upon the surface under inspection (metal–nonmetal).

The possibility of sputtering uranium-containing materials and pure metals by fission fragments (large

Translated from Atomnaya Énergiya, Vol. 40, No. 5, pp. 395-398, May, 1976. Original article submitted July 1, 1975.

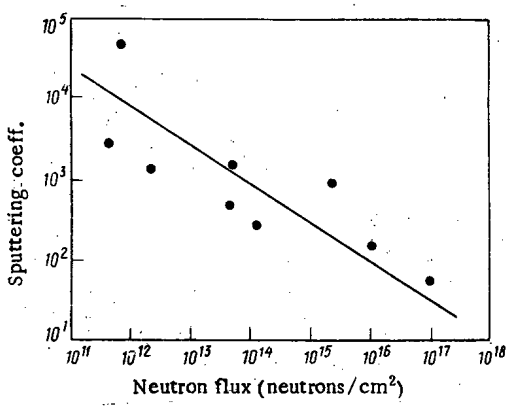

Fig. 1. Dependence of the sputtering coefficient (^{235}U atoms per fragment) upon the neutron flux.

conglomerates torn from the surface) was not clearly established. Investigations of the effect are certainly of interest.

The present article reports on an investigation of surface sputtering under the influence of fission fragments; solid-state track detectors were employed. A thin film of uranous–uranic oxide enriched with ^{235}U was inserted into the setup consisting of an emitter (thin uranous–uranic oxide film with a thickness of 4 mg/cm^2 on aluminum foil) and a collector (aluminum disk with a diameter of 10 mm); the emitter was separated from the collector by a 0.5-mm-thick diaphragm with an internal diameter of 3.5 mm. The setup with the quartz tube was evacuated to high vacuum and irradiated in a VVRTs reactor. After irradiation, the collector was withdrawn from the setup, brought into contact with a glass plate, and irradiated again in the reactor with a neutron flux of 10^{12}–10^{15} neutrons/cm^2. After etching in 1.4% hydrofluoric acid solution, the glass detectors were inspected under an optical microscope and photographed. Before the secondary irradiation, the concentration of uranium on the collectors was determined from the alpha activity with the aid of a semiconductor alpha detector and the "Amur" instrument set.

The sensitivity of the solid-state track detector technique amounted to 10^{-12} g for uniformly distributed uranium atoms; the "Amur" instrument set had a sensitivity of 10^{-9} g uranium.

In order to determine the dependence of the sputtering coefficient upon the neutron flux, the emitter–collector assemblies were irradiated in a reactor with various integral doses of thermal neutrons. After that, the uranium concentration on the collectors was determined with the above methods and the coefficient of ejection was calculated with the well-known equations of [10].

At low irradiation doses, the sputtering coefficient can reach several thousand uranium atoms per fragment (Fig. 1). An analogous overall dependence of the sputtering coefficient upon the dose has been described in [11, 12], though the neutron flux exceeded 10^{14} neutrons/cm^2.

Since particularly at low irradiation doses the highest sputtering coefficients were observed, it was logical to assume that the increase is related to the initial state of the surface of the layer subjected to sputtering [13]. In the initial moments of irradiation, substantial changes can occur in the surface layer, because when the irradiation with neutrons and the bombardment of the layer with fission fragments leaving the uranous–uranic oxide sample begin, stresses can be generated on the surface sections through which the fission fragments pass; protruding pieces, "islands," can be torn off if they are located in the zone in which the track of a fission fragment is effective; and sections which are not very well joined with the base layer can be destroyed.

A surface which had not been initially prepared was subjected to sputtering, i.e., a surface which had not been ground, polished, or modified with some other operation for leveling and smoothing the surface. When a cross section profile of such a uranous–uranic oxide layer was inspected with an optical microscope, many coarse irregularities, pits, and protrusions could be recognized on the sample surface. Therefore, the fact that pieces containing a large number of uranium atoms are torn from the emitter at the beginning of emitter irradiation can be one of the reasons for the noticeable increase in the coefficient of ejection. The high sensitivity of the track detectors and observations of the distribution of the material precipitated on the collector made it possible to follow the changes in the uranium precipitation process while the flux of the irradiating neutrons was increased.

Some characteristic formations which could be recognized on the collectors with solid-state track detectors are shown in Fig. 2. At a neutron flux of 10^{12}–10^{14} neutrons/cm^2, pieces which on the track detector are visible as dense "stars" with a size of 30–50 μ (Fig. 2a and b) are present on the collector surface.

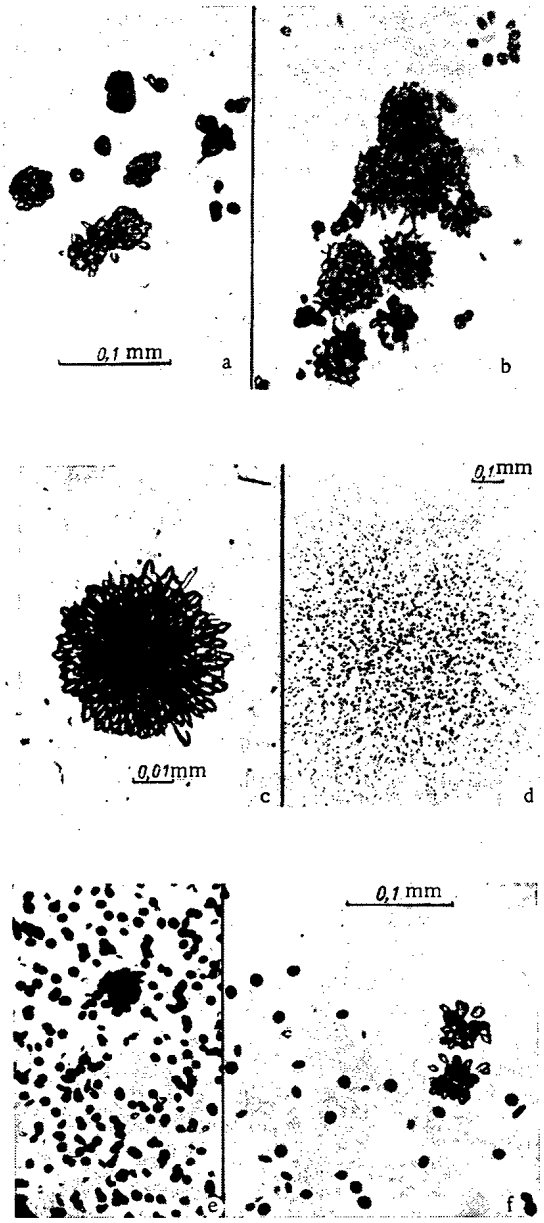

Fig. 2. "Stars" on the detector surface in the case of primary (emitter–collector) and secondary (collector–detector) irradiation (neutrons/cm^2): a) 10^{11}, 10^{14}; b) 10^{13}, $6 \cdot 10^{12}$; c) $\sim 10^{13}$, 10^{14}; d) 10^{13}, 10^{14} (large "dissected star"; distance between the collector and the detector 0.5 mm); e) 10^{16}, $6 \cdot 10^{13}$; f) 10^{16}, $6 \cdot 10^{12}$, respectively.

Both the size of a "star" on a detector and the track density in the detector depend upon the dose of the secondary irradiation and the amount of material in the piece precipitated on the collector. In the case of a secondary irradiation with a neutron flux of 10^{15} neutrons/cm^2, pieces, each of which contains less than 10^6 uranium atoms, give one or two fragments leaving on the side of the detector. When such a detector is analyzed, one cannot detect an accumulation of uranium atoms on the collector, because the entire field of the detector is uniformly covered with individual tracks. "Stars" can be obtained only from pieces containing at least 10^7–10^8 uranium atoms.

When the size of "stars" was estimated, pieces which on the collector had linear dimensions of less than the range of the fission fragments in the particular material (several microns) were considered as point sources. The critical angle of incidence was assumed as 35° for glass [14]; the track diameter after etching was assumed to be 7-9 μ. It is possible to show for these conditions that pieces of the material on the collectors must result in "stars" with a diameter between 30 and 40 μ on the track detector. When the distance between the collector and the detector is increased to several dozen or more microns, the tracks in the glass of the detector appear as "porous (dissected) stars." When the collector with a detector spaced 0.5 mm from it was irradiated for a second time, images of the uranium pieces were obtained in the form of "dissected stars" (see Figs. 2c and d). "Stars" of large diameter and with dissected structure can also result from a collector or detector surface which is contaminated by occasional aerosol particles containing uranium (Fig. 3) or can be found after irradi-

Fig. 3. "Dissected" background "stars" obtained upon irradiating a track detector of glass which was in contact with a collector of pure aluminum; thermal neutron flux ~ 10^{14} neutrons/cm^2.

ating collectors containing large pieces of the material (10^9 or more ^{235}U atoms) with small doses (<10^{12} neutrons/cm^2). The number of tracks in the form of prongs can be easily estimated in a "dissected star." Calculations have shown that the "stars" can be formed by pieces having a diameter of ~ 2000 Å, which contain up to 10^9 uranium atoms and, in certain cases, up to 10^{11} uranium atoms at a diameter of several thousand angstroms.

It should be noted that in [4] the dose of the secondary irradiation of the collector, which was in contact with a detector, amounted to 10^{14} neutrons/cm^2 and less. Therefore, one could expect the appearance of dense "stars" with the dimensions indicated. Conglomerates containing ~ 10^4 atoms cannot cause "stars" under these conditions.

The α activity of the collectors was measured with the "Amur" set of instruments and was much greater than the α activity obtained by counting individual tracks. At low doses, the field of the detectors is practically free of individual tracks. This indicates that the sputtering of the surface of uranous–uranic oxide occurs in the initial stages of irradiation mainly by breaking off pieces of the material.

When the irradiation dose increases, the distribution of the material on the collector changes. The field of the collector is covered with a uniform layer of sputtered uranium; the number of the "stars" on the detector decreases and almost reaches zero at a neutron flux of the order of 10^{16}–10^{17} neutrons/cm^2. Individual "stars" are found on the collector boundary where the diaphragm protects the surface from the direct fission fragments leaving the emitter (see Fig. 2e and f).

The decrease in the number of "stars" on the detector and, accordingly, the disappearance of large (>10^6 atoms) pieces from the collector surface can be related to the destruction of the pieces under the influence of the flux of fission fragments flying from the emitter and developing within the pieces under the influence of the neutron irradiation; the decrease in the number of "stars" and the disappearance of large pieces can also be related to a decrease in the number of pieces torn away from the emitter when the homogeneity increases and the surface roughness of the emitter is reduced. Examples are known in which the surface of a metal was polished by bombardment with α particles [15]; a dependence of sputtering coefficient upon the microrelief of the surface [16] was observed when thin films of curium were sputtered.

We may assume that at sufficiently high neutron flux densities, a certain equilibrium between the number of large pieces recently precipitated on the collector and the number of pieces destroyed by the flux of fission fragments is established. Similar conclusions were drawn in [17, 18] when the decrease in the size of crystallites in the surface layers of uranium oxide and in thin polycrystalline metal films subjected to a flux of fission fragments was interpreted.

LITERATURE CITED

1. M. Rogers, J. Nucl. Mater., 15, 65 (1965).
2. J. Bierlein and B. Mastel, J. Appl. Phys., 35, 2188 (1964).
3. O. Gautsch and E. Ruedl, J. Nucl. Mater., 3v, 290 (1964).
4. K. Verghese and R. Piascik, J. Appl. Phys., 40, No. 4 (1969).
5. A. Whapham and M. Makin, Phil. Mag., No. 7, 1441 (1962).
6. J. Biersack, D. Finik, and P. Mertens, J. Nucl. Mater., 53, 194 (1974).
7. M. Kaminsky and S. Das, J. Nucl. Mater., 53, 162 (1974).
8. T. Blewitt et al., J. Nucl. Mater., 53, 184 (1974).
9. T. Bierlein and B. Mastel, J. Nucl. Mater., No. 7, 32 (1962).

10. M. Rogers and J. Adam, J. Nucl. Mater., 6, 182 (1962).
11. M. Rogers, J. Nucl. Mater., 22, 103 (1967).
12. P. Peterson and M. Thorpe, Nucl. Sci. and Eng., 29, 425 (1967).
13. V. A. Bessonov, At. Énerg., 37, No. 1, 52 (1974).
14. H. Khan and S. Durrani, Nucl. Instrum. and Methods, 98, No. 2, 229 (1972).
15. N. Riehl, Kerntechnik, 3, No. 12, 518 (1961).
16. V. K. Gorshkov and P. A. Petrov, At. Énerg., 30, No. 1, 49 (1971).
17. M. Rogers, J. Nucl. Mater., 16, 298 (1965).
18. A. Goland, in: Studies in Radiation Effects, D. Dienes (editor), Ser. A., Phys. and Chem., Vol. 1 (1966), p. 159.

REVIEWS

RADIATION DEFECTS IN GRAPHITE

T. N. Shurshakova, Yu. S. Virgil'ev, and I. P. Kalyagina

UDC 621.039:532.21

The extensive utilization of graphite in nuclear technology makes it necessary to study the behavior of graphite under the influence of neutron irradiation. The various defects which develop in graphite substantially influence its basic properties, particularly at temperatures below 300°C. Therefore, graphite is periodically restored by annealing in reactors having a low temperature of operation [1].

Despite a large number of publications, to date a reliable model of the radiation defects in graphite has not been developed, because the type of the defects depends not only upon the conditions of irradiation (temperature, dose accumulated, and intensity of the damaging flux) but also upon the structure of the carbon materials. Investigations of the radiation damage (nature of the defects, their number and activation energies) are important from the viewpoints of theory and practical applications.

Electron microscopy is used to study defects in graphite single crystals and in carbonic materials having

TABLE 1. Activation Energy (eV) for the Formation and Movement of Point Defects in Graphite [2, 3]

Type of defect	Formation		Movement	
	expt.	theor.	expt.	theor.
Vacancy	>6,6 7,3±1 2,4—4,2	10,7	3,0±0,5 5,45±0,05	4
Double vacancy	—	~7	—	—
Interstitial C atom	6,75±0,4	9,76 9,90	0,45±0,05 2,8±0,2	0,140 0,016
Vacancy + interstitial atom	11,5±2 neutrons 36,5 neutrons	—	—	—
C–C	—	—	0,9±0,1	—

Remark. The activation energy on the base plane is indicated in the numerator; the activation energy in perpendicular direction is indicated in the denominator.

Translated from Atomnaya Énergiya, Vol. 40, No. 5, pp. 399-408, May, 1976. Original article submitted January 24, 1975.

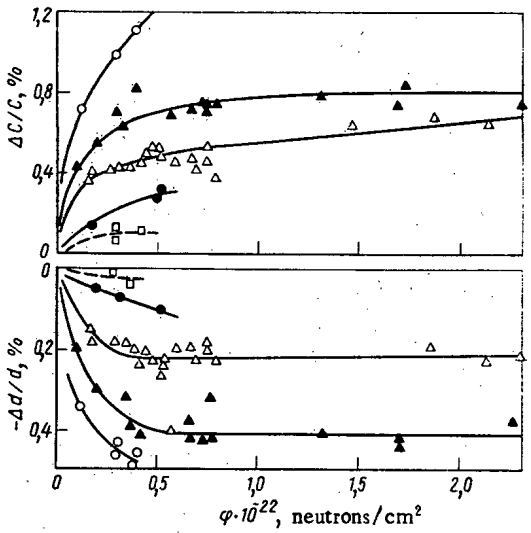

Fig. 1. Dependence of the relative change in the parameters of the crystal lattice of graphite [2] upon the accumulated dose at various temperatures (°C) : ○) 300; ▲) 350–440; △) 450–600; ●) 650; □) 900–1350.

a high degree of perfection of the crystal lattice. When radiation defects are studied in polycrystalline graphite, the structure-dependent properties are restored by thermal annealing and radiative annealing.

We discuss below papers describing research on radiation defects in synthetic graphite materials, among them materials which were intensively irradiated. When the relation between the defects and the changes in the properties of graphite during its irradiation is to be analyzed, a systematic order must be established in the publications in regard to the influence of the radiation defects upon the various properties of the graphite in the light of the present concepts concerning the mechanism of radiation-induced damage to materials.

At the present time, most of the authors assume that neutron irradiation creates point defects, vacancies, and interstitial atoms in the structure of graphite. The equilibrium concentration of these defects depends upon the intensity of the damaging flux, the time and the temperature of irradiation, etc. The resulting defects do not exist in isolated form. Under certain conditions the defects interact and reduce the internal energy of the crystal. It was theoretically calculated that the energy of migration of isolated atoms amounts to ~ 0.016 eV [4] and, according to recent data [3], to 0.14 eV. The corresponding value for vacancies is 4 eV (see Table 1). The high mobility of the interstitial atoms causes them to associate into C_2 and C_3 pseudomolecules at 78°K [4]. At temperatures in excess of 110°K, the molecules form $(C_2)_n$ accumulations. Since the $(C_2)_2$ molecules disintegrate into the simpler components C_2 and since the latter migrate, a peak appears at a temperature of ~200°C on the curve representing the liberation of the stored energy during annealing.

Accumulations of 2–4 interstitial atoms [5] were detected (by scattering of slow neutrons) in graphite which had been irradiated at ~ 30°C. The size of the accumulations increases at this irradiation temperature with increasing dose and, finally, saturation is reached. The size of the accumulations and the distances between them increase in the interval 30–600°C with the temperature of irradiation [6, 7].

After irradiation with $(0.6–6.0) \cdot 10^{20}$ neutrons/ cm^2 at 350°C or higher temperatures, the accumulations have a size of 30–40 Å and reach 200 Å upon irradiation at ~ 650°C. It was assumed [4] that when the dimensions of the molecular accumulations increase, the accumulations can transform into hexagonal structures. These are basically new atomic planes formed by condensation of molecules. The binding energy in such a complex is obviously equal to the sublimation energy of 7.4 eV [3]. At temperatures in excess of 1000°C, the atoms of the new planes interact with free vacancies and, hence, the new planes disappear. Vacancies which are formed during irradiation usually remain isolated and are hardly mobile at temperatures of up to 350°C; but when the temperature is increased further, the vacancies become mobile [7] and condense into stable accumulations corresponding to the removal of a part of an atomic plane [8]. These structural disturbances can be destroyed only by self-diffusion processes having an activation energy of 7–8 eV [3].

It is also assumed that the form of the defects depends upon the degree of perfection of the crystal structure in carbonic materials [2]. However, there exist no methods of directly observing the defects in materials having a low degree of perfection of the crystal structure. In materials having a high degree of perfection of the crystal structure, the type of admixtures and their amounts noticeably influence the damage to the structure [9]. The degree of radiation-induced damage is a function of the following three variables: intensity of the damaging flux, and time and temperature of irradiation [10]. A 100-fold increase in the intensity of irradiation is equivalent to a noticeable reduction of the irradiation temperature.

Irradiation of graphite results in the accumulation of radiation-induced defects and, hence, in a distortion of the crystal lattice. At low irradiation temperatures, the spacing c of the planes in axial direction increases (Fig. 1) owing to isolated point defects and small groups of them [11, 12]; at the same time a compression takes place on the base plane.

An empirical formula [14]

$$r = 1.034 + \frac{0.51}{n} \tag{1}$$

can be used to describe the dependence which was observed in some investigations [13] between the order n of binding (number of electron pairs participating in the chemical bond) and the length of the C—C bond.

The authors of [14] have considered the possible positions of the shifted atoms and vacancies in the crystal lattice of graphite and have analyzed the variation of n in the above formula; the conclusion was that the expansion of the lattice parallel to the c axis and the compression on the base plane are caused by vacancies. However, since the calculations are not in a satisfactory quantitative agreement with the experimental results, defects in the form of interstitial atoms must noticeably contribute to the expansion of the lattice in the direction of the c axis.

The reduced increase in the parameter c in graphite upon increasing irradiation doses and temperatures is associated with the coagulation of the interstitial atoms into larger compounds [9]. The broadening of the profile of the diffraction lines upon increasing the irradiation dose means particularly that the size of the regions of coherent scattering decreases because the crystallographic planes are distorted. The crystal structure can become completely amorphous at very high irradiation doses.

The net result of changes in the crystal structure is that the physical properties of the graphite samples are modified.

The changes in the lattice parameters correspond to the changes in the macrodimensions only at low irradiation doses. At neutron fluxes exceeding 10^{20} neutrons/ cm^2, the expansion of a recrystallized pyrolytic graphite sample in the direction of the c axis considerably exceeds the increase in the parameter c. This is explained by the development of the aforementioned molecular accumulations whose dimensions are comparable with the size of the crystallites [15]. Other authors [7] believe that the lack of correspondence results from defects on the boundaries of the crystallites.

A compression of the sample occurs on the base plane. The dependence of the changes in the sample dimensions upon the radiation dose is complicated: The high-temperature setting of any graphite is replaced by a "swelling" which may reach 100% at high irradiation doses. In [16] the changes which occur in the sample dimensions in broad temperature and irradiation dose intervals were explained by the dynamics of both the formation and the transformation of complexes and accumulations. The conclusion was that the secondary "swelling" of graphite is caused by the oriented formation of a vacancy-induced porosity in the lattice.

The mechanical properties are basically determined by point defects. Polycrystalline graphite has increased strength and brittleness after irradiation. Its hardness increases and reaches saturation at a neutron flux density of $7.2 \cdot 10^{18}$ neutrons/ cm^2 ($E \geq 1$ MeV); thereafter the hardness decreases [9]. When graphite is irradiated at temperatures of 56-140°C with a neutron flux density of up to $1 \cdot 10^{20}$ neutrons/ cm^2, the relative increase in the hardness depends linearly upon the absolute value of the neutron flux density; the observed effect decreases exponentially with increasing irradiation temperature [9]. Electron-microscopical investigations of the radiation defects [7] have shown that the hardness reaches its maximum when the average spacing of the defects amounts to 20-50 interatomic distances. When the size of the defects increases further by coagulation, the spacing of the accumulations increases, which results in a decrease in hardness.

In the case of synthetic graphite, the modulus of elasticity of the first kind increases during irradiation. At low temperatures (up to 300°C), the change in the modulus of elasticity is nonmonotonic: A sharp increase at neutron fluxes of $\sim 10^{20}$ neutrons/ cm^2 is followed by a decrease, whereafter the absolute value of the modulus increases again. At temperatures in excess of 300°C, the modulus of elasticity increases gradually; its absolute value stabilizes and is constant at neutron fluxes of up to $1.5 \cdot 10^{22}$ neutrons/cm^2. The increase in the modulus of elasticity is related to dislocation locking [2]. This effect can also be explained by the influence of defects upon the elastic deformation of the lattice. The presence of interstitial atoms can reduce the effective spacing of the layers. But the dislocation mechanism is generally accepted. A decrease in the absolute value of the modulus is explained by changes in the aggregate state of the interstitial atoms during the irradiation process.

The radiation defects in graphite are per se electron traps and create an excess concentration of hole-type charge carriers by reducing the Fermi level in the valence band of graphite. Therefore, when the irradiation dose is increased, the Hall coefficient changes its sign from negative to positive, reaches its maximum, and decreases gradually. Layer defects are per se scattering centers which reduce the mobility of the charge carriers. Since the effect of the reduced mobility is superimposed on the effect of the increased charge carrier concentration, the resistivity of an irradiated sample exceeds the initial resistivity. The diamagnetic susceptibility decreases, because the Fermi level in the valence band is reduced.

Electroparamagnetic resonance studies made it possible to identify the paramagnetic centers with simple types of defects, namely with interstitial atoms and vacancies [17]. Measurements of the electroparamagnetic resonance in pyrolytic carbon [18] have confirmed the assumption that trapped paramagnetic centers are related to interstitial atoms and their simplest complexes of the type $(C_2)_n$ [19]. The relatively low activation energy ($E_{min} \sim 0.5$ eV) of the movement of complexes of interstitial atoms [20] facilitates their annealing at temperatures of up to 1000°C; this is in good agreement with a reduction of the concentration of trapped paramagnetic centers. Nonlocalized paramagnetic centers are associated with vacancies and radiation-induced dislocations which have developed in the layers.

Calculations of the concentration of defects accumulated in pyrolytic graphite (which is identified with a single crystal) are made under the assumption that interestitial atoms and vacancies exist in the form of individual defects, small groups, and, in some number, in the form of loops [21]. These defects change the linear dimensions X_c and X_a because the lattice parameters are modified. The changes can be considered the reason for the anisotropic internal pressure which is proportional to the vacancy concentration C_v and the concentration C_i of interstitial atoms. In this case the formulas for the concentration of defects [22] assume the form

$$C_i = \frac{\Delta C/C + 1.43\Delta a/a}{2.8}, \tag{2}$$

$$C_v = \frac{-21.4\Delta a/a - \Delta C/C}{2.8}. \tag{3}$$

These dependencies are valid only at low temperatures and for low irradiation doses when only point defects and small compounds thereof exist. When both the dose and the temperature of irradiation are increased, the probability of forming large defect accumulations increases and, hence, the modification of the lattice parameters is retarded, whereas the concentration of the defects decreases. The total number of displaced atoms, which was theoretically calculated with the cascade model of Kinchin and Peace, substantially exceeds the defect concentration calculated with formulas (2) and (3) [23]. This means that, during irradiation, an intense annealing of the defects takes place.

It was attempted [14] to explain the observed changes in the parameters and to estimate the defect concentration in irradiated graphite with the aid of the dependence of the carbon atom spacing upon the order of the bond, i.e., $r = f(n)$. It was found with the well-known relations of [22] that in the case of graphite irradiated at temperatures of up to 100°C, $\Delta a/a = -0.4\%$ and $\Delta c/c = 4.6$; the concentrations of vacancies and interstitial atoms are the same and amount to 1.4%. Estimates of the vacancy concentrations from the above dependence render $r = f(n) \sim 1.8\%$ (from $\Delta a/a$) and 3.2% from $\Delta c/c$. The value of 3.2% is evidently too high, because a part of the expansion in c direction can be explained by the influence of complexes of interstital atoms.

The type of defects and their migration energy are usually determined when changes in the physical properties of materials are studied in the course of thermal annealing and radiation-induced annealing.

Defect annealing is defined as the disappearance of defects from a crystal oversaturated with defects, when the crystal is heated above the irradiation temperature at which the defects accumulated.

Radiation-induced annealing takes place under the influence of a second irradiation at an increased temperature. Such a secondary irradiation of graphite containing radiation defects reduces the total damage to the samples to a greater extent than conventional heating to the same new temperature, but without irradiation [24].

In order to determine the defects which were formed in a crystalline material after its irradiation, thermal annealing is usually employed. The extent of annealing and its rate depend upon the mobility of the defects proper. Excess defects can be removed from the crystal basically by redistributing the defects to sinks and by recombination.

The theory of thermal annealing has been well developed [11, 25] but an analysis of the determination of the activation energy with one of the methods indicated [26] is not possible if one of the properties changes nonmonotonically. For example, the microhardness of irradiated pyrolytic graphite first increases upon isothermal

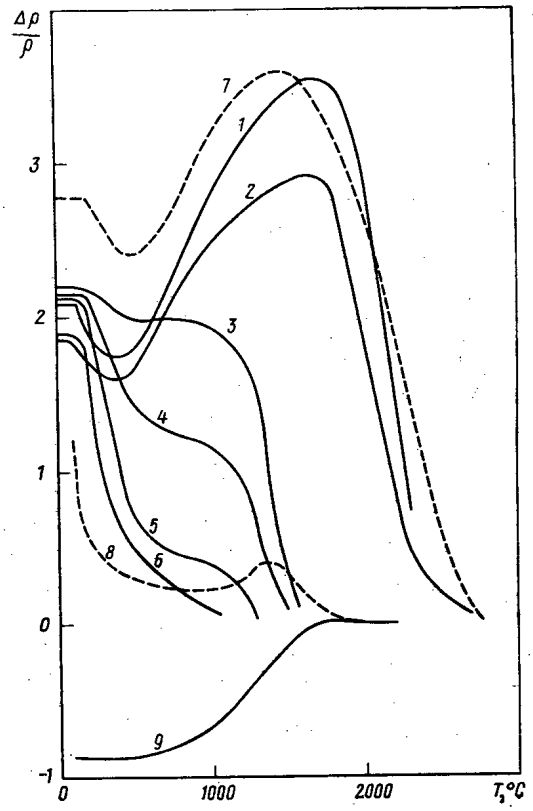

Fig. 2. Dependence of the relative change in the electrical resistivity upon the temperature of annealing: 1-6) Gor' kii Metallurgical Plant graphite irradiated under various conditions with the following doses: $7 \cdot 10^{21}$, $7 \cdot 10^{21}$, $7 \cdot 10^{20}$, $\sim 10^{20}$, $\sim 2 \cdot 10^{19}$, and $\sim 10^{18}$ [32] neutrons/cm^2, respectively; 7) graphite for nuclear applications, $5.42 \cdot 10^{21}$ [30]; 8) WSF graphite, $8.4 \cdot 10^{18}$ [12]; 9) pyrolytic graphite, additionally treated at 2400°C, $9 \cdot 10^{20}$. The samples were initially irradiated at 50-250°C.

annealing and decreases only thereafter to the initial microhardness values [27].

The defects which were accumulated during irradiation become mobile owing to their activation by thermal annealing and undergo further transformations.

Small groups of interstitial atoms were found in electron-microscopical investigations of the annealing processes in thin films of natural graphite crystals which had been irradiated at 50°C [28]. When the temperature of annealing is increased, the groups become larger, but disappear at temperatures in excess of 1700°C. Owing to the condensation of vacancies at 1700°C, loops with a radius of 150 Å appear; the loops grow at 750 Å at 2600°C, but the area of all the loops is constant thereafter. The number of condensed vacancies, which amounted to ~ 0.5% of the total number of atoms, was calculated.

The electron-microscopical investigations of [3] have shown that dislocation loops with a diameter of <50 Å acquire a noticeable mobility at ~ 1000°C, but the motion of large loops is impeded. During annealing at ~ 1500°C, the loops become shorter and disappear completely at 2200°C. The changes in both type and concentration of defects during annealing affect mainly the structural properties of the material.

An analysis of the changes in the half-width of the (002) and (110) lines during thermal annealing of graphite irradiated at low temperatures has shown that the processes which occur upon heating to 1000°C are very intensive. For example, the broadening of the (110) line is reduced by 50% after heating to 2000°C; after that, the rate of annealing is reduced. In order to restore the form of the (002) line to about 50%, annealing at 600°C suffices [9].

Thus, a considerable portion of the lattice distortions is restored even at low temperatures; this is probably explained by an annealing of those distortions which were caused by relatively unstable defects, because the total disappearance of the line broadening is accomplished only at 2500°C.

In the case of PGA graphite which had been irradiated at 200°C with a neutron flux of $3.5 \cdot 10^{20}$ neutrons/cm^2 ($\Delta c/c \approx 4\%$), the recovery of the parameter c takes place at temperatures of up to 650°C but terminates completely only at 1800°C [29].

The recovery of the parameter *a* is insignificant at temperatures of up to ~ 1000°C in the thermal annealing of graphite which had been irradiated at 200°C with a neutron flux of $8.6 \cdot 10^{20}$ neutrons/cm^2. However, the recovery of the parameter terminates at 1800°C. The recovery of the parameter *a* increases the size of the samples on the base plane [29].

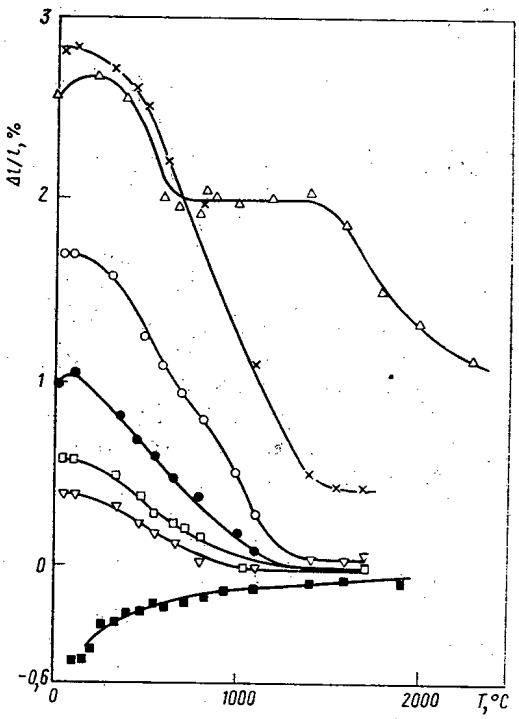

Fig. 3. Restoration of the length of various graphite samples irradiated with the following neutron fluxes (10^{21} neutrons/cm^2) in dependence upon the temperature of the thermal annealing for restoration: ×, ○, ●, □, ▽) 2.18, 1.63, 1.02, 0.11, and 0.46, respectively (CSF graphite, T = 30°C [9]); △) 7 (Gor'kii Metallurgical Plant graphite, T ≈ 100–150°C; ■) 0.9 (pyrolytic graphite, additionally treated at 2400°C; T = 140°C [27]).

The parameters c and *a* are annealed in a wide temperature interval between 200 and 2000°C, but the annealing is most effective at temperatures above ~ 1200°C. This means that groups of vacancies have a stronger influence upon the decrease in the parameter *a* and the size of the samples than individual isolated vacancies.

Annealing of pyrolytic graphite which earlier had been irradiated at 170–200°C with $7 \cdot 10^{19}$ neutrons/cm^2 [18] has shown that the rates at which the susceptibility of localized and nonlocalized paramagnetic centers is restored are not identical. Since localized centers associate with individual interstitial atoms or the simplest complexes of such atoms, their annealing takes place even at 1000°C; this is in good agreement with the reduction of their concentration.

But the excess concentration of nonlocalized paramagnetic centers, which stems from vacancies and dislocation in the defect layer, is completely annealed only at ~ 2000°C.

The change of the Hall coefficient R_x at the beginning of the annealing is small, because numerous positive "holes" are present in the irradiated graphite [30, 31]. The ensuing increase in R_x at increasing temperatures of annealing up to 1300°C is basically associated with the annihilation of traps during the healing of structural damages; the sharp drop of R_x at temperatures above 1400°C can be explained by the influence of conduction electrons which stem from the rapid shift of the Fermi level to the bottom of the unfilled upper band. The competing decrease in the concentration and the increase in the mobility of the charge carriers account for the plateau at temperatures of 700–1000°C. The R_x maximum at ~ 1300°C coincides with the maximum of the electrical resistivity. Such a peak is observed on the R_x curve only in the case of irradiation with high neutron fluxes (~ 10^{20} neutrons/cm^2).

The restoring of the electrical properties is impeded at increasing doses and irradiation temperatures. All radiation defects which cause the increase in the electrical resistivity of graphite are completely removed only at 2400°C.

Interestingly enough, when samples of pyrolytic graphite obtained at 2100°C were irradiated at 140°C, the electrical resistivity was reduced approximately 10 times in the direction perpendicular to the plane of precipitation. When these samples were annealed at temperatures in excess of 800°C (Fig. 2), the electrical resistivity increased and was fully restored at T ≈ 2000°C. Pyrolytic graphite with a structure of greater perfection, which before irradiation had undergone additional annealing at 2400°C [27], had an electrical resistivity which was restored at a lower temperature (1600°C).

Both the rate and the extent to which the dimensions of a sample are restored depend upon the initial structure of the material, the temperature, and the accumulated dose. It was established in [12] that, after low-temperature irradiation (30°C) of CSF graphite (Fig. 3) with a neutron flux of up to 10^{21} neutrons/cm^2, the

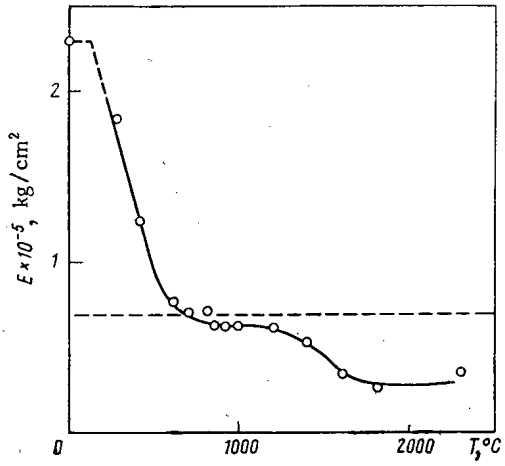

Fig. 4. Influence of the temperature of annealing upon the relative change in the modulus of elasticity of graphite of the Gor'kii Metallurgical Plant, irradiated with a dose of $7 \cdot 10^{21}$ neutrons/cm^2 at 100-150°C.

restoration of the dimensions during thermal annealing practically ended at 1200°C. In the case of samples which had been irradiated with a greater neutron flux ($2.2 \cdot 10^{21}$ neutrons/cm^2), annealing at 1700°C did not suffice for the complete restoration of the initial dimensions (the remaining change amounted to ~ 0.4%).

The work of [33] reported on the thermal annealing of samples of pyrolytic graphite which had been initially irradiated at various temperatures. The irradiation increased the linear dimensions of the sample in the direction of the c axis and caused a compression on the base plane. Annealing below 1000°C implied a slow restoration of the linear dimensions in the direction of the c axis, because small groups of interstitial atoms merged into larger groups which required a smaller volume. At temperatures in excess of 1000°C, the rate of annealing was substantially increased, because the loops of interstitial atoms disappeared (this was established with electron microscopy). The annealing was actually completed at 2000°C.

It was observed at the same time that the dimensions of pyrolytic graphite which had been irradiated at 250°C are restored at temperatures above 1000°C and that the restoration ends much more slowly than after irradiation at 170°C.

The compression of a sample in the direction of the *a* axis is restored at annealing temperatures above 1000°C; this agrees with the results pertaining to graphite single crystals [29]. But the reduction of the dimensions in the direction of the *a* axis during high-temperature irradiation of graphite is not completely restored. It was observed in investigations of the thermal annealing of pyrolytic graphite samples with various degrees of perfection of the crystal structure irradiated at 140°C with a neutron flux of $9 \cdot 10^{20}$ neutrons/cm^2 that the restoration of the sample length is the better the higher the quality of the structure [27]. After annealing at 600°C, the restoration of the sample length of the initial pyrolytic graphite (precipitated at 2100°C) amounted to only 11%, whereas the corresponding value for a sample treated at 2800°C was 23%.

Stronger damage to the crystal lattice of graphite at increasing doses (or reduced irradiation temperatures) helps the defects to become fixed; this is a hindrance to the restoration of the sample length [12, 32].

Two shape-changing processes account for the complicated laws governing the restoration of the sample length [34]. The first process encompasses the generation of defects which can be annealed and which resemble the defects created by low-temperature irradiation. This implies an increase in the sample size X_c of the crystalline regions in the direction of the c axis and a compression of the sample dimension X_a in the direction of the *a* axis.

The second process is a compression which cannot be eliminated by annealing and which reminds one of the ordering of the structure during the development of graphite. It is assumed that this process occurs basically in the less perfect regions of polycrystalline graphite. According to other theories, the compression which cannot be annealed is caused in the course of the irradiation by the development of stable, collapsed vacancy groups or by the loss of vacancies from the crystallites via trapping by an edge dislocation.

At high irradiation temperatures, the changes in the sample dimensions originate mainly (according to the authors of [35]) from the compression which cannot be annealed and which decreases with increasing perfection of the material (e.g., by treating the material at temperatures of up to 3200°C).

A considerable compression, which could not be annealed and which was of the order of 1.9% in the direction perpendicular to the axis of extrusion, was observed in the thermal annealing of PGA graphite which had been

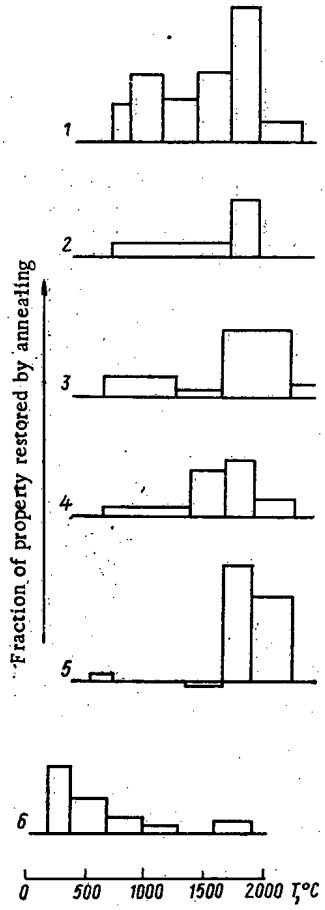

Fig. 5

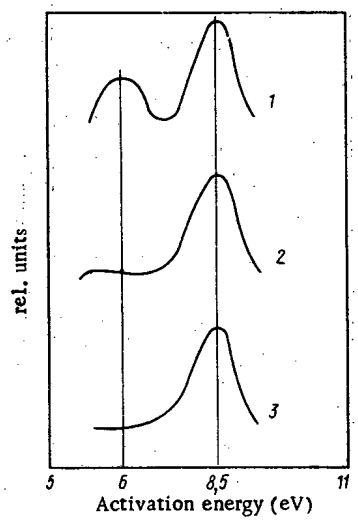

Fig. 6

Fig. 5. Dependence of the degree of restoration of the sample properties upon the temperature of annealing [29, 33, 37]: 1, 2) parameters c and *a*, respectively; 3, 4) length parallel to the c axis and on the base plane, respectively; 5) specific electrical resistivity; 6) modulus of elasticity.

Fig. 6. Distribution of the activation energy during the restoration of the various properties of NC graphite which had been irradiated at 1060°C with a neutron flux of $2 \cdot 10^{21}$ neutrons/cm^2 [46]: 1) interplanar spacing; 2) dimensions of crystallites; 3) specific electrical resistivity.

irradiated in the PLUTO and DIDO reactors. But in the direction parallel to the above axis, the sample dimensions were completely restored.

The restoration of the mechanical properties (strength, modulus of elasticity, and hardness) begins at low temperatures and proceeds intensely up to 1000°C, because individual interstitial atoms or small groups thereof disappear. It was noted in [36] that, after annealing at 2000°C, the modulus of elasticity was 10% smaller than before irradiation in a direction parallel to the axis of extrusion. The results (Fig. 4) indicate that this reduction of the modulus of elasticity is observed after annealing above 1000°C and reaches 40% at 1600°C. A further increase in the temperature of annealing does not modify the value of the modulus of elasticity which can be reached.

Thermal annealing at 900°C [9] reduces the hardness of graphite which had been previously irradiated with a neutron flux of $1.2 \cdot 10^{20}$ neutrons/cm^2; the hardness then comes close to the hardness of the nonirradiated material.

In the isochronous annealing, the microhardness of pyrolytic graphite which had been irradiated at low temperatures (140°C) first increases substantially and only at temperatures above 800°C decreases to the value which is characteristic of the nonirradiated material [27]. This effect reminds one of the increase in the elec-

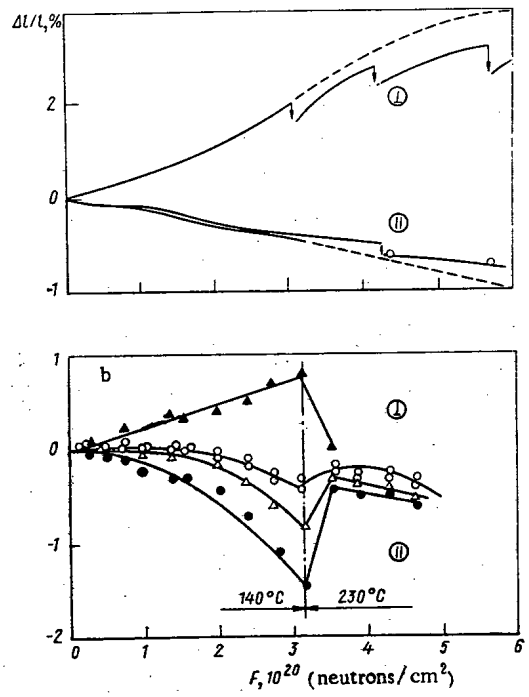

Fig. 7. Dependence of the relative change $\Delta l/l$ of the length upon the accumulated dose: (a) - - - -) irradiation at 150°C; ———) irradiation-induced annealing at 300°C [39]; (b) irradiation at 140°C, dose $8 \cdot 10^{20}$ neutrons/cm^2, radiation-induced annealing at 230°C [27]. Deformation (%): ▲) 5; ○) 10; Δ) 30; and ●) 40.

trical resistivity in isochronous annealing and is explained by the development of simple defects during the decomposition of defects of greater complexity in the course of annealing [27].

The above experimental results are very clearly illustrated by the histograms (Fig. 5) which represent the degree to which the properties are restored at various temperatures of annealing. The histograms were constructed in work on the parameters of the crystal lattice and dimensional changes on the base plane [29], on the electrical resistivity and the modulus of elasticity [37], and on dimensional changes in the direction of the c axis [33]. It follows from the histograms that the modulus of elasticity is almost completely restored at 1000°C, whereas the expansion of the samples and the lattice parameter in the direction of the c axis is only partially restored. In the latter case (Fig. 5a) two clear maxima are observed; the sharpest of the maxima corresponds to the temperature interval 1200-1500°C. This confirms that vacancies and vacancy complexes contribute most significantly to the increase in the parameter c during irradiation [14].

The beginning of an intense restoration of the macrodimensions in the direction of the c axis of samples and the recovery of the electrical resistivity correspond to this temperature interval (Fig. 5, histograms 3 and 5).

The activation energy which was calculated for the annealing of the electrical resistivity of irradiated polycrystalline graphite was 1.27-1.72 eV at 100-800°C; 2.5 eV at 1100-1400°C; and 4.35-5.22 eV at 2400°C [38].

The spectra of the activation energy, which were calculated from the changes in the interplanar spacing, the spectra of the dimensions of the crystallites, and the spectra of the electrical resistivity of isotropic NC graphite irradiated at 1060°C with a neutron flux of $2 \cdot 10^{21}$ neutrons/cm^2 are shown in Fig. 6 [46]. It follows from the data that the restoration of these properties of graphite irradiated at high temperatures with a strong neutron flux is associated with the annealing of extremely stable defects having an activation energy equal to the energy of self-diffusion of the atoms of this material.

As indicated above, radiation-induced annealing increases the rate at which the properties of graphite are restored, because radiation-induced annealing provides additional heat which is obtained from the dissipation of the energy transferred from the neutrons to the carbon atoms.

It was noted in one of the first papers on graphite [12] that subsequent 150°C irradiation of graphite samples which initially had been irradiated at 30°C compensates by 40% for the swelling of the samples. In order to obtain this effect by thermal annealing, the samples would have to be heated to a temperature of several hundred degrees centigrade.

The annealing of PGA graphite samples at 150°C and radiation-induced annealing at 300°C (Fig. 7a) considerably reduced the expansion [39] of the samples, because the reversal of the temperature to 150°C did not imply an expansion of the sample to the earlier value. Therefore the radiation-induced swelling of PGA graphite

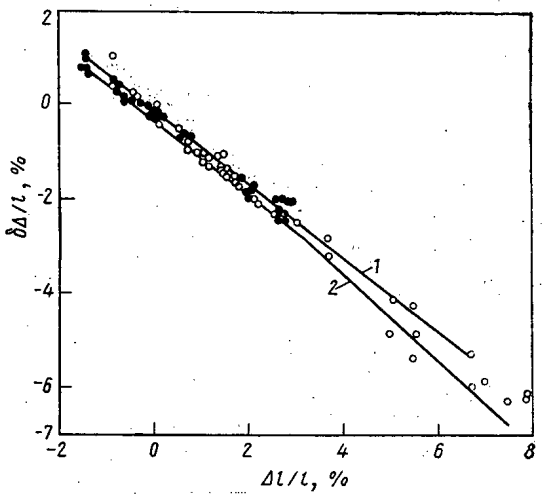

Fig. 8. Restoration of the length of graphite samples during annealing in dependence upon the radiation-induced dimensional changes after an initial irradiation at 140°C: 1) thermal annealing for 2 h at 500°C (●); 2) radiation-induced annealing at 230°C with a neutron flux of $2 \cdot 10^{20}$ neutrons/cm^2 (○).

in radial direction was smaller than that observed in the case of irradiation at a constant temperature of 150°C. The effect was not so significant in the direction parallel to the axis of compression.

In [27] anisotropic graphite samples (the base material was Gor'kii Metallurgical Plant graphite annealed under various deformations of 5-40%) were irradiated at 140°C with a neutron flux of $8 \cdot 10^{20}$ neutrons/cm^2. Then some of the irradiated samples were irradiated at the higher temperature 230°C, whereas some other samples were annealed at 500°C for 2 h (Fig. 7a and b). Obviously, the radiation-induced and the thermal annealing reduced the changes in the dimensions of the samples under inspection: both the expansion and the compression decreased.

In both forms of annealing, the restoration of the dimensions was directly proportional to the previously observed radiation-induced changes in the sample dimensions (Fig. 8). In order to obtain the effect by thermal treatment, annealing at higher temperatures (500°C) than radiation-induced annealing was required.

The total activation energy for the migration of defects during irradiation can be determined from the dependence of the various properties of graphite upon the irradiation dose at several temperatures. Based on the theory of radiation-induced imperfections [40], the authors of [41] derived an equation which describes the dependence of the relative change of the lattice parameter ($\Delta c/c$) upon both dose and temperature of irradiation:

$$\frac{\Delta c}{c} = \frac{bD}{1 + b\beta D}, \tag{4}$$

where $b = b_0 \exp(E/RT)$; $\beta = \beta_0 \exp(-q/RT)$; b_0 and β_0 denote constants; and E and q are the total activation energies for the migration and the formation of accumulations, respectively.

At neutron fluxes $<10^{21}$ neutrons/cm^2, the increase in the lattice parameter stabilizes; then $1 \ll b\beta D$ and Eq. (4) assumes the simplified form:

$$\frac{\Delta c}{c} \approx \frac{1}{\beta} = \beta_0^{-1} \exp(q/RT). \tag{5}$$

It follows from Eq. (5) that the changes of the parameter depend only upon the temperature of irradiation.

When the quantities b and β, which were derived from the experimental curves, are used to construct a curve in ln b (ln β), T^{-1} coordinates, it is possible to determine the total activation energy for the irradiation temperatures of 90-800°C.

A similar approach can be used to analyze the dependencies of other properties of materials upon the irradiation dose (the properties considered are: thermal conductivity [42], electrical resistivity [43], tensile strength in compression and modulus of elasticity [44], and electroparamagnetic resonance [45]). The total activation energies which were obtained are much lower than those calculated from the data for thermal annealing (q = 0.24 and 0.11 eV for the parameters c and a, respectively). This means that during irradiation mainly defects in the form of isolated interstitial atoms and quasi-molecules are in motion.

LITERATURE CITED

1. A. Powell, 2nd Geneva Conference, 1958, Report No. 462.
2. B. Kelly, Radiation-Induced Damage to Solids [Russian translation], Atomizdat, Moscow (1970).
3. W. Reynolds, Physical Properties of Graphite, Elsevier, Amsterdam–London–New York (1968).
4. T. Iwata and H. Suzuki, in: Proc. IAEA Symp. "Radiation Damage in Reactor Materials," Vienna (1963), p. 565.
5. D. Martin and R. Henson, Phil. Mag., 9, 659 (1964).
6. I. F. Pravdyuk, S. G. Konobeevskii, and A. D. Amaev, in: 3rd International Conference on the Peaceful Use of Atomic Energy, 3, 610 (1964).
7. W. Reynolds and P. Thrower, AERE-R-4862 (1965).
8. W. Bollman, Phil. Mag., 5, 621 (1960).
9. S. E. Vyatkin et al., Nuclear Graphite [in Russian], Atomizdat, Moscow (1967).
10. H. Bridge, in: Proc. IAEA Symp. "Radiation Damage in Reactor Materials," Vienna (1963), p. 531.
11. J. Deans and J. Vignard, Radiation-Induced Effects in Solids [Russian translation], Izd-vo Inostr. Lit., Moscow (1960).
12. W. Woods, L. Boop, and J. Fletcher, in: Metallurgy of Nuclear Power Engineering and Effect of Irradiation upon Materials [Russian translation], Metallurgizdat, Moscow (1956), p. 593.
13. S. V. Shulepov, in: Physics of Carbonic Graphite Materials [in Russian], Izd. Chelyabinsk. Gos. Ped. In-ta (1968), p. 13.
14. V. A. Nikolaenko, S. I. Alekseev, and P. A. Platonov, Preprint [in Russian] IAÉ-2124 (1971).
15. J. Simmons, in: Proc. Symp. "Uranium and Graphite," London, No. 11, 7580 (1962).
16. Yu. S. Virgil' ev and I. P. Kalyagina, At. Énerg., 31, No. 5, 497 (1971).
17. J. Hove and I. Mollelland, J. Chem. Phys., 26, 1028 (1957).
18. A. S. Kotosonov et al., in: Construction Materials on the Basis of Graphite [in Russian], Vol. 8, Metallurgiya, Moscow (1974), p. 117.
19. T. Iwata, in: Proc. Symp. on Carbon, Tokyo, Nippon Toshi Center, June 20-23, 1964, Vol. 1, p. 228.
20. H. Harker and J. Horsley, Phil. Mag., 16, 139 (1967).
21. R. Henson and W. Reynolds, Carbon, 3, 277 (1965).
22. B. Gray, J. Brocklehurst, and B. Kelly, in: Proc. IAEA Symp. "Radiation Damage in Reactor Materials," Vienna, June 1969, Vol. 11.
23. P. A. Platonov, V. I. Karpukhin, and O. K. Chugunov, Preprint [in Russian] IAÉ-2266 (1973).
24. H. Fan and K. Lark-Horovitz, The Effects of Radiation on Materials, Rushold (1958).
25. A. Damasque and J. Deans, Point Defects in Metals [Russian translation], Mir, Moscow (1966).
26. V. A. Nikolaenko, V. I. Karpukhin, and S. I. Alekseev, Preprint [in Russian] IAÉ-1094 (1966).
27. Yu. S. Virgil' ev, R. N. Ivanova, and V. G. Makarchenko, in: Construction Materials on the Basis of Graphite [in Russian], Vol. 8, Metallurgiya, Moscow (1974), p. 95.
28. H. Heerschap and P. Delavignette, J. Nucl. Mater., 12, 349 (1964).
29. P. Goggin, Carbon, 1, 189 (1964).
30. T. Tsuzuku and Sh. Arai, J. Appl. Phys., 10, 5 (1971).
31. A. Pacault and A. Marchand, J. Chim. Phys. et Phys. Chim. Biol. (1969).
32. V. I. Klimenkov and Yu. N. Aleksenko, in: Transactions of the Session of the Academy of Sciences of the USSR on the Peaceful Use of Atomic Energy [in Russian], Izd-vo Akad. Nauk SSSR, Moscow (1955), p. 325.
33. B. Kelly et al., in: Proc. 5th Conf. on Carbon, Pergamon Press, New York–London (1962).
34. D. Halas and H. Yoshikawa, in: Proc. 5th Conf. on Carbon, Vol. 1, Pergamon Press, New York–London (1962), p. 249.
35. P. A. Platonov et al., in: Construction Materials on the Basis of Graphite [in Russian], Vol. 8, Metallurgiya (1973), p. 105.
36. B. Kelly, J. Nucl. Mater., 7, 279 (1962).
37. W. Reynolds and J. Simmons, in: Proc. 5th Conf. on Carbon, 1, No. 4, 225, Pergamon Press (1962).
38. D. Bowen, Phys. Rev., 76, 12 (1949).
39. B. Gray, Rep. TR9, 1858 (1968).
40. M. Balarin and O. Hanser, Phys. State Solids, 10, 475 (1965).
41. Yu. S. Virgil' ev, At. Énerg., 30, No. 3, 312 (1971).
42. Yu. S. Virgil' ev and V. G. Makarchenko, Izv. Akad. Nauk SSSR, Neorganicheskie Materialy, 9, No. 10, 1703 (1973).
43. Yu. S. Virgil' ev and V. G. Makarchenko, Izv. Akad. Nauk SSSR, Neorganicheskie Materialy, 9, No. 9, 1546 (1973).

44. Yu. S. Virgil' ev, At. Énerg., 36, No. 6, 479 (1974).
45. A. S. Kotosonov et al., in: Construction Materials on the Basis of Graphite [in Russian], Vol. 6, Metallurgiya, Moscow (1971), p. 77.
46. G. Engle et al., Corros. Abstracts, 58, No. 3, 195 (1971).

ASYMPTOTIC SOLUTION OF A γ-RAY TRANSPORT EQUATION

L. D. Pleshakov

UDC 539.171.015

A kinetic equation is derived that describes the transmission of radiation to large distances; an asymptotic solution is derived, which fully describes the scattered γ-ray spectrum. This solution takes three different forms, which are governed by the relation between the γ-ray energy at the source E_0 and the value of E_{min}, which corresponds to the minimum in the attenuation coefficient $\mu(\lambda)$. The spatial relationships derived here and by U. Fano, J. Res. Nat. Bur. Stds., 51, 95 (1953) coincide for $E_0 > E_{min}$; for $E_0 \approx E_{min}$ they differ somewhat. In the first case, the spatial dependence includes that derived in [1] as a special case.

The spectrum has been determined for cases where $\mu(\lambda)$ may be approximated by an exponential or polynomial of the first, second, or third degrees. These functions have a simple analytical form and can be used without a computer to calculate the spectra at any large distance from the source.

For $E_0 < E_{min}$, when the attenuation coefficient is approximated by the polynomial $\mu(\lambda) = \mu_0 + \mu_1(\lambda - \lambda_0) + \mu_2(\lambda - \lambda_0)^2 + \mu_3(\lambda - \lambda_0)^3$, the energy flux density distribution takes the form

$$I(x, \lambda-\lambda_0) = \frac{\lambda_0^2 b}{\lambda\mu_0} \exp(-\mu_0 x) \frac{(\mu_0 x)^{\frac{\bar{b}}{\mu_1}}}{\Gamma\left(\frac{\bar{b}}{\mu_1}+1\right)} \left[\frac{\mu_1}{\mu_0}(\lambda-\lambda_0)\right]^{\frac{\bar{b}}{\mu_1}-1} \times$$

$$\times \frac{\exp\left\{-\frac{\bar{b}}{\mu_1}\frac{1}{\sqrt{\frac{4\mu_1\mu_3}{\mu_2^2}-1}}\left[\operatorname{arctg}\frac{1+\frac{2\mu_3}{\mu_2}(\lambda-\lambda_0)}{\sqrt{\frac{4\mu_1\mu_3}{\mu_2^2}-1}} - \operatorname{arctg}\frac{1}{\sqrt{\frac{4\mu_1\mu_3}{\mu_2^2}-1}}\right]\right\}}{\left[1+\frac{\mu_2}{\mu_1}(\lambda-\lambda_0)+\frac{\mu_3}{\mu_1}(\lambda-\lambda_0)^2\right]^{\frac{1}{2}\frac{\bar{b}}{\mu_1}+1}},$$

where λ_0 is the γ-ray wavelength at the source, x is the distance from the source, $b = 2\pi r_0^2 n$;, r_0 is the classical electron radius, n is the electron density in the material, $\bar{b}$ is an eigenvalue that determines the γ-ray transmission at large distances, and $\Gamma(x)$ is the γ function.

The spectra given by the analytical solution and by the method of moments show that the analytical solution can be used to calculate a spectrum from distances greater than ten times the mean free path for virtually any medium and for most source γ-ray energies.

(No. 840/8034. Paper received October 1, 1974, abstract December 25, 1975, complete text 0.65 printers sheets, 5 Figs., 8 Refs.).

EFFECTS OF POLARIZATION ON γ-RAY TRANSMISSION BY MATTER

L. D. Pleshakov

UDC 539.171.015

The kinetic equation for γ-ray transmission in matter should incorporate the polarization of the scattered γ rays, since γ rays after Compton scattering are polarized somewhat in a direction perpendicular to the scat-

Translated from Atomnaya Énergiya, Vol. 40. No. 5, pp. 411-417, May, 1976.

tering plane even if not initially polarized [1]. The kinetic equation in matrix form and incorporating the polarization has already been derived [2]; however, no criteria are available for incorporating the polarization. Usually, the effects of the polarization are determined for a given particular case by comparing the results with and without correction for the polarization effects.

Here it is shown that, even in the very simple plane-parallel case with γ rays propagating from an unpolarized source, one needs to solve a system of two coupled integrodifferential equations. If the small-angle approximation applies, the system reduces to the usual kinetic equation neglecting polarization. Consequently, that equation may be solved in the small-angle scattering approximation, and exact solutions obtained by numerical methods (for instance, by the method of moments) will give accuracy no higher than experiment.

We introduce the parameter η, which enables one to judge how far the small-angle scattering approximation is applicable and consequently when one can neglect polarization effects. The value of η may be calculated as a function of Z and for various source energies, which allows one to predict under what conditions the polarization effects will be maximal or minimal. If $\eta \ll 1$ at distances of 10-15 mean free paths from the source, comparison with detailed calculations by Monte Carlo and moment methods shows that the contribution from polarization effects to the radiation transport at any distance from the source does not exceed a few percent.

These results define the lower bound (as regards γ-ray source energy) to the use of small-angle scattering and hence the lower bound to the use of the kinetic equation neglecting polarization effects. Approximately, this bound lies for elements with $Z < 10$ and $10 < Z < 50$ at $E_0 = 0.8$-1.0 and 0.5-0.7 MeV, respectively. For elements with $Z > 50$, the limit lies at a source γ-ray energy such that one can assume that the scattering occurs at free electrons. Below this limit the polarization effects must be incorporated. The maximum contribution from the polarization effects for γ rays at large distances from the source should occur in light media with $Z < 10$ at source energies E_0 of about 100 keV.

LITERATURE CITED

1. V. B. Berestetskii, E. M. Lifshits, and L. P. Pitaevskii, Relativistic Quantum Theory [in Russian], Pt. 1, Nauka, Moscow (1968), p. 398.
2. G. Fano, L. Spencher, and B. Berger, γ-Ray Transport [Russian translation], Gosatomizdat, Moscow (1963).

(No. 841/8416. Paper received July 14, 1975, abstract November 25, 1975, complete text 0.45 printers sheet, 1 Table, 4 Refs.).

THE REACTIONS BETWEEN URANYL CHLORIDE AND ZIRCONIUM TETRACHLORIDE IN A SODIUM CHLORIDE – POTASSIUM CHLORIDE MELT

T. F. Babikova, Yu. S. Sokolovskii, and M. M. Sroelova

UDC 546.791.6'131-143:546.831' 131-143

A study has been made of the interaction of UO_2Cl_2 and $ZrCl_4$ in an NaCl–KCl melt at 700°C, with uranium concentrations of 5-25 wt.% and $UO_2Cl_2/ZrCl_4$ ratios of 0.5-2.0.

The reagent products were identified by chemical and spectrophotometric methods; also, the molten NaCl –KCl–(UO_2Cl_2 + $ZrCl_4$) mixture was tested for resistance to reduction (with zinc) and to decomposition on reducing the partial pressure of chlorine by flushing the cell with helium.

It was found that the interaction of UO_2Cl_2 with $ZrCl_4$ occurs without change in the valency of the uranium, and also without deposition of solid phases (UO_2, ZrO_2) or gaseous ones (Cl_2), being restricted to the formation of complexes, which are linked by oxygen bridges into chains of U–O–Zr type.

(No. 842/8111. Paper received December 9, 1974, complete text 0.45 printers sheet, 3 Figs., 2 Tables, 5 Refs.).

DIFFERENTIAL MACROSCOPIC SCATTERING COEFFICIENTS FOR LOW-ENERGY γ RAYS IN AIR

S. N. Sidneva and A. S. Strelkov

UDC 539.166.3

Two types of scattering have to be considered in determining the transport of low-energy γ rays in air ($E \leq 100$ keV): coherent (Rayleigh) and incoherent (Compton), in both cases on the basis of electron binding in the atom. The differential macroscopic coefficients for these processes for air take the form

$$d\mu_R(E, \Phi) = \frac{d\sigma_T}{d\Omega} \sum_z n_z F_z^2(E, \Phi)\, d\Omega =$$

$$= 0.0019291 \left(\frac{2}{r_0^2} \frac{d\sigma_T}{d\Omega}\right) F_R(E, \Phi) \sin\Phi\, d\Phi \ [\mathrm{cm}^2/\mathrm{g}];$$

$$d\mu_c(E, \Phi) = \frac{d\sigma_c^{K-N}}{d\Omega} \sum_z n_z S_z(E, \Phi)\, d\Omega =$$

$$= 0.0019291 \left(\frac{2}{r_0^2} \frac{d\sigma_c^{K-N}}{d\Omega}\right) S_c(E, \Phi) \sin\Phi\, d\Phi \ [\mathrm{cm}^2/\mathrm{g}],$$

where $d\delta_T/d\Omega$ is the differential cross section for Thomson scattering, $d\delta_c^{K-N}/d\Omega$ is the Klein–Nishina scattering cross section, S_Z is the incoherent-scattering function for an atom, F_Z is the atomic form factor, r_0 is the classical electron radius, and n_Z is the number of N, O, and Ar atoms in a gram of air.

The available published evidence for S_Z and F_Z at $10 \leq E \leq 100$ keV and angles $0 \leq \Phi \leq 180°$ has been used to tabulate the following curves:

$$d\mu_{c,R}/d\Omega;\ \frac{d\mu_R}{d\Omega}\Big/\frac{d\mu_T}{d\Omega};\quad \frac{d\mu_c}{d\Omega}\Big/\frac{d\mu_c^{K-N}}{d\Omega} \text{ and}$$

$$\int_0^{\Phi} \frac{d\mu_{c,R}}{d\Omega} \sin\Phi\, d\Phi \Big/ \int_0^{\pi} \frac{d\mu_{c,R}}{d\Omega} \sin\Phi\, d\Phi$$

which are the distributions for the scattering probabilities for given angles, which enable one to find scattering angles in simulating paths in statistical calculations.

The differential interaction coefficients can be used in analytical calculations by representing F_R and S_c as

$$F_R(E, \Phi) = a_1 \exp(a_2 I + a_3 I^2);$$

$$S_c(E, \Phi) = b_1 [1 - \exp(b_2 I + b_3 I^2)]$$

(here $I = (E_{keV}/12.34) \sin \Phi/2$), which approximate the calculated F_R and S_c with avarage error of ~ 5-10%.

To simplify statistical calculations for low-energy quantum scattering it is best to use weighted interaction cross sections, which provide the scattering angles readily.

It is convenient to take $(d\mu_R^*/d\Omega) = c_1 \exp(-c_2 I^2)\, 0.0019291$ as the weighted cross section for Rayleigh interaction, for $c_1 = 226.8$; $c_2 = 9.704$ for $0 \leq I \leq 0.5$ and with $c_1 = 16.94$; $c_2 = 0.57$ for $0.5 < I \leq 2$; $c_1 = 3.83$; $c_2 = 0.254$ for $2 < I \leq 4$ and $c_1 = 0$ for $I > 4$. Use of the weighted cross section in this form gives the following simple relationship for Φ:

$$\sin\Phi/2 = \sqrt{-\frac{1}{N} \ln(M - \xi L)},$$

where L, M, and N are numerical coefficients and $\xi \in [0, 1]$ is a random number.

A published method [P. Cavanaugh and A. Chilton, Nucl. Sci. Engng., 53, No. 2, 256 (1974)] can be used to determine Φ for Compton interaction.

Numerical evaluation of the statistical weights, which balance out the bias in the result,

$$W_{c,R} = \frac{d\mu_{c,R}}{\mu_{c,R}} \Big/ \frac{d\mu_{c,R}^*}{\mu_{c,R}^*},$$

gives W_R in the range 0.6–2, with W_c in the range 0.8–1.8, which values are quite acceptable from the viewpoint of smooth convergence in statistical calculations.

(No. 839/8434. Paper received July 18, 1975, complete text 0.6 printers sheet, 2 Tables, 13 Refs.).

γ-RAY MONITORING OF REACTOR POWER

A. B. Dmitriev and V. S. Shepel'

UDC 539.074.22

When a γ-ray detector is used to monitor reactor power, a problem arises in adequate separation of the prompt and delayed components of the γ rays. A differential ionization γ chamber has been used, whose sections are connected differentially and which differ in spectral sensitivity for γ rays. The sensitivity relation between the sections is taken such that the current difference is almost zero with the reactor shut down. A description of the differential chamber is given.

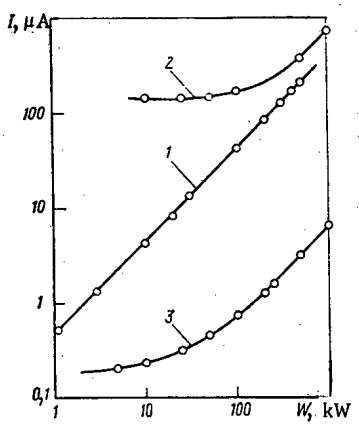

Fig. 1. Current in the γ-chambers as a function of reactor power.

Figure 1 shows the current in the γ-chambers as a function of reactor power; curve 1 is for the differential chamber at the edge of the core and set to zero with the reactor shut down; curve 2 is for an ordinary two-electrode chamber at the same point, and curve 3 is for a two-electrode chamber in the reactor shield behind the reflector. These curves illustrate clearly the advantages of the differential γ chamber, whose current is directly propertional to the reactor power above 1 kW. If the apparatus has a limit of detection of 10^{-9} A, no unbalance in the differential chamber as a result of shift in the delayed γ-ray spectrum occurs for a period of 12 h after shutting down the reactor. This method of power monitoring provides an adequate output signal and can be used with traditional methods in reactor monitoring and control systems.

(No. 843/8175. Paper received January 22, 1975, abstract June 6, 1975, complete text 0.3 printers sheet, 2 Figs., 8 Refs.).

NEUTRON-ACTIVATION ASSAY OF URANIUM AND THORIUM IN ROCKS WITH AN ANTICOINCIDENCE SPECTROMETER

V. R. Burmistrov and T. N. Madiyanov

UDC 543.53

The scope for determining uranium and thorium in geological specimens by instrumental neutron activation has been examined; the sensitivity has been improved by combining an anticoincidence spectrometer [2] with the standard method [1] of irradiation with resonant neutrons. This reduces the background by a factor 4, which improves the sensitivity by the corresponding factor. The following isotopes and γ lines were employed: ^{239}Np for uranium and ^{233}Pa for thorium (T of 2.35 and 27.4 days, E_γ of 228 and 278 or 312 keV, respectively).

TABLE 1. Activation-Analysis Results for Uranium and Thorium in Rocks

Standard rock	Element	Content (%) given by other methods	Activation-analysis results		
			content %, $P = 0,95$	No. of parallel meas.	coeff. of variation, %
Ur -240s	U Th	0,24 —	0,232±0,009 (9,9±0,2) 10^{-3}	10 10	5,5 10
Ur - 47s	U Th	$4,7 \cdot 10^{-2}$ —	(4,7±0,14) 10^{-2} (2,2±0,16) 10^{-3}	10 10	4 10
D-8	U Th	(1,2—1,3) 10^{-4} $4,7 \cdot 10^{-4}$	(0,83±0,14) 10^{-4} (6,7±0,7) 10^{-4}	5 9	13 13,6
224-b/67	U Th	$2,1 \cdot 10^{-4}$ $1,8 \cdot 10^{-3}$	(2,1±0,3) 10^{-4} (2,3±0,1) 10^{-3}	5 9	12 7

The sample of mass 0.5 g is exposed to an epithermal neutron flux of about $5 \cdot 10^{10}$ neutrons/cm^2-sec for 3 h, with the γ rays recorded by a Ge (Li) detector of volume 25 cm^3 and resolution 7 keV at 661 keV.

Rock samples of four types were examined: standstones, limestones, granites, diorite, gabbro, porphyrite, etc. The limits of detection were $(4-8) \cdot 10^{-6}$ for uranium and $(5-10) \cdot 10^{-6}$% for thorium; isolated minerals (sphalerite, pyrite, chalcopyrite, and galena) gave poor results: $(2-4) \cdot 10^{-4}$ for uranium and $(2-7) \cdot 10^{-4}$% for thorium. There was interference from Zn, Sb, As, Cd, and Ba.

Tests were also made to determine the uranium and thorium concentration ranges within which there was no self-screening; if a cadmium filter was used, self-screening began to make itself felt at uranium concentrations of $5 \cdot 10^{-1}$% and thorium concentrations of 2%. If no cadmium was used, the effect became appreciable at 5% uranium, whereas there was no effect for thorium up to 10% concentration.

Many of the specimens had previously been analyzed in various laboratories by other methods: isotope dilution, emanation, track methods, x-radiography, luminescence, and radiometry. The results for the range $(10^{-5}-2 \cdot 10^{-1})$% agreed with those from activation analysis. Table 1 gives the results for uranium and thorium in standard rocks, for which the concentrations were known.

The uranium contents for the standard rock Ur-240s and UR-47s are certified values (thorium not determined). The uranium and thorium have been determined in various laboratories for specimens D-8 and 224-b/67, but the values have not been certified.

LITERATURE CITED

1. E. Steinnes and D. Brune, Talanta, 16, No. 9, 1260 (1969).
2. V. R. Burmistrov et al., in: Industrial Activation Analysis [in Russian], Fan, Tashkent (1974), p. 46.

(No. 844/8187. Paper submitted January 30, 1975, complete text 0.35 printers sheet, 1 Fig., 1 Table, 9 Refs.).

A DEVICE FOR NEUTRON FLUX AND SPECTRUM MEASUREMENT IN A REACTOR CHANNEL

F. M. Arinkin, G. A. Batyrbekov,
Z. B. Bekmurzaeva, V. N. Kiselev,
and Yu. A. Sobolev

UDC 621.039.55:621.039.573

Tests inside reactors on highly enriched fuel assemblies often require a specified neutron spectrum, a given heat dissipation and heat distribution within the fuel pins, and other such conditions. The present device uses absorbing screens made of ^{3}He and cadmium, which allows one to meet some of these requirements.

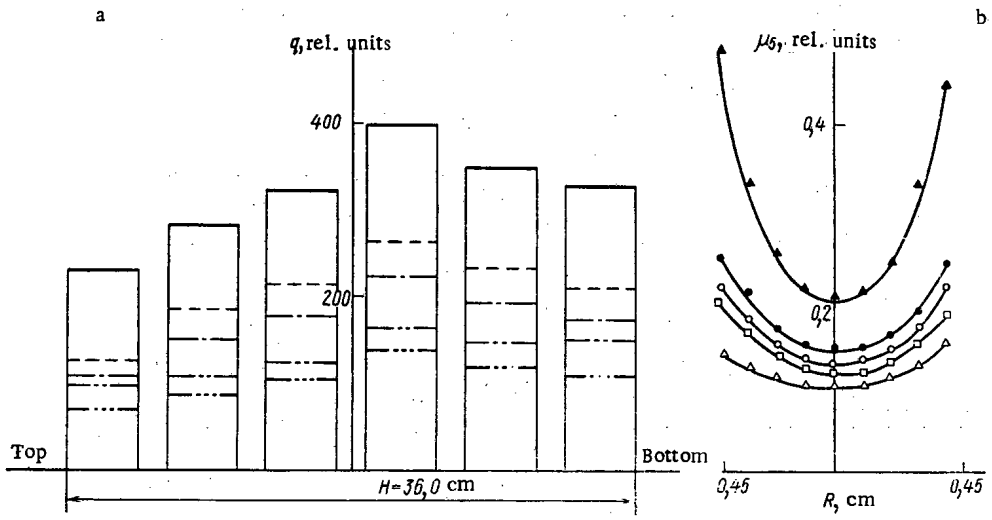

Fig. 1. a) Vertical distribution of energy release in rod assemblies: ——)Pd = 0; — — —) 1.2; —·—) 7.6; —·· and —···) 0 and 7.6 (assemblies surrounded by cadmium shield; b) distribution of ^{235}U fission density along a diameter in a rod model: ▲) Pd = 0; ●) 1.2; ○) 7.6; □ and △) 0 and 7.6 (assemblies surrounded by cadmium shield).

The device consists of three coaxial cylinders made of stainless steel of wall thickness 2 mm, which are welded to a common base and flange. The height of the active part is 580 mm. The ^3He is supplied to the cavity formed by two of the cylinders with a distance of 7 mm between the walls. If necessary, a cadmium sheet of thickness 0.5 mm can be placed in the specimen chamber. The chamber is connected to a cylinder containing ^3He and a collecting system with shutoff valves and gauges. The system contained six vertical fuel-pin models of height 30 mm, which were made of UO_2 tablets enriched to 90% in ^{235}U and of diameter 9 mm. The fuel-pin models were separated by inserts of height 40 mm. The pins were placed in a heat-transfer graphite sleeve and set up in the cavity. The following neutron characteristics were dependent on the ^3He pressure: ^{235}U fission rate within the device, total energy release within the pins as determined calorimetrically with thermal-analysis equipment [1], the detailed energy distribution in radius and height as determined by autoradiography [2], and the distribution of the thermal and fast neutron fluxes in the core and working cavity.

Figure 1a shows the distribution of the energy release over the height of an assembly for various Pd. The mean energy release (from absorption by ^3He) falls almost by a factor 2 for Pd = 7.6 (P is gas pressure in atm and d is gas layer thickness in cm). The attenuation factor for the fission density in ^{235}U was measured by a fission chamber and found as 2.3; when a cadmium screen was used, the effect from the ^3He was much less; at the same Pd, the energy release (by absorption in ^3He) was reduced by a factor 1. 2. The skewness in the distributions (the dip on the left side) is due to the control devices. Figure 1b shows the ^{235}U fission density over the cross section of one of the pins. The energy deposition decreases as the gas pressure increases, while the fission distribution becomes much more even along the radius and along the length. The nonuniformity factor (ratio of the maximum emission density to the average) falls from 1.61 to 1.44 for the radius at Pd = 7.6, while the figures for the height are from 1.57 to 1.39.

The distribution of the thermal and fast neutron fluxes were measured with activation detectors, which showed only slight deviations in the neutron distributions within the core. The measurements were in good agreement with calculations performed in the S_4 approximation.

LITERATURE CITED

1. Yu. L. Tsoglin et al., in: Neutron-Flux Measurement on Reactors and Accelerators [in Russian], Vol. 1, Izd. Standartov, Moscow (1972), p. 151.
2. A. Ertaud and P. Zaleske, J. Phys. Radium, 14, 191 (1953).

(No. 845/8231. Paper received March 10, 1975, complete text 0.45 printers sheet, 4 Figs., 4 Refs.).

NEUTRON-FLUX STABILIZATION FOR REACTOR CHANNELS

A. N. Kosilov, A. P. Kryukov,
V. T. Neboyan, P. T. Potapenko,
E. S. Timokhin, and A. P. Trofimov

UDC 621.039.55

Research-reactor operation requires automatic control or at least stabilization of the neutron flux at the exit from an experimental channel.

It is shown that a local neutron-flux transducer can be used in the reflector with a scatterer to deflect thermal-neutron flux from a tangential vertical channel [1]. This device has been used with the IRT-2000 reactor at the Moscow Physics Research Institute to examine the performance of local regulation systems to stabilize and control neutron fluxes in horizontal and vertical channels near the scatterer for various control laws.

The transducer was a graphite scatterer in the form of a cylinder 35 mm in diameter and height 70 mm, which was enclosed in an aluminum tube and worked with a KNK-53 ionization chamber. The scatterer and chamber were placed in a VÉK-2 vertical channel; the scatterer was at the level of the center of the core, while the chamber was 400 cm above this, under the shielding plug [2]. The position of the scatterer with respect to the chamber could be altered.

The current from the ionization chamber was plotted as the function of the position of the scatterer relative to the core, and this closely reflected the neutron flux distribution over the height of the core.

The reactor control system consisted of a rod integral-power regulator in conjuction with a neutron-flux regulator; there were no artificial links between the regulators. The local regulator was examined in the local-flux stabilization mode and in the integral-power stabilization mode on introducing local reactivity perturbation with manual control rods, and also in the mode in which the local neutron flux was varied at constant integral power and the mode with stabilization of the local neutron flux with variation in the integral power.

In all experiments the thermal neutron flux at the exit from the nearest horizontal channel was measured. The control system maintained the present value to ±1%. This method of stabilizing neutron flux can be applied to other research reactors, with considerable gain in experiment performance.

LITERATURE CITED

1. A. P. Kryukov and B. S. Kaminskii, in: Neutron-Flux Measurement on Reactors and Accelerators [in Russian], Vol. 2, Izd. Standartov, Moscow (1972), p. 96
2. G. A. Bat', A. S. Kochenov, and L. P. Kabanov, Research Reactors [in Russian], Atomizdat, Moscow (1972).

(No. 846/8234. Paper received March 10, 1975, complete text 0.45 printers sheet, 5 Figs., 4 Refs.).

OPTIMIZATION IN QUANTITATIVE ACTIVATION ANALYSIS

M. G. Davydov and A. P. Naumov

UDC 543.53

An optimization function is given for activation analysis, which amounts to quantitative determination of element concentrations in a matrix subject to specified lower limits. The optimium analysis conditions are to be defined by locating the minimum cost for a multielement analysis S:

$$S=\sum_{i=1}^{q}\frac{\alpha_1 t_{\mathrm{irr}\,i}+\alpha_2 t_{\mathrm{c}i}+\alpha_3 t_{\mathrm{co}\,i}+\alpha_{4i}}{n_i}+\alpha$$

subject to the condition

$$f_m\equiv\frac{C_{1m}}{C_{Qm}}\geqslant 1;\quad 1\leqslant m\leqslant q,$$

where α_1, α_2, and α_3 are the costs of unit irradiaton time, unit cooling time, and unit counting time; t_{irri}, t_{ci}, t_{coi} are the irradiation, cooling, and counting times in determining element i; α_{4i} is the cost of auxiliary operations of element i; α is the cost of preparing standards, monitors, and so on; n_i is the number of elements to be determined at the same time as element i (including the latter); q is the number of elements to be determined altogether; C_{1m} is the lower bound to the possible concentration of element m in the sample, and C_{Qm} is the limit of detection for element m.

It has been found [L. Currie, Anal. Chem., 40, 586 (1968)] that

$$C_{Qm} = K_Q \sigma (C_{Qm}),$$

where $1/K_Q$ is the maximum acceptable relative error in determining the concentration of element m in the analysis and $\sigma(C_m)$ is the variance of the concentration for element m.

As σ (C_{Qm}) has to be known, an expression is derived for σ (C_m) for the relative method of γ-activation analysis, which incorporates the instrumental error. As monitoring is widely used in practical analysis, an expression is derived for σ (C_m) for this case also. Criteria are also given for correcting the instrumental error for C_{Qm}. The condition for existence of C_{Qm} is used to draw up specifications for the equipment parameters that have to be provided for an optimum to exist.

(No. 847/8328. Paper received May 21, 1975, complete text 0.45 printers sheet, 13 Refs.).

LETTERS TO THE EDITOR

CORRECTION FOR TIME OF FALL IN NEGATIVE-REACTIVITY DETERMINATION BY ROD-DROP

O. A. Elovskii

UDC 621.039.562:621.039.519

The rod-drop method is one method of determining negative reactivity from small values up to above 1 for β_{ef} [1]. The integral form of the method (the integral count method [2]) provides a simple realization of high statistical accuracy no matter what the reactivity. The method presupposes a stepwise change in the reactivity in a critical reactor. The finite time of rod drop is neglected in the interpretation which results in a systematic error, which can be appreciable [3-5]. The point model has been applied to the kinetics subject to certain assumptions to provide a reasonably rigorous analysis of the systematic error arising from the finite time of fall. In that case, the change in the neutron density n(t) on introducing the reactivity ρ^* (t) into a critical assembly is described by a standard system of equations:

$$\frac{dn(t)}{dt} = \frac{\rho^*(t) - 1}{\Lambda^*} n(t) + \sum_{i=1}^{6} \lambda_i C_i(t); \tag{1}$$

$$\frac{dC_i(t)}{dt} = -\lambda_i C_i(t) + \frac{a_i}{\Lambda^*} n(t), \tag{2}$$

where $\Lambda^* = \Lambda/(\beta ef)$; $\rho^*(t) = \rho(t)/(\beta ef)$, and the other symbols are usual ones.

The integration in (1) and (2) for instantaneous injection of negative reactivity $\rho^*(t) = -\rho_0^*$ leads via simple steps to an expression used in the integral-count method:

$$\rho_0^* = \frac{n(0)\left(\Lambda^* + \sum_{i=1}^{6} a_i/\lambda_i\right)}{\int_0^\infty n_0(t)\,dt}, \tag{3}$$

Translated from Atomnaya Énergiya, Vol. 40, No. 5, pp. 418-420, May, 1976. Original article submitted July 15, 1975.

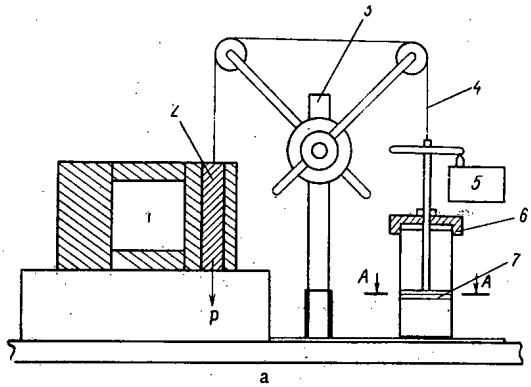

Fig. 1. Experimental system: 1) reactor; 2) control rod; 3) support; 4) cable; 5) electronic equipment; 6) cylinder containing water; 7) piston; φ angular size (deg) of sector in piston; t_0 (sec) rod fall time.

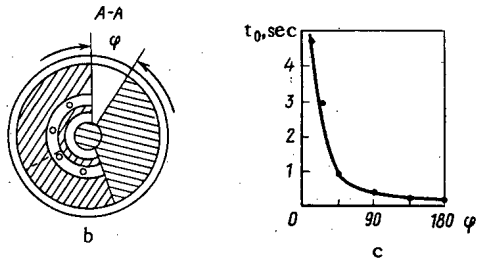

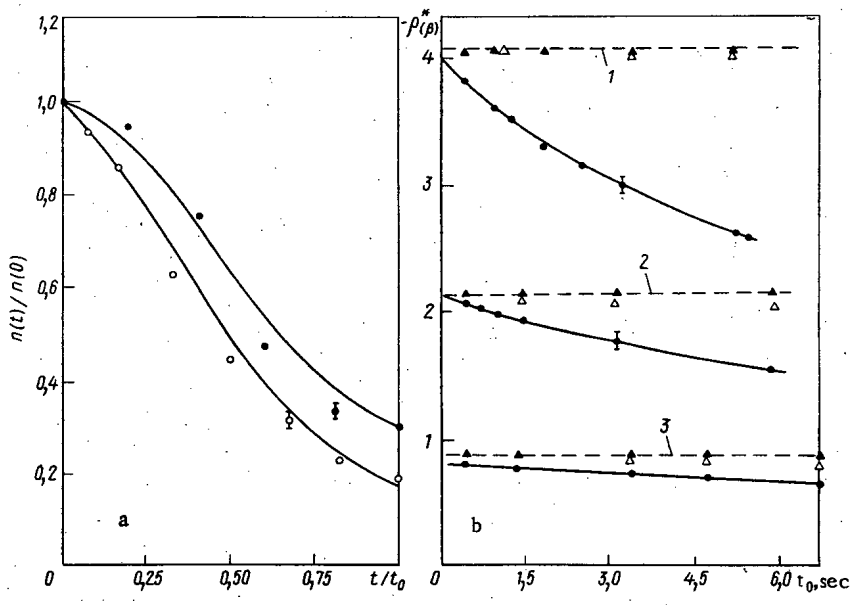

Fig. 2. Results: a) flux change produced by rod for $\rho_0^* = 2.15$ (○ and ● for t_0 of 0.5 and 6 sec, respectively); b) reactivity as a function of rod fall time (● neglecting actual motion as in (3); ▲ and Δ incorporating real motion in accordance with (8) and (5), respectively); (γt_0, ρ^*) calculated from (4) by Nairi-1 computer; -----) independently measured reactivity [1) $\rho_0^* = -4.05 \pm 0.002$; 2) $\rho_0^* = -2.15 \pm 0.01$; 3) $\rho_0^* = -0.81 \pm 0.005$].

where n(0) is the neutron density in the critical reactor, while ρ_0^* and n_0 (t) here and subsequently relate to instantaneous reactivity change.

In practice, the reactivity change occurs in a finite time t_0 in accordance with a law determined as a whole by the reactor design and characteristics. In that case, the value of $\rho_0^* t_0$ given by (3) on the basis of the real n(t) contains an error.

Simple steps from (3) allow one to relate $\rho^*_{t_0}$, as derived from the measurements to ρ^*_0; for this purpose we introduce the factor

$$\gamma(t_0, \rho^*) = \frac{\int_0^\infty [n(t) - n_0(t)]\, dt}{n(0)\left(\Lambda^* + \sum_{i=1}^{0} a_i/\lambda_i\right)}, \tag{4}$$

whose value by definition is responsible for the systematic error in the reactivity for a finite drop time. Then from (3) and the expression for γ (t_0, ρ^*), we get

$$\rho^*_0 = \frac{\rho^*_{t_0}}{1 - \rho^*_{t_0}\gamma(t_0, \rho^*)}. \tag{5}$$

As$(\Lambda^*/n)(dn/dt) \ll \rho^*$ (t), from (1) we have

$$n(t) = \frac{\Lambda^* \sum_{i=1}^{6} \lambda_i C_i(t)}{\rho^*(t) + 1}. \tag{6}$$

Integration in (2) with all the delayed-neutron groups gives

$$\Lambda^* \sum_{i=1}^{6} \lambda_i C_i(t) = \sum_{i=1}^{6} a_i \exp(-\lambda_i t) + \sum_{i=1}^{6} a_i \lambda_i \exp(-\lambda_i t) \int_0^t n(\tau) \exp(\lambda_i \tau)\, d\tau. \tag{7}$$

Usually, the reactivity as a function of time during rod drop is closely described by $\rho^*(t) = -bt^2$; the latter may be used with (2) and (6) on the assumption that there is a single effective group of delayed neutrons, which gives an analytical solution for n(t). Then (4) and (5) give a solution for ρ^*_0 in terms of measured quantities only:

$$\rho^*_0 = \rho^*_{t_0}\left[1 + \left(\frac{\rho^*_{t_0} + 1}{\sqrt{\rho^*_{t_0}}} \operatorname{arctg} \sqrt{\rho^*_{t_0} - 1}\right) \frac{t_0}{\sum_{i=1}^{6} \frac{a_i}{\lambda_i}}\right]. \tag{8}$$

Although (8) has been derived on the assumption that the error is small, the results are satisfactory even if the error is around 10%; estimates show that good results can be obtained if in calculating γ $(t_0\rho^*)$ one assumes that $\int_{t_0}^{\infty} [n(t) - n_0(t)]\, dt \approx 0$. Then one can derive ρ^*_0 from (5) by using tables for γ (t_0, ρ^*), as calculated for the law of variation in ρ^* (t) with possible values for t_0 and $\rho^*_{t_0}$, and in (4) for γ (t_0, ρ^*) the integration is performed over the finite time interval t $(0 \le t \le t_0)$.

This approach can be applied to the systematic error arising from the finite time of rod drop and has been tested for rods in a fast critical assembly. One of the dropping control rods had a drop time adjustable by connection to a mobile piston (Fig. 1a). This piston moved in a cylinder containing water. The time of fall was adjustable between 0.5 and 6 sec by adjusting the size of the hole in the piston (varying the angle φ in Fig. 1b and c). Control rods of different diameters could also be used to vary the reactivity. The time course of the neutron flux as measured on dropping the rod (Fig. 2a) agreed well with that calculated from (6), where the reactivity change was approximated by $\rho^*(t) = -bt^2$ $(b = \sigma^*_0/t_0^2$; when the rod began to move, the scalers were started (Fig. 1), which recorded the pulses from 6 neutron detectors (SNM-11 counters), which were placed within the reactor at a reasonable distance (about 1.5 m). The reactivity was calculated from (3) on the basis of the contribution to n(t) from the natural background. For each t_0 and ρ^*_0 we performed several rod drops; Fig. 2b shows the results from the drop method as averaged over all channels for each t_0. The systematic error was elminated by using (5) and (8). A calculation on the basis of the actual rod motion gave results that agreed closely with those from other methods of reactivity measurement (Fig. 2b).

I am indebted to E. S. Matusevich and V. Ya. Pupko for valuable comments on the work, and to M. E. Kolchin, A. L. Shmotin, K. M. Kotov, L. M. Razina, and V. D. Tsverave for assistance in the experiments and in processing the results.

LITERATURE CITED

1. J. Kipin, Physical Principles of Reactor Kinetics [Russian translation], Atomizdat, Moscow (1967).
2. W. Hogan, Nucl. Sci. Engng., 8, 518 (1960).
3. V. Ya. Pupko, in: Theoretical and Experimental Aspects of Nonstationary Neutron Transport [in Russian], Atomizdat, Moscow (1972), p. 192.
4. L. Bveitenhuber and H. Huber, Atomkernenergie, 15, 259 (1970).
5. J. Bouzik, S. Hvaščevski, and K. Jablonsky, At. Énerg., 30, No. 4, 381 (1971).

AN INVESTIGATION OF THE PARAMETERS OF A CRITICAL ASSEMBLY

É. Ya. Tomsons, V. V. Bute,
V. V. Gavar, A. S. Dindun,
U. A. Kruze, and É. Ya. Platatsis

UDC 621.039.51

The loading of the fissionable material of a nuclear reactor depends directly upon the number and geometrical shape of the fuel elements and their arrangement in the active zone and also upon the composition and thickness of the neutron reflector (water, graphite). The reactivity equivalent of the regulators of a critical assembly depends upon the composition of the active zone and the neutron reflector and also upon their location in the reactor.

The nuclear physical parameters of three configurations under investigation of a critical assembly consisting of fuel assemblies (FA) are compared in this article.

Characteristics of a Critical Assembly. We use in the critical assembly the four-tube fuel assembly of the IRT-M reactor [1] manufactured of a uranium–aluminum alloy and containing on the average 170 g of uranium enriched 90% in ^{235}U. The average height of the uranium layer in the fuel assembly is 580 mm. The fuel assembly occupies a cell in the active zone having the cross section 71.5 × 71.5 mm. It is possible to extract the central tube of the fuel assembly and install in its place a channel for a control rod or an experimental channel.

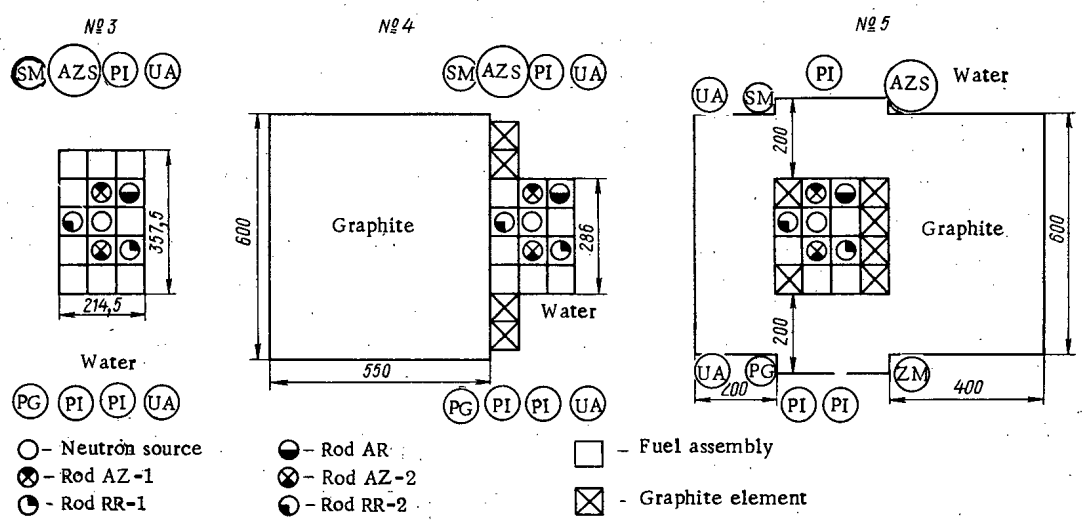

Fig. 1. Diagram of the configurations of the No. 3, 4, and 5 critical assemblies.

Translated from Atomnaya Énergiya, Vol. 40, No. 5, pp. 420-422, May, 1976. Original article submitted December 13, 1975.

TABLE 1. Basic Nuclear Physical Parameters of the Configurations of the Critical Assembly

Parameters	Configurations		
	№ 3	№ 4	№ 5
No. of fuel assemblies, pieces	15 (3 × 5)	12 (3×4)	10 (2×4)+2
Amount of ^{235}U in the active zone, g.	2501	1964	1612
Neutron multiplication factor of an infinite active zone K_∞	1,84	1,84	1,84
Effective multiplication factor K_{eff}	1,0082	1,0053	1,0069
Material parameter of critical assembly B^2, cm^2	$1,62 \cdot 10^{-2}$	$1,62 \cdot 10^{-2}$	$1,62 \cdot 10^{-2}$
Eff. fraction of delayed neutrons β_{eff}	0,00824	0,00824	0,00824
Eff. contribution of reflector, cm:			
end reflector — water	6,5	6,5	6,5
side reflector — water	5,4—5,6	5,4—5,6	—
side reflector — graphite	—	8,15	8,15
Compensating power of rods, $\Delta K/K$			
AR	$2,16 \cdot 10^{-2}$	$1,32 \cdot 10^{-2}$	$4,60 \cdot 10^{-3}$
RR-1	$2,16 \cdot 10^{-2}$	$2,61 \cdot 10^{-2}$	$3,10 \cdot 10^{-2}$
RR-2	$2,77 \cdot 10^{-2}$	$3,70 \cdot 10^{-2}$	$2,67 \cdot 10^{-2}$
AZ-1	$4,08 \cdot 10^{-2}$	$2,70 \cdot 10^{-2}$	$2,50 \cdot 10^{-2}$
AZ-2	$4,08 \cdot 10^{-2}$	$4,60 \cdot 10^{-2}$	$3,83 \cdot 10^{-2}$

The critical assembly is located in an aluminum tank 2.5 m in diameter with a height of 2.0 m and a volume of 9.8 m^3 [2]. Two vertical columns are mounted in the tank along which the frame of the active zone can be moved by servomotors to a height of 2.0 m at a speed of 0.21 mm/sec. The elements of the active zone and the graphite reflector are attached to the frame.

The critical assembly is controlled by a single automatic regulating rod AR and by two compensating rods RR-1 and RR-2, and protection is controlled by two emergency protection rods AZ-1 and AZ-2 (Fig. 1). All the rods are manufactured of Duraluminum tubes 20 × 1 mm in size filled with boron carbide (530 g of B_4C per rod), with the exception of the rod AR of the critical assembly of configuration No. 5, which is manufactured of Kh18N10T steel (tube 20 × 4 × 1755 mm in size). During the starting-up, a plutonium—beryllium neutron source with an intensity of $1 \cdot 10^6$ neutrons/sec is introduced into the center of the active zone.

The monitoring of the control and protection of the critical assembly is accomplished by three neutron counters of the SMNO-5 type, the ratemeters PI_1-4, PI_2-4, and PI-5, six type KNK-56 ionization chambers, power control devices PG (UI-12, M-95) and SM (ÉPPV-51), protection amplifiers UA_1-9, UA_2-9, and AZS (AZS-2M), and an automatic regulation system ZM (ZM, UR-8, ÉMU).

Nuclear Physical Characteristics of Configurations No. 3, 4, and 5 of the Critical Assembly. The neutron moderator of the critical assembly is water. The upper and lower neutron reflectors consist of water and the aluminum end elements of the fuel assemblies. The side reflector of configuration No. 3 consists of water; that of configuration No. 4 of water, a graphite prism 550 mm thick, 600 mm wide, and 500 mm high, and four graphite slugs of the same dimensions as the fuel assemblies; and that of configuration No. 5 consists of graphite from 200 to 470 mm thick (see Fig. 1).

The critical loading of the active zone with the water neutron side reflector was attained at 15 fuel assemblies and with the graphite reflector at 10 fuel assemblies (see Table 1).

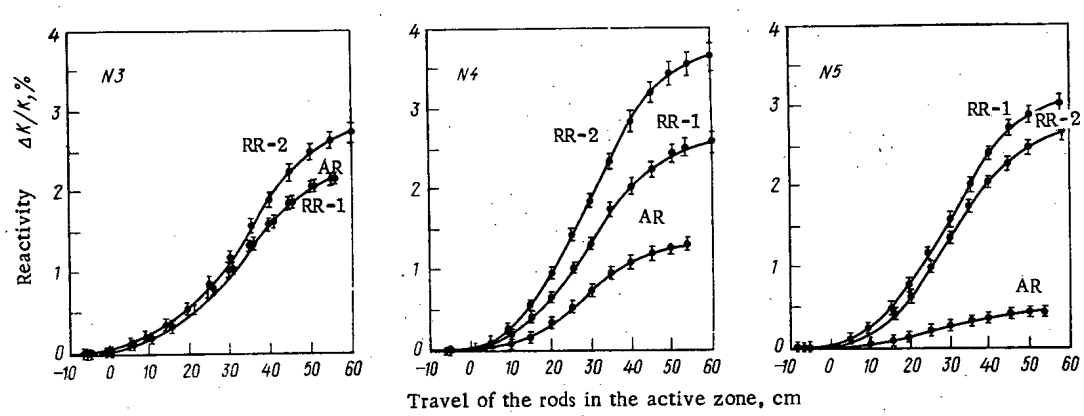

Fig. 2. Variation of the compensating power of the reactivity of the control rods AR, RR-1, and RR-2.

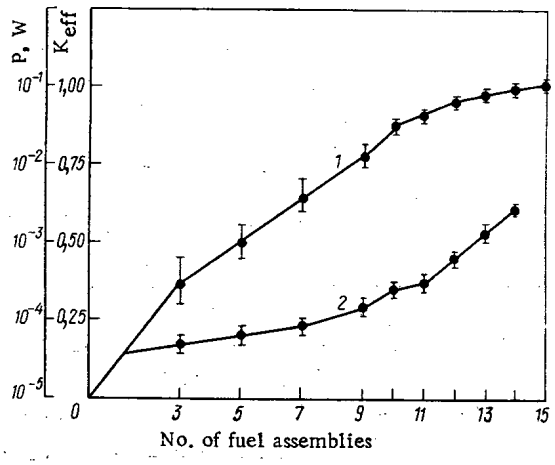

Fig. 3

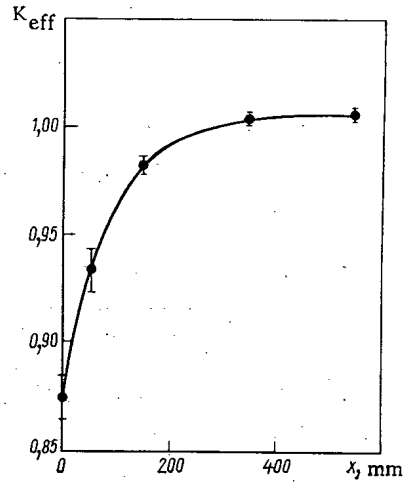

Fig. 4

Fig. 3. Variation of the effective neutron multiplication factor (1) [$K_{eff} = f(n)$] and the power (2) of configuration No. 3 of the critical assembly in the process of the critical loading of the active zone.

Fig. 4. Variation of K_{eff} of the critical assembly as a function of the thickness of the single-sided graphite side reflector.

Thus the replacement of the water neutron side reflector by a graphite one decreases the critical loading of the assembly by 35.6%.

The compensating power of the control rods of the critical assembly (Fig. 2) depends upon their location and the surrounding medium (see Table 1). The total compensating power of the rods AR, RR-1, and RR-2 of configuration No. 3 of the critical assembly is $\Delta K/K = 6.72 \cdot 10^{-2}$, and that of all the rods of SUZ is $\Delta K/K = 14.4 \cdot 10^{-2}$. Due to interference of the rods, their compensating power is decreased by 5.5%. The reactivity of the rods was measured by the method of the asymptotic period of the reactor.

In the process of the critical loading of configuration No. 3 the variation of the multiplication factor and the power of the critical assembly were measured for the arrangement of the SMNO-5 neutron counters and the neutron source as shown in Fig. 1 (Fig. 3). During the loading of from one to 14 fuel assemblies the thermal power of the critical assembly, produced by the neutron source, increased by a factor of 83 and amounted to $\sim 3 \cdot 10^{-3}$ W. The effective neutron multiplication factor of the critical assembly of 15 fuel assemblies without a neutron reflector, determined by the successive weighing of the fuel assemblies, is equal to 0.55.

The graphite reflector 600 × 550 × 800 mm in size of configuration No. 4 of the critical assembly increased the neutron multiplication factor by 0.136 (Fig. 4). The neutron multiplication factor for the medium of an active zone of infinite dimensions and the material parameter cited in Table 1 are close to the calculated values obtained by the use of the diffusion-age double-group method ($K_{\infty}^{calc} = 1.866$, $B^2_{calc} = 1.56 \cdot 10^{-2}$ cm^2). The calculated values are determined in the presence of all the fuel tubes in the fuel assemblies.

Thus the minimum critical loading of the reactor with a graphite side reflector consists of 10 fuel assemblies and contains 1612 g of ^{235}U. The replacement of the water side reflector of the active zone by the graphite one reduces the critical loading of the reactor by 35.6%. The interference of the rods decreases the compensating power of a rod by 5.5%. A singlesided graphite side reflector 550 mm thick increases the neutron multiplication factor of the reactor by 0.136. The experimental data are close to the calculated values obtained by the double-group diffusion-age method.

LITERATURE CITED

1. P. M. Egorenkov et al., Preprint IAE-1707, Moscow (1968).
2. É. Ya. Tomsons et al., Izv. Akad. Nauk LatvSSR, Ser. Fiz. i Tekh. Nauk, No. 4, 82 (1968).

AMPULE DEVICES IN THE VVR-M REACTOR FOR IRRADIATING CARBON-BASED MATERIALS

G. Ya. Vasil'ev, Yu. S. Virgil'ev,
V. G. Makarchenko, and Yu. P. Semenov

UDC 621.039.55

Materials are commonly irradiated in reactors to evaluate their scope for use in reactors, and also in research on the structure of matter; this has required a variety of ampule devices and special channels for specimen irradiation. Many descriptions have been given of such devices [1, 2].

Here we describe the ampules used in the VVR-M reactor, with results on the irradiation conditions. The devices were intended for handling graphite specimens in the core, and also in vertical channels in the beryllium reflector (V-2BS), and in the water behind the beryllium reflector (V-15S). The maximal thermal-neutron flux density ($n_t v_0$) and the fast-neutron flux density Φ_f are listed in Table 1.

These devices provide a comparatively simple means of producing several temperature zones simultaneously; the specimens are heated by the γ rays absorbed by the graphite and by the neutron scattering. The temperatures ranged from 70-90°C to 800-850°C. The temperatures were regulated by adjusting the gaps between the specimens and the ampule walls, and also by introducing steel screens. It was not intended to provide very precise temperature control.

The steel screens were centered within the body by three-point contacts; within the screens, or directly within the ampule in the absence of screens, there were hollow cylinders with dense graphite at the bottom, with grooves on the outer surfaces, which provided for inserts to produce centering with a given gap. Layers of the specimens were placed between the inserts (Fig. 1). There were also gaps between the inserts along the length of the ampule. In some cases, the inserts were insulated by plates of thickness 2-8 mm made of pyrolytic graphite, whose thermal conductivity perpendicular to the deposition plane is almost zero.

The irradiation temperature was determined by means of diamond indicators [3]; a graphite capsule having the size of the specimen (diameter 4 mm and length 40 mm) was drilled with a hole containing a few milligrams of diamond powder. These specimens were placed at various points in the ampule. The irradiated powder was annealed isochronously with successive rises in temperature, with measurement of the lattice parameter. This was performed by powder methods with K_α radiation (cobalt) in VRS and RKU cameras of diameters 143 and 114 mm, respectively. The error in determining the lattice parameter was ±0.005 Å.

The diamond could be replaced as a temperature indicator by natural graphite or by some material based

TABLE 1. Flux Densities (neutrons/cm^2 · sec) in the VVR-M Reactor

Channel or cell	$n_t v_0$	Φ_f ($E_f > 1$ MeV)	Φ_f ($E > 0{,}18$ MeV)
Core, cells b-1 and l-1	$7 \cdot 10^{13}$	$(5{,}1-6{,}4)\,10^{13}$	$(10{,}6-13{,}4)10^{13}$
V-2BS channel in beryllium reflector	$4 \cdot 10^{13}$	$3 \cdot 10^{12}$	$5{,}5 \cdot 10^{12}$
V-15S channel in water behind reflector	$5 \cdot 10^{12}$	$1{,}4 \cdot 10^{11}$	$2{,}6 \cdot 10^{11}$

Translated from Atomnaya Énergiya, Vol. 40, No. 5, pp. 423-425, May, 1976. Original article submitted January 15, 1975.

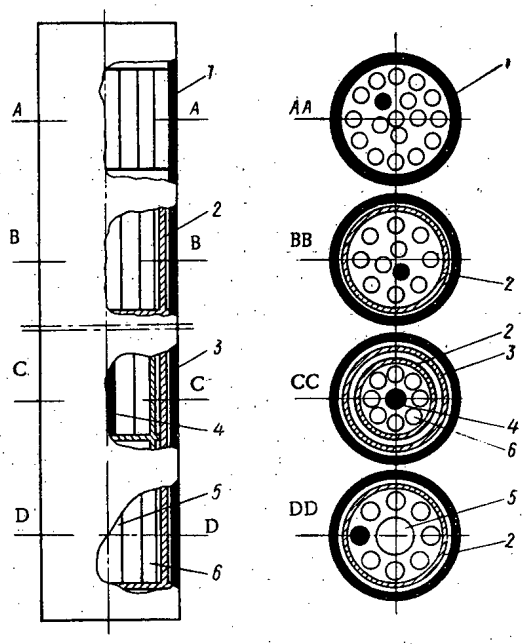

Fig. 1

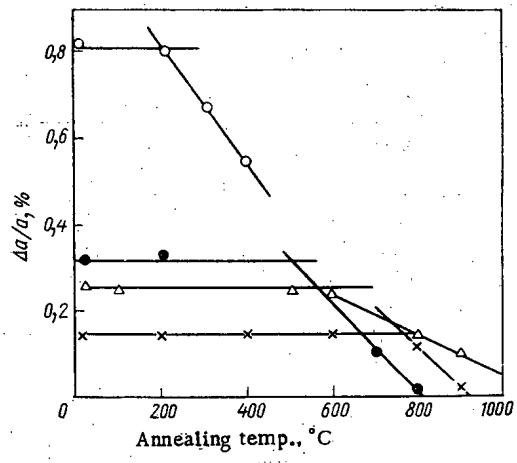

Fig. 2

Fig. 1. Ampule for irradiating graphite in VVR-M core: 1) body; 2) graphite liner; 3) heat screen; 4) diamond indicator; 5) internal integral liner; 6) specimens.

Fig. 2. Determination of irradiation temperature by diamond indicator for ampule assemblies as in Fig. 1: ○) A, 200°; ●) B, 500°; Δ) D, 570°; ×) C, 760°C.

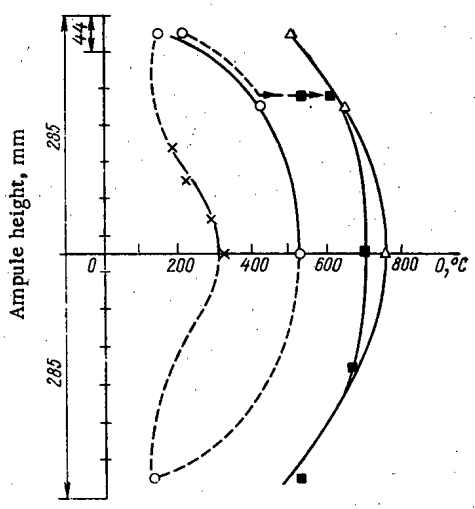

Fig. 3.

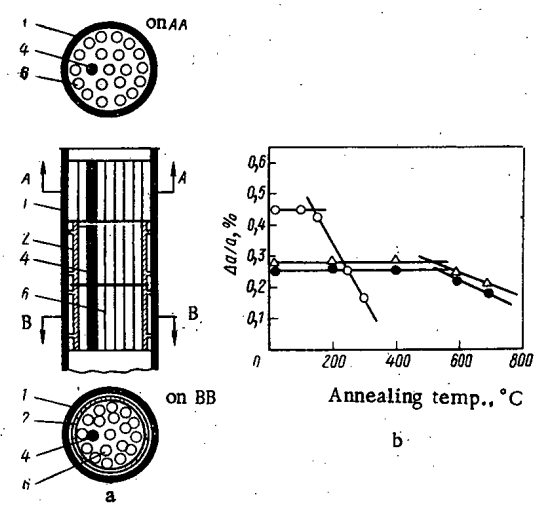

Fig. 4

Fig. 3. Temperature as a function of height for ampules of various designs used in the core: ×) no screens or liners; ○) with liners; ■) with liners and screen; Δ) the same, evacuated (height of ampule and one liner shown on left).

Fig. 4. a) Ampule for irradiation in the VVR-M reflector (symbols as Fig. 1); b) effects of annealing on lattice parameter of diamond indicator: ○) A, 150°; Δ, ●) B, 500 and 550°C.

on it, and this should enable one to measure the specimen temperature directly, e.g., temperatures measured with natural graphite and diamond indicators were, respectively, 160 and 190°C. The difference in these temperatures was due to a certain temperature gradient along the ampule. This was most pronounced in low-temperature irradiation. On the other hand, the recovery of the c lattice parameter of artificial graphite starts

at a higher annealing temperature because the material is more defective than natural graphite, which hinders recovery on annealing.

Figures 2 and 3 show some of the results. These were used with other data to construct the temperature distribution for each of the various styles of ampule. The irradiation field in the reactor was symmetrical, as was the disposition of the specimens in a tube, so the number of temperature indicators could be restricted. As a rule, they were usually placed only along one-half of an ampule.

Figure 1 shows various styles of internal sample assembly for unchanged external dimensions. If the specimens were placed one after the other without gaps (Section AA, Fig. 1), the temperatures varied from 140°C at the edge of the reactor to 325°C in the median plane of the core. The inserts spaced the specimens from the water-cooled walls, which raised the temperature appreciably (to 500°C). If a massive rod of dense graphite was placed at the center of an insert (Section DD, Fig. 1), the temperature could be increased by 50-70°C. An additional steel screen between the ampule wall and the insert raised the temperature at the center to 760°C. A further increase of 40-60°C was attained by using a screen in the form of a sealed cylinder evacuated and filled with argon to 10^{-1}-10^{-2} mm Hg; this means that evacuation was largely without effect at 600°C and above.

Figure 3 shows the distribution of the working temperature along the device for various styles of assembly as determined with diamond indicators. If the screen was inserted only along parts of the ampule, the temperature fell sharply outside the screen (shown by arrow in Fig. 3). The inserts of pyrolytic graphite were very effective, and screens and washers of pyrolytic graphite insulating the specimens from the walls raised the temperature from 140 to 400-500°C.

Specimens in the reflector channels were irradiated in aluminum tubes, whose construction is shown in Fig. 4. The graphite temperature did not exceed 140-200°C without spacing. If the specimens were placed in copper holders with a gap of 1 mm from the wall, the graphite temperature rose to 500-550°C. In the channel behind the beryllium reflector, the low flux intensity caused the lattice-parameter change in the diamond to be small, so we were unable to determine the irradiation temperature in this way. One expects that materials showing a larger change in lattice parameter such as natural graphite would be more effective.

It has thus been shown that simple elements such as inserts, screens, and insulating pyrolytic graphite components can be used in irradiating carbon materials in the VVR-M reactor to produce temperatures between 70-90 and 800°C in a single tube without evacuating the specimens.

LITERATURE CITED

1. N. F. Pravdyuk et al., in: Effects of Nuclear Radiations on Materials [in Russian], Izd. Akad. Nauk SSSR, Moscow (1962), p. 34.
2. I. Snepvangers, RCN-INT 65-095, Petten (1965).
3. V. I. Karpukhin and V. A. Nikolaenko, Temperature Measurement with Irradiated Diamonds [in Russian], Atomizdat, Moscow (1971).

NEUTRON-SPECTRUM STRUCTURE NEAR A RESONANT ABSORPTION LINE

A. I. Dod', I. M. Kisil',
and I. P. Markelov

UDC 539.125.5.173.162.3

When neutrons from a δ-type source are moderated in an unbounded elastically scattering medium [1], one gets Plachek oscillations, namely oscillations about the asymptotic value. If one takes a negative source as the perturbation, namely an absorption resonance of finite width, then this leads to averaging of the oscillations over the width of the resonance. Moreover, if this negative source is localized, as in a heterogeneous reactor, the oscillation effect will decay away from the source.

Here we report experiments and calculations on the deviation of the neutron flux after the first collision from the asymptotic distribution in a uranium–graphite lattice at energies below the 6.68-eV resonance in ^{238}U.

The maximum energy loss on scattering of a 6.68-eV neutron of carbon transfers the neutron to the main resonance of gold at 4.9 eV, which allows one to use the activation of gold indicators to record the radial distribution of the neutron flux below the 6.68-eV resonance in ^{238}U. The flux distribution for the asymptotic spectrum below that resonance was measured from the activation of ^{115}In, which has its main resonance at 1.49 eV.

The experiments were done with a uranium–graphite reactor having a lattice step of 20 × 20 cm and fuel rods in the form of natural metallic uranium of diameter 3.5 cm [2]. There was a gap of thickness 4.5 mm between the uranium and the graphite, which was partly filled with aluminum. The activity distributions for ^{115}In and ^{197}Au were used to determine the coefficient K_p^e, which represents the reduction in the neutron flux in the region of the first-collision energy after the 6.68 eV resonance of ^{238}U, by comparison with the flux in the asymptotic spectrum as a function of distance r_i from the fuel rod:

$$K_p^e = \frac{[A(r_i)/A(r_0)]_{In} - [A(r_i)/A(r_0)]_{Au}}{[A(r_i)/A(r_0)]_{In}}, \quad (1)$$

where r_0 is the distance from the center of the uranium rod to the cell boundaries.

A connection was applied for the neutrons absorbed in the ^{235}U by using rods containing 2 and 0.71% ^{235}U, and also containing partly depleted uranium. Then the values of $A(r_i)/A(r_0)$ for each point were extrapolated to zero ^{235}U content. Measurements with the 2%-enriched uranium and the depleted uranium were performed with inserts of height 240 mm, which were placed in the central cell as part of a rod of natural uranium. The detectors of diameter 14 mm were surrounded by cadmium of diameter 20 mm and thickness 0.5 mm for irradiation. The thicknesses of the ^{197}Au and ^{115}In detectors were respectively 1.3 and 1 mg/cm^2. Figure 1 shows the distribution of the activities of ^{115}In and ^{197}Au along the radius for zero-enrichment uranium, together with the value of K_p^e.

We determined from theory the nonasymptotic deviations of the flux due to the negative source (resonance at 6.68 eV in ^{238}U) from the activity difference in gold detectors in a heterogeneous cell with and without correction for the finite energy transferred to the carbon. The neutron flux was derived by the usual method of determining neutron spatial and energy distribution [3]; this involves solving integral equations for many layers, which are linked by the first-collision probabilities. The energy structures of the interaction cross sections throughout the energy range were recovered in terms of the known or mean statistical parameters of the resonances. The calculations were performed twice for each cell with the above uranium enrichments: with an exact scattering core for the carbon and with a hydrogen-type core. The results were extrapolated to zero

Translated from Atomnaya Énergiya, Vol. 40, No. 5, pp. 425–426, May, 1976. Original article submitted May 4, 1975.

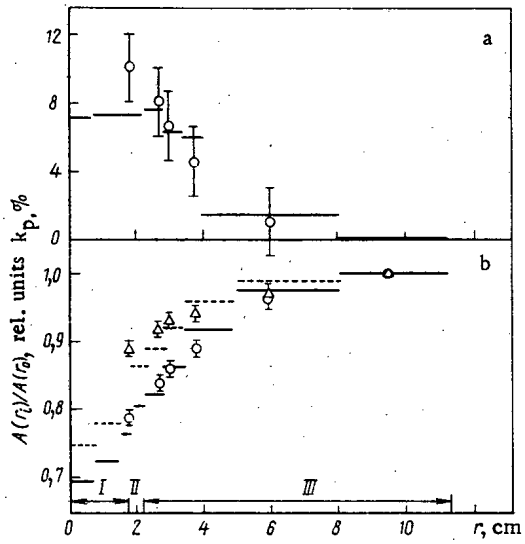

Fig. 1

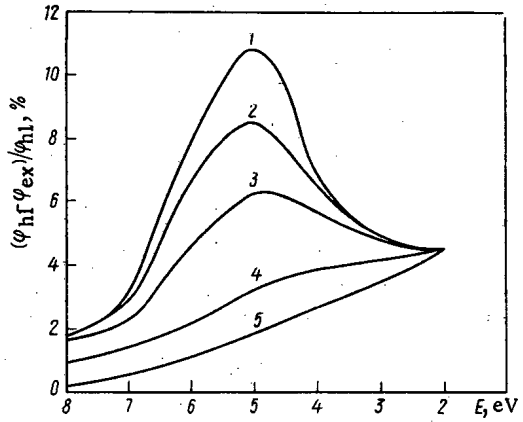

Fig. 2

Fig. 1. Radial distribution of K_p and activity in gold and indium detectors: a) K_p: ——) K_p^t; ○) K_p^o; b) activity. Calculations: ——) exact; ------) hydrogen-like scattering. Measurements: ○) gold; Δ) indium; I) uranium; II) gap; III) graphite.

Fig. 2. Energy dependence of the difference between the neutron fluxes for exact and hydrogen-like scattering for moderator layers at distances (cm) from cell center of: 1) 2.2-2.8 cm; 2) 2.8-3.4 cm; 3) 3.4-4.9 cm; 4) 4.9-8.0 cm; 5) 8.0-11.3 cm.

uranium enrichment. Figure 1 shows the calculated activity distributions for the gold detectors for the exact and hydrogen-like cores for zero-enriched uranium, together with the K_p^e, determined from the activities.

Figure 2 gives the ratios of the flux differences for the hydrogen-like case φ_{hl} and the exact case φ_{ex}, in each case with respect to the flux in the hydrogen-like case.

It is clear that there is no asymptotic deviation of the first-collision neutron flux in a urainium-graphite assembly on account of the 6.68-eV resonance in ^{238}U, which reduces the neutron flux and thus the activation of the gold by about 10% near a fuel rod and within it. The deviation falls to zero as one recedes from the rod. The actual deviation must be larger, as Fig. 2 shows, as the maximum capture cross section for the resonance in gold is somewhat shifted with respect to the minimum in the effect for the nonasymptotic deviations.

These results thus show that the neutron flux has a complex structure in a heterogeneous material near a resonance. Apart from the direct neutron depletion by the resonance, and the associated flux depression near the resonance, there is a substantial flux depression away from the resonance throughout the cell on account of a marked reduction in the overall neutron flux density.

This deviation in the flux density past the 6.68-eV resonance in ^{238}U must be allowed for in interpreting measurements with gold detectors in heterogeneous systems if the moderator is oxygen, carbon, or beryllium, especially when the fuel contains ^{238}U.

If the moderator produces a neutron-energy change comparable with the effective width of the ^{238}U resonances, deviations will occur even within the resonance, which will produce the neutron flux in it and hence the resonance integral. Our calculations indicate that a uranium–graphite reactor with a 20 × 20 cm lattice and fuel rods of natural metallic uranium of diameter 3.5 cm should give 9% fall in the effective resonance integral for the 6.68-eV resonance of ^{238}U on account of the nonasymptotic deviation. If necessary, the effects of the deviations on the measured effective resonance integral can be eliminated by surrounding the uranium block by a cavity [4].

We are indebted to B. G. Dubovskii for assistance in organizing the experiments, to E. B. Pugacheva for assistance in the calculations, and to V. V. Orlov and G. Ya. Rumyantsev for valuable discussions.

LITERATURE CITED

1. G. Plachek, Phys. Rev., 69, No. 9-10, 423 (1946).
2. Yu. Yu. Glazkov et al., At. Énerg., 11, No. 1, 5 (1961).

3. A. I. Dol', Izv. Akad. Nauk BSSR, Ser. Fiz. Énerg. Nauk, No. 3, 5 (1972).
4. E. Hellstrand, J. Appl. Phys., 28, 1493 (1957).

CALORIMETER MEASUREMENT OF THE HEAT RELEASED BY IRRADIATED NUCLEAR FUEL

A. P. Kirillovich, P. S. Gordienko, and V. P. Buntushkin

UDC 621.030.59:621.039.526

Calorimetric methods are widely used in nuclear power for research in materials science, radiation damage, and radiation energy measurement for radioactive decay [1]. Considerable importance attaches to calorimetric measurement of the heat released by irradiated fuel and other radioactive materials, since existing computational methods are fairly laborious and of poor accuracy (±20%) on account of lack of reliable evidence on the radioisotope composition of fission products and also nuclear constants. The subject is of particular interest for fast reactors, which are of high energy output per unit volume and high residual heat release in the fuel.

Here we consider a design of a calorimeter intended for remote measurement of heat release from fuel rods and other radioactive materials; results are presented for irradiated rods from the BOR-60 reactor.

Construction. The following major specifications form the basis of the design: simplicity and reliability under the conditions of remote operation in a hot cell; high and constant sensitivity over a wide range of heat outputs, and unvarying performance in the presence of intense α, β, and γ radiations. Conduction-type calorimeters (Calvet type) [2] meet these requirements most completely. A double (differential) calorimeter of this type (Fig. 1) was built for measuring the specific heat output from radioactive materials.

The calorimeter unit proper was a copper cylinder having two holes each of diameter 30 mm containing Chromel–nickel thermobatteries, which were insulated from the copper block by mica inserts of thickness 0.1-0.2 mm. The sample of radioactive material in a copper tube was placed in one of the ceramic tubes, which were closed by heat-insulating plugs. Around each tube there were 12 thermobatteries, which were connected in series and served to monitor the heat flux.

A thermobattery was a mica substrate of size 30 × 10 × 0.8 mm on which there were 30 turns of Chromel wire of diameter 0.3 mm; a layer of nickel of thickness up to 100 μ was deposited electrolytically on one side of the substrate on the Chromel wire. See [3] on the technique of making such thermobatteries. The calorimeter unit with its thermal insulation was placed within the body and set up in the shielded cell on a rotating stand. The calorimeter was served by manipulators. The measuring system consisted of an F-116 dc amplifier, interface unit, and ÉPP-09 recording potentiometer. The minimum measurable heat output was $0.9 \cdot 10^{-7}$ W.

The maximum sensitivity was dependent on the number of thermobatteries used, as well as on the diameter of the Chromel wire, the thermophysical characteristics of the insulators between the batteries, and the performance of the secondary instruments such as the amplifier and recorder. The best performance in our system was represented by a calibration factor of $0.5 \cdot 10^{-7}$ W/mm.

The thermo-emf developed by a battery is

$$E = \frac{K\varepsilon}{\lambda} \Phi,$$

where K is the fraction of the heat flux passing through the battery, ε is the thermo-emf of the Chromel–nickel couples, λ is the thermal conductivity of the material, and Φ is the heat flux from the calorimeter cell.

Translated from Atomnaya Énergiya, Vol. 40, No. 5, pp. 427-428, May, 1976. Original article submitted May 4, 1975; revision submitted July 7, 1975.

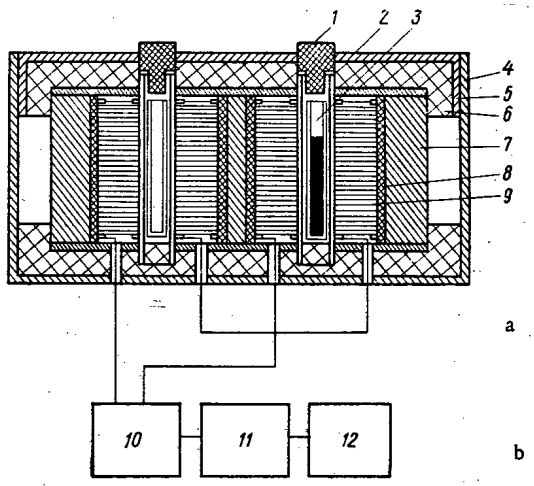

Fig. 1

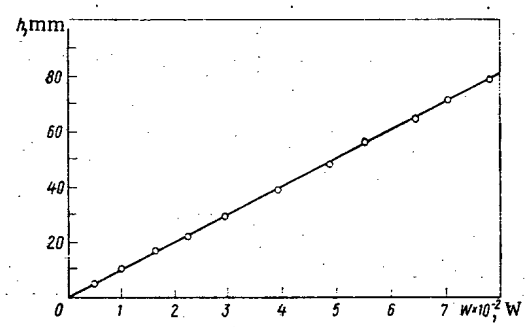

Fig. 2

Fig. 1. a) Calorimeter unit; b) measuring system for energy release in fuel assemblies and processing products: 1) insulating plugs; 2) ceramic tube; 3) ampule with specimen; 4) body; 5) lid; 6) insulating disks; 7) copper block; 8) liners; 9) thermopiles; 10) dc amplifier; 11) matching unit; 12) pen recorder.

Fig. 2. Instrument reading as a function of thermal power produced in calorimeter chamber.

All the major working characteristics were determined before the measurements were started, in particular the sensitivity and time-constant for heat loss from the calorimeter cell. The sensitivity was determined with a standard electrical heater placed in the working volume. The current and voltage to the heater were measured with classical M-82 instruments. The known power input went with the readings of the recorder (ÉPP-09 potentiometer) in the steady state to give the sensitivity as

$$K = W/h,$$

where W is the power deposited in the working volume in W and h is the instrument reading in mm.

Figure 2 shows that the sensitivity remained constant for heat outputs between the milliwatt and watt levels. The time constant was found graphically by the method of [2] and was 1.5 min for our conditions.

The irradiated fuel specimen was prepared for measurement as follows. After the assembly had been extracted from the reactor and the sheath had been removed from the fuel rod, the fuel in the form of tablets or granules was carefully mixed, and an average sample of about 10 g was taken from a mass of 300 g by repeated quartering, this then being ground up and further mixed. Small weighed amounts of this sample (100-2000 mg) were placed in copper tubes, which were weighed on remote-controlled balances to 0.001 g and transmitted for measurement of the residual heat release.

The error in determining the specific thermal power output from irradiated fuel materials is dependent on many factors such as the error in the output instrument readings, error in measuring the current and voltage to the calibrated heater, and the mass of the sample.

The specific thermal power output from any radioactive product or any heat-producing source generally is defined by

$$P = \frac{UI}{h}\frac{h'}{m},$$

where I and U are the current and voltage to the calibration heater, and h and h' are the readings of the output instrument during the sensitivity determination and the output measurement, with m the mass of the sample.

The maximum relative error in determining the specific heat output was calculated from

$$\frac{\Delta P}{P} = \frac{\Delta U}{U} + \frac{\Delta I}{I} + \frac{\Delta h}{h} + \frac{\Delta h'}{h'} + \frac{\Delta m}{m}$$

and did not exceed ±5% for our conditions. This error remained constant over wide ranges in the heat output. The limits to the use of the device for measuring the output in watts with an error not exceeding ±5% are governed by the linear part of the relation of sensitivity to heat putput.

Results. This apparatus has been used to measure the specific heat output for irradiated fuel from the BOR-60 reactor after various irradiation times; the output after a burnup of 89,226 MW-day/ton U after operation for 452 effective days and cooling for 3 months was 95.8 W/kg (mean of 5 measurements). Fuel from the end screens gave only 5% of the thermal power quoted above for the core fuel. When the cooling times were increased to 6 and 10 months respectively, the specific heat output for core material fell to 25.0 and 16.9 W/kg respectively. The operation was also tested on specimens of high-activity materials, with specific heat outputs from 0.1 to 550 W/kg.

The system has been operated for 2 yr in a shielded cell and subject to α, β, and γ radiations; no changes have been detected in the characteristics such as the sensitivity and time constant.

LITERATURE CITED

1. V. M. Kolyada and V. S. Karasev, Reactor-Radiation Calorimetry [in Russian], Atomizdat, Moscow (1972).
2. E. Calvet and H. Prat (editors), Recent Progress in Microcalorimetry, Pergamon Press (1963).
3. P. S. Gordienko et al., in: Machines and Instruments for Materials Testing [in Russian], Moscow (1971).

STRUCTURAL CHANGES IN IRRADIATED DYSPROSIUM TITANATE

V. M. Kosenkov, T. M. Guseva,
S. A. Alekseeva, and V. K. Nevorotin

UDC 621.039.53

As nuclear-power engineering has progressed, the workload and the length of the operating period of nuclear reactors have been steadily increased. At the same time, greater demands have been placed upon the absorbing materials used in the reactors. One promising development is the use of rare-earth metal (REM) compounds as absorbing materials. However, REM oxides are unstable in water, and react to form hydroxides, which leads to an increase in absorbent volume. One method of increasing the corrosion resistance is to stabilize the REM oxides with oxides of tungsten, titanium, etc. [1, 2]. This leads to the formation of compounds MeO_x, $n \cdot Me''O_y$, which are stable in aqueous medium and have no polymorphic transformations in the range 20-1000°C. Change in volume accompanies structural transformations induced on irradiation, but for REM compounds no information is available on this subject.

Materials and Method. Samples of $Dy_2Ti_2O_7$ were obtained in tablet form (diameter 7 mm, height 10 mm), by pressing together powders of the appropriate oxides and then sintering under the conditions given in [3].

Samples sealed in a hermetic stainless-steel ampule were irradiated for 328 days in the active zone of a VK-50 reactor. The flux of fast neutrons was $1.4 \cdot 10^{13}$ neutrons/cm^2 · sec and the total flux $3.6 \cdot 10^{20}$ neutrons/cm^2; for thermal neutrons, the corresponding figures were $1 \cdot 10^{12}$ neutrons/cm^2 · sec and $2.8 \cdot 10^{19}$ neutrons/cm^2. The temperature of the samples was ~ 500°C. The samples were heated as a result of the occurence of the (n, γ) reaction and of γ absorption in the active zone. The indicated temperature was achieved by introducing radial gaps between the samples and the ampule.

The irradiated samples and the reference samples were investigated on a long-range dilatometer, the linear dimensions were measured, and an x-ray analysis was carried out on a DPD-4 long-range diffractometer (K_α Cu radiation).

Results and Discussion. X-ray photographs of unirradiated samples (Fig. 1a) show the presence of a solid solution of Dy_2O_3 in $Dy_2Ti_2O_7$. It is known [4] that the compound $Dy_2Ti_2O_7$ of pyrochlore type can dissolve large quantities of Dy_2O_3. The lattice parameter for the unirradiated crystal is a_{ini} = 10.121 ± 0.004 Å, which

Translated from Atomnaya Énergiya, Vol. 40, No. 5, pp. 428-431, May, 1976. Original article submitted May 15, 1975.

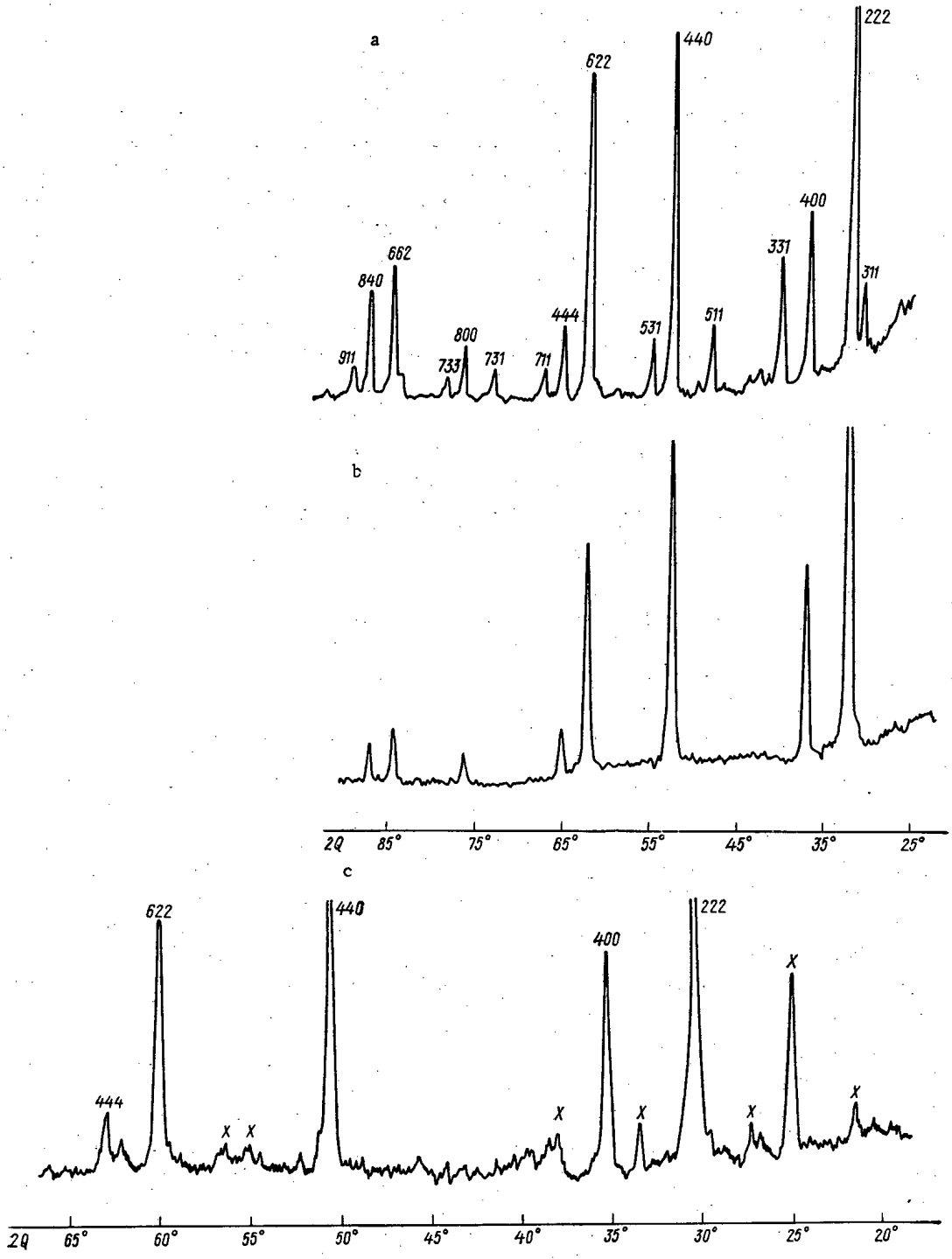

Fig. 1. X-ray diagrams for $Dy_2Ti_2O_7$: a) unirradiated sample; b) irradiated sample; c) irradiated sample with the presence of x phase.

corresponds to 34 mole % Dy_2O_3. Irradiation leads to considerable structural changes in the crystal lattice. The most pronounced effect on the x-ray photographs of the irradiated samples is the complete elimination of lines with odd indices (Fig. 1b). At the same time there is a redistribution of the intensity of the remaining lines. Measurement of the shift in these lines (10.62) and (12.00) shows that after irradiation the lattice parameter increases by 1% (a_{irr} = 10.222 Å).

Two methods were used to determine the change in the external dimensions of the sample after irradiation: direct measurement using a micrometer, and dilatometric analysis. Measurement of the length of the same sample before and after irradiation revealed an increase of 1 ± 0.02% in the external dimensions. For the dilatometric analysis, irradiated and unirradiated samples were heated to 1000°C. An increase of 1% in the

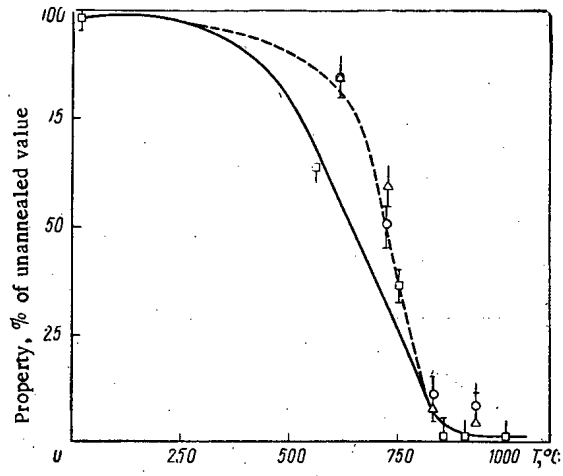

Fig. 2. Effect of annealing on properties of irradiated $Dy_2Ti_2O_7$: ○) lattice parameter; □) elongation of sample; Δ) ratio of line intensities (I_{331}/I_{400}).

linear dimensions was established by this method also. Thus, the swelling of the samples under irradiation was the result not of cracking nor of pore formation, but of increase in the parameter of the crystal lattice due to structural transformations.

The x-ray diagram of the irradiated sample in Fig. 1b corresponds to the fluorite lattice. It is known [4] that $Dy_2Ti_2O_7$ at high temperatures dissolves Dy_2O_3 with gradual transition from pyrochlore to fluorite structure. At 1700°C 52.4 mole % Dy_2O_3 is dissolved, and the structure is completely transformed to fluorite with lattice parameter 10.36 Å. Irradiation may lead to a change in the transition temperature [6, 7], and a configurational change in the structure [5]. However, the x-ray diagrams of a number of irradiated samples contain new lines (Fig. 1c), indicating decomposition of $Dy_2Ti_2O_7$ and the formation of a new phase. It was not possible to identify the new lines. However, although x-ray photographs were not taken for all the samples before irradiation, there is indirect proof that these lines are the consequence of irradiation. On annealing, these additional lines, like other aftereffects of irradiation, gradually disappear and the x-ray diagram is restored to its initial form (see Fig. 1a). Small differences (see Fig. 1b-c) may also result from variations in the conditions of irradiation of the samples in different parts of the ampule or from certain differences in the conditions in which the samples were prepared.

In Fig. 2 changes in the properties of the irradiated samples on annealing are shown. At 600-700°C the linear dimensions are restored more rapidly than the x-ray characteristics but at higher temperatures the two rates become equal. Annealing for 2 h at 815°C removes 90% of the increase in the lattice parameters and at the same time the intensity of the lines of the pyrochlore structure is restored, the additional lines disappear, and the sample dimensions are restored.

The results obtained indicate that irradiation of dysprosium titanate leads to structural transformations that are associated with a significant change in volume ($\Delta v/v = 3\%$). This is very important in considering the dimensional stability of the absorbing core in the moderator rods and shielding of atomic reactors. It is necessary to investigate these effects in order to find materials that undergo minimal change in volume on irradiation.

LITERATURE CITED

1. R. Crick, N. Berard, and D. Wilder, J. Nucl. Mater., 27, No. 1, 97 (1968).
2. C. Leitten and R. Beaver, Nucl. Appl., 4, No. 6, 398 (1968).
3. V. E. Réi, Production of Moderator Rods for Nuclear Reactors [in Russian], Atomizdat, Moscow (1965), p. 246.
4. N. A. Toropov et al., State Diagrams for Silicate Systems [in Russian], No. 1, Nauka, Leningrad (1969).
5. E. V. Kolontsova and É. E. Kulago, Kristallografiya, 17, No. 6, 1197 (1972).
6. O. Hauser and M. Schenk, Phys. State Solid, 18, 547 (1966).
7. M. Schenk, Phys. State Solid, 36, K101 (1969).

SEPARATION OF ISOTOPIC MIXTURES OF HYDROGEN IN THE HYDROGEN – PALLADIUM SYSTEM

B. M. Andreev, A. S. Polevoi, and O. V. Petrenik

UDC 621.039.3:546.11.02

The two-component system consisting of molecular hydrogen and hydrogen dissolved in palladium is characterized by a high value of the equilibrium coefficient α for the separation of hydrogen isotopes [1-4], if the volume of the palladium is much greater than that of the hydrogen [1]. In consequence, many authors regard this system as promising for use in the separation processes associated with the localization and concentration of tritium [4, 5]. However, in the literature there is a lack of information on the kinetics of isotopic exchange, which is required in order to determine optimal conditions for the separation of hydrogen isotopes in counterflow columns. The aim of the present paper is to study the effects of the basic parameters of the separation process (temperature, pressure, load) on the rate of interphase isotopic exchange.

Procedure for Investigating the Kinetics of Interphase Isotopic Exchange. The method used to study the kinetics was to make incremental changes in the concentration at the column inlet of one of the components being separated, and to measure the change in the edge of the substance at the outlet [6]. A diagram of the apparatus is given in Fig. 1. The main part is an exchange column (length 80 cm, diameter 5 mm) filled with palladium black of grain size 0.3-0.5 mm. After preliminary heating and evacuation by a prevacuum pump, the palladium black was saturated with hydrogen of known isotopic composition, held in a calibrated glass vessel. From measurements of the pressure in the glass vessel, the capacity of the palladium black for hydrogen was determined. The hydrogen blown through the column (a mixture of protium with deuterium or tritium) was first passed through a system of traps cooled with liquid nitrogen, and its pressure and temperature were maintained by means of a manostat and an electrical heating coil. The gas flow rate was monitored using a rheometer. The pressure in the apparatus was held constant by means of a pressure regulator and was measured using a mercury manometer. Samples to be tested for deuterium were taken by means of a tap and an ampule, and analyzed spectrographically on a DS-1 monochromator [7]. Samples to be tested for radioac-

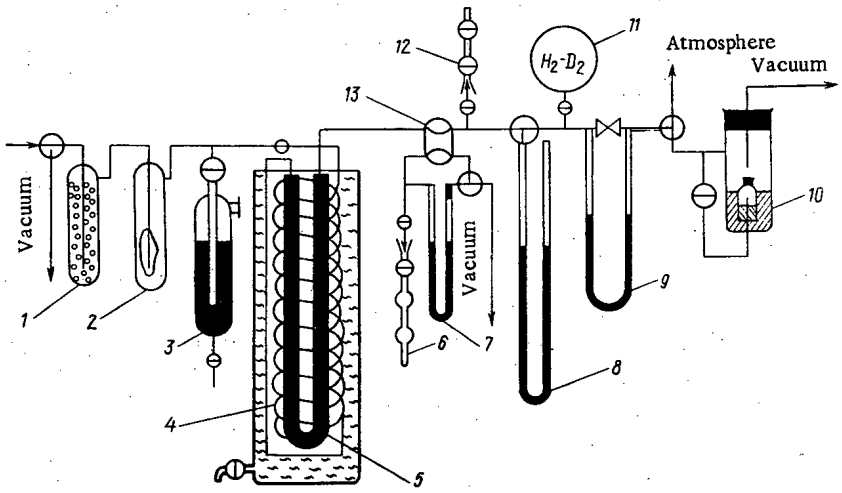

Fig. 1. Diagram of the apparatus: 1, 2) system of cooled traps; 3) manostat; 4) heating coil; 5) exchange column; 6) ampule; 7) manometer; 8) mercury manometer; 9) rheometer; 10) pressure regulator; 11) calibrated glass vessel; 12) flow ampule; 13) tap.

Translated from Atomnaya Énergiya, Vol. 40, No. 5, pp. 431-433, May, 1976. Original article submitted May 21, 1975; revision submitted January 15, 1976.

TABLE 1. Effect of Load w and Pressure P on Efficiency of Separation of Hydrogen–Deuterium mixtures at 19-25 and 100°C

T°, C	P, mm Hg	w, cm/sec	HTU, cm
100	737	1,14	1,0±0,7*
100	735	2,84	1,3±0,7
100	735	7,10	1,0±0,7
100	737	9,94	2,4±1,0
21 †	750	1,76	1,3±1,0
25 †	732	2,76	2,8±1,0
25 †	750	3,74	2,4±0,7
23 †	770	3,74	2,8±1,0
20	747	4,54	2,6±0,7
21	745	5,68	2,5±1,0
21	746	10,65	2,7±1,0
25	750	10,65	2,8±1,0
21	750	14,75	2,7±0,7
22	540	16,60	2,3±0,7
20	522	15,50	2,9±1,0
19	500	18,30	3,2±1,0
22	422	17,10	2,4±0,7
19	200	7,36	2,3±0,7
21	746	9,35	3,2±1,0

*The error in the value of HTU found from the yield curve of protium washed from palladium is less than in the inverse experiments.

†Experiments conducted in a column of length 64 cm and diameter 6 mm.

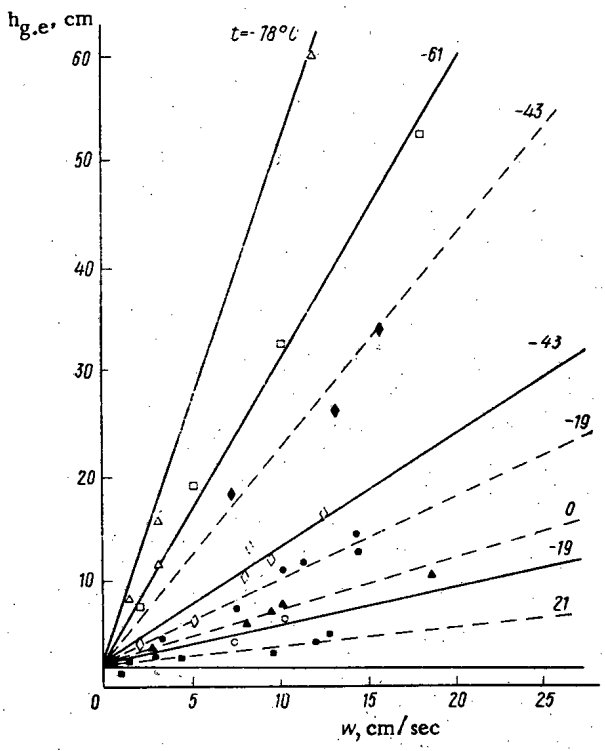

Fig. 2. Dependence on load w of HTU for the separation of hydrogen–deuterium and hydrogen–tritium isotopic mixtures.

tive tritium were taken in a flow ampule and measured using an SBM-8 gas-filled counter working in the saturation mode.

Results for External-Diffusion Kinetics. The dependence of the rate of interphase isotopic exchange on load and pressure was investigated at temperatures between 20 and 100°C for hydrogen–deuterium isotopic mixtures. From the results (Table 1) it is evident that, regardless of the load w and pressure P, the height

corresponding to transfer unity (HTU) calculated from the change in gas concentration is $h_{g.e} \approx 2$ cm. Evidently, the mass-transfer process is limited by the diffusional resistance in the gas phase, and the diffusional coefficient of external mass release β_g is a linear function of the load. This conclusion drawn from the data of Table 1 regarding the limiting stage of the interphase isotopic exchange is confirmed by the results of [8], in which change of temperature in the range 20-40°C was found to have no effect on the efficiency of chromatographic separation of hydrogen isotopes on palladium, and also by the experimental data obtained on the separation of the isotopes H_2 and D_2 in a column of diameter 3 mm filled with palladium black of grain size 1.0-1.5 mm. At pressure P = 760 mm Hg, linear gas velocity w = 3.0 cm/sec, and temperature 20, 40, and 60°C, the degree of separation was, respectively, 121, 86, and 53.4; taking into account the temperature dependence of the separation coefficient α according to [2], this corresponds to a constant value of HTU.

Kinetics in the Internal-Diffusion Region. Experiments at negative temperatures showed a sharp deterioration in the efficiency of mass exchange. In Fig. 2 results are shown for experiments at negative temperatures for hydrogen–deuterium (continuous lines) and hydrogen–tritium (dashed lines) isotopic mixtures. Starting from the additive relations between the total coefficient of mass exchange K_g and the coefficients determining the external and internal diffusional resistance, $1/K_g = 1/\beta_s + \alpha/\beta_g$, we consider the diffusional components of the HTU

$$h_{g.e} = h_g + \alpha h_s/\lambda = h_g + \alpha G/\beta_s a S,$$

where $h_g = G/\beta_g aS$; $h_s = L/\beta_s aS$; G, L are the fluxes of gaseous hydrogen and of hydrogen dissolved in palladium, kmole/h; S is the column cross section, m^2; a is the specific surface of phase contact, m^2/m^3; λ is the ratio of fluxes ($\lambda = L/G$); β_s is the coefficient of internal mass release, kmole/m^2.

Since h_g = const, a linear dependence of $h_{g.e}$ on the value of G should be observed. The slope of the straight line will depend upon the ratio $\alpha/\beta_s a$, i.e., with increase in the internal-diffusion stage of mass transfer and the phase-contact surface (or with increase in α), the dependence of $h_{g.e}$ on the load becomes weaker (Fig. 2).* The dependence of log ($\beta_s a$) on 1/T was used to determine the value of the activation energy for the internal-diffusion process, the limiting stage of mass transfer at negative temperatures. For hydrogen–deuterium and hydrogen–tritium mixtures it was found to be 4.9 ± 0.4 kcal/mole, which is in good agreement with published values of activation energy for the diffusion of hydrogen atoms in β-phase palladium, obtained by different methods: 3.9 kcal/mole by NMR spectroscopy [9]; 6.8 kcal/mole electrochemically [10]; 5.7 kcal/mole from the permeability of palladium foil [11].

According to the date of [4, 11], deuterium atoms diffuse at a higher rate in palladium, and tritium atoms at a lower rate (the diffusion rate for the tritium is less by a factor of approximately 1.5 than that for deuterium). The ratio of coefficients of internal mass release in the separation of hydrogen–deuterium and hydrogen–tritium isotopic mixtures calculated at -19 and -43°C corresponds to the ratio of rates of diffusion of atomic deuterium and atomic tritium in β-phase palladium. From the results obtained it follows that a high efficiency of interphase isotopic exchange can be obtained only if internal-diffusional resistance is absent. In this case, HTU is almost independent of temperature, pressure, and load, and the optimal conditions for separation correspond to the largest linear velocity of the gas for which there is no negative effect due to longitudinal mixing.

LITERATURE CITED

1. E. Wicke and G. Nernst, Bunsenges. Ber., Phys. Chem., 68, 224 (1964).
2. M. M. Domanov, B. M. Andreev, and S. É. Gil'burd, Trudy MKhTI im. D. I. Mendeleeva, 67, 104 (1970).
3. B. M. Andreev and M. M. Lomanov, Zh. Fiz. Khim., 49, No. 5, 1260 (1975).
4. G. Sicking, Bunsenges. Ber., Phys. Chem., 76, No. 8, 790 (1972).
5. Tritium Control Technology, N AT-33-1-GEN-53, US Atomic Energy Commission (1973).
6. M. S. Safonov, V. K. Piryaev, and V. I. Gorshkov, Zh. Fiz. Khim., 44, No. 4, 975 (1970).
7. E. S. Neduma et al., Isotopenpraxis, 6, No. 11, 211 (1970).
8. J. Hoy Science, No. 161, 464 (1968).
9. K. M. MacKay, Hydrogen Compounds of the Metallic Elements, Spon, London (1966).
10. N. A. Galaktionova, Hydrogen in Metals [in Russian], Metallurgiya, Moscow (1967).
11. B. Bonn et al., Phys. Chem., 76, No. 12, 1213 (1972).

*The relative error in determining $h_{g.e}$ at negative temperatures is 10-15% on average.

MAGNETIC SUSCEPTIBILITIES OF BERYLLIDES

V. P. Gladkov, V. I. Petrov,
A. V. Svetlov, D. M. Skorov,
and V. I. Tenishev

UDC 621.317.412:549.2:546.45

Faraday's method has been applied with fields of 3-5 kOe at room temperature to measure the magnetic susceptibilities of two-component heterogeneous alloys of beryllium with rare-earth and other metals. Alloys made by arc melting contained $MeBe_{13}$, $MeBe_{12}$, or other higher beryllides. The magnetic susceptibility was a linear function of concentration (Fig. 1).

The relationship was extrapolated to the concentration of the corresponding beryllide to derive the atomic susceptibility χ_A for over 20 beryllides (Table 1). Beryllides of scandium, yttrium, cerium, neodymium, chromium, and iron were made specially. The χ_A derived by direct measurement agreed within the error of measurement with the extrapolated values. There was also agreement within 10-15% with published values for $CeBe_{13}$ [1], $EuBe_{13}$, and $YbBe_{13}$ [2].

Most of the rare-earth beryllides are high paramagnetics, as are the beryllides of vanadium, chromium, manganese, uranium, and thorium; the other compounds were weakly paramagnetic or diamagnetic.

Figure 2 shows the susceptibilities of rare-earth beryllides and oxides in relation to atomic number; the two curves are of the same form for the beryllides and oxides of the trivalent rare-earths, which shows that the rare-earths take the trivalent form in the beryllides. This agrees with data on the lattice parameters of beryllides [3] and the data of [1], which shows that cerium in its beryllide is trivalent and also partially tetravalent; Klemm's data [2] also show that europium and ytterbium are trivalent in their beryllides.

The analogy with the rare-earth oxides indicates that the atomic susceptibilities of the beryllides of praesodymium, promethium, and samarium should be $\sim +400 \cdot 10^{-6}$, $+150 \cdot 10^{-6}$ and $+70 \cdot 10^{-6}$ cgs magnetic units respectively.

Figure 3 shows the Z dependence of the magnetic susceptibility for ions of the 3d metals in ionic compounds and in the beryllides $MeBe_{12}$, Me_5Be_{21}, etc; transition-metal beryllides differ from ionic compounds in that the maximum susceptibility occurs at the middle of the transitional series.

Elements of the 4d and 5d series usually show magnetism weaker than that for the 3d metals in compounds; the measured susceptibility for niobium beryllide was close to zero. One expects that the beryllides of the 4d

TABLE 1. Atomic Susceptibilities of Beryllides at 293°K

Compound	χ_A, 10^{-6} cgsm units	Berryllide	χ_A, 10^{-6} cgsm units
$CaBe_{13}$	−10±2	$NdBe_{13}$	+390±5
$ScBe_{13}$	−0,5±0,5	$EuBe_{13}$	+350±50
$TiBe_{12}$	+8±2	$GdBe_{13}$	+2340±60
VBe_{12}	+22±2	$TbBe_{13}$	+3090±60
$CrBe_{12}$	+292±1	$DyBe_{13}$	+3600±50
$MnBe_{12}$	+78±2	$HoBe_{13}$	+3150±60
$FeBe_{12}$	+6±0,5	$ErBe_{13}$	+2460±50
$CoBe_{12}$	−3±2	$TmBe_{13}$	+1700±30
Ni_5Be_{21}	+12±2	$YbBe_{13}$	+480±10
$CuBe_3$	0,0±0,5	$LuBe_{13}$	−0,5±0,5
YBe_{13}	−0,2±0,5	$HfBe_{13}$	−10±2
$NbBe_{12}$	−3±2	$ThBe_{13}$	+160±10
$LaBe_{13}$	−0,7±1	UBe_{13}	+269±2
$CeBe_{13}$	+131±1		

Translated from Atomnaya Énergiya, Vol. 40, No. 5, pp. 433-434, May, 1976. Original article submitted June 25, 1975

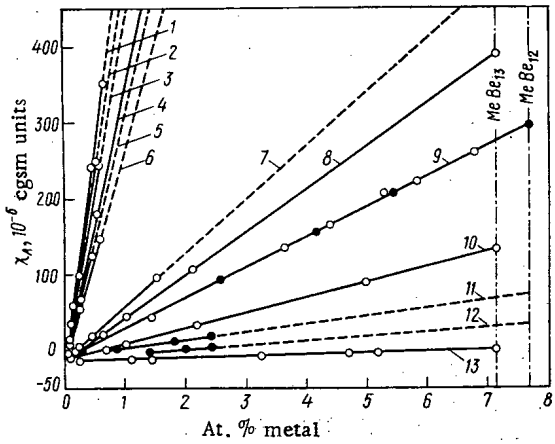

Fig. 1

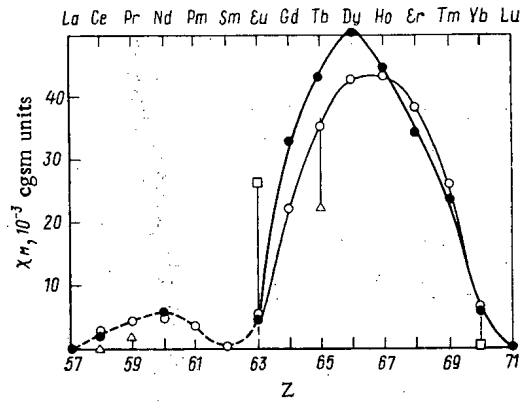

Fig. 2

Fig. 1. Concentration dependence of the atomic susceptibility for binary beryllium alloys at 293°K ($\chi_A = \chi A$, with χ the specific (mass) susceptibility and A the mean atomic mass of the alloy): 1) Be-Dy; 2) Be-Ho; 3) Be-Tb; 4) Be-Eu; 5) Be-Gd; 6) Be-Tm; 7) Be-Yb; 8) Be-Nd; 9) Be-Cr; Be-U; 10) Be-Ce; 11) Be-Mn; 12) Be-V; 13) Be-Y; Be-Sc; Be-Lu; ●, ○) alloys containing the phases $MeBe_{12}$ and $MeBe_{13}$.

Fig. 2. Room-temperature molar magnetic susceptibilities of rare-earth beryllides and oxides in relation to atomic number Z ($\chi_M = \chi M$, with χ the specific susceptibility and M the molecular weight of the compound); ○) $MeO_{3/2}$ (trivalent rare-earths) [4, 5]; Δ) the same for rare-earths showing valency +4 [4, 5]; □) the same for rare-earths showing valency +2 [4, 5]; ●) $MeBe_{13}$, our results.

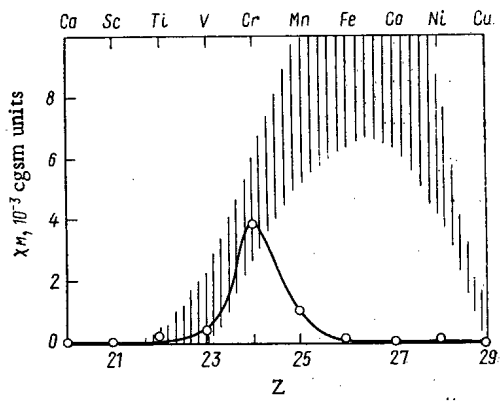

Fig. 3

Fig. 3. Magnetic susceptibilities at 293°K for transition-metal ionic compounds [4, 5] (hatched region) and beryllides (solid line).

and 5d metals will be found to be weak paramagnetics or diamagnetics.

These results can be utilized in research on the physical properties of alloys and compounds, and also in physicochemical analysis of beryllium alloys.

LITERATURE CITED

1. G. Olcese, Atti. Acad. Lincei, Rend. Sc. Fiz Mat. e Nat, 40, 1052 (1966).
2. W. Klemm and W. Mühlpfordt, J. Rev. Chimie Minerale, 5, 561 (1968).
3. P. I. Krysyakevich et al., Kristallografiya, 8, 595 (1963).
4. P. W. Selwood, Magnetochemistry [Russian translation], Izd. In. Lit., Moscow (1958).
5. Ya. G. Dorfman, Structure and Magnetic Properties [in Russian], GTTL, Moscow (1955).

CONFERENCES AND MEETINGS

RADIOCHEMISTRY AND NUCLEAR TECHNOLOGY AT THE 11TH MENDELEEV CONGRESS OF GENERAL AND APPLIED CHEMISTRY

É.V. Renard

The 11th Mendeleev Congress on General and Applied Chemistry took place Sept. 22-26, 1975 in Alma-Ata. The Congress, which was organized by the Academy of Sciences of the USSR and the Academy of Sciences of the Kazakh SSR, the Department of the Chemical Industry of the USSR, and the Mendeleev All-Union Chemical Society, was devoted to the basic problems of modern chemistry and chemical technology.

About 2500 delegates and guests, among them 200 foreign scientists, participated in the Congress. More than 900 reports were presented, read, and discussed in the plenary and sectional sessions. The abstracts of the reports (more than 1500) were published by Nauka Press (Moscow, 1975) in the form of sectional collections of papers.

Sixteen sections convened: organic chemistry and technology of organic substances, biochemistry, physical chemistry, chemical physics and catalysis, geochemistry and cosmochemistry, analytic chemistry, chemistry and technology of high-molecular compounds, theoretical principles of chemical technology, electrochemistry, chemistry of metals and metallurgy, petroleum chemistry, chemistry and technology of silicates, chemistry in agriculature, and chemical literature and chemical education.

The section "Radiochemistry and Nuclear Technology" (presided by Academician B. P. Nikol' skii) appeared for the first time on that Congress. Six sessions took place and more than 40 reports were presented and discussed; the reports concerned theoretical radiochemistry and the chemistry of radioactive elements, nuclear technology, analytic chemistry and the chemistry of preparations, and the chemistry of hot and new atoms.

Problems related to the theory of the structure of actinide compounds received great attention in this section. It could be concluded from investigations of the properties of the new compounds (complex nitrates and chlorides of tri- and tetravalent f elements, lanthanides and actinides, with organic cations, tertiary ammonium bases) that the degree of covalency of the bond increases in the series U(IV) <Np(IV) <Pu(IV). A theoretical explanation was given for the nonmonotonic drop of the strength of the An–O bond in AnO_2^{2+} in the series U–Np–Pu–Am. The progress and the development tendencies in the coordination chemistry of uranium were considered and a noticeable increase in the interest in the chemistry of penta- and trivalent uranium, organic uranium compounds, and the chemistry of uranium alloys was observed. For example, a volatile sandwich complex, uranocene, was recently obtained (by sublimation in vacuum at 150°C).

A large group of reports provided information on new actinide compounds. The chemical, thermal, and radiative properties of the new actinide fluorides NpF_5, PuF_5, and $NpOF_4$ and of the fluorides of hepta- (Np, Pu) and hexavalent (Np, Pu, Am) actinides were determined and described. The laws of the periodic system were used to determine and to prove a similarity to tantalum from the ^{243}Am reaction with neon nuclei of nilsborium in the form $NsBr_5$.

It was established that the residues resulting from the dissolution of metallic uranium, thorium, and plutonium in halogene hydride acids form a new class of coordination compounds, i.e., they are mixed oxygen-containing hydrides (oxo-, hydroxo-, and peroxohydrides, but no peroxides). Volatile adducts, namely hexafluoro-acetylacetonate and pivaloyl-trifluoro-acetonate of Am(III) with tri-n-butylphosphate, were obtained for the first time; there are chances for separating elements by using the volatility of intercomplex compounds of radioactive elements.

The chemism of extraction processes was treated in some of the reports. The suitability of fluorine and chlorine containing diluents for extraction was investigated. The search for and the production of a large number

Translated from Atomnaya Énergiya, Vol. 40, No. 3, pp. 435-438, May, 1976.

of phosphor-containing and nitrogen-containing cyclic and linear polydentate extractants are continued and their capability of extracting uranium, plutonium, and neptunium is examined. Extractants with high affinity to Pu(IV, VI) and even selective extractants for Pu(III) have been found (extractant with piperidyl radicals).

Despite the low selectivity, the efficiency of organic acids (in the extraction of ^{90}Sr) can be increased in various ways by increasing the separation coefficient of the pairs Sr–Ba and Sr–Ca to 12-14.

Several reports considered the mathematical description and the modeling of extraction processes and ion exchange. The quantitative description of the combined extraction of rare-earth elements in an extraction system using the Talspey process was successfully attempted. It was shown that there are good chances for the mathematical modeling of all the operations in the extraction technology of fuel element restoration. The mathematical analysis of the uranium and plutonium separation scheme with the so-called expulsive re-extraction was of great interest (no reducing agents are employed).

A semiempirical method of calculating the separation coefficients of trivalent rare-earth elements and transplutonium elements in extraction systems was developed. The method is based on the differences in the formation energies of metal complexes in the two phases. Progress was made in the mathematical description of the dynamics of the ion-exchange process in the separation of Am and Cm when data on the statics of sorption were used.

The kinetics of oxidation–reduction reactions, extraction and complex-formation in solutions, and the utilization of agents (ascorbic acid, hydrazine, hydroxyl amine) which do not form salts and which are suitable for the stabilization of the valencies of Np and Pu in the aqueous regeneration of fuel elements of atomic electric power stations were considered in detail. Important data on the kinetics of the reaction of Np(IV) with Pu(IV) were presented. The oxidation of Pu(IV) and other elements in a solution with ozone and the stability of ozone in nitrate media were investigated; ozone is a possible saltless stabilizer of the valency of actinides in the regeneration of the fuel elements of atomic electric power stations.

Problems related to the kinetics of extraction with the systems Pu(IV)–tri-n-octyl amine and Zr(IV)–tri-n-butyl phosphate were discussed. Investigations of the kinetics of extraction are of great importance for the regeneration of the fuel of atomic electric power stations by extraction in fast extraction units.

The re-extraction operations of metals from extractants can be accelerated by a preliminary reaction which takes place in the organic phase between the complex-forming agent introduced into the organic phase or the reducing agent and the metal. It is promising to make use of the differences in the kinetics of complex formation of metals in solutions with complicated complex-forming agents of the type of aminopolyacetic acids (DTPA, ÉDTA, NTA, and others).

Rare valency states (II, IV, VI, VII) of actinides were investigated, for example, the divalent state of the remote actinides (Cf, Es, Fm, Mv, 102) which was detected with the method of cocrystallization; this divalent state is a novel phenomenon. The stability of this state increases with increasing serial number of the element (in contrast to the second subgroup of lanthanides). However, beginning from Mv, the average valency of the actinides begins to increase again. New data were obtained on the ability of Am, Cm, Bk, Cf, Es, and Pm to be reduced to the divalent state in melts of halogenides. Heptavalent americium, which instantaneously oxidizes Np(VI) and Pu(VI) to the heptavalent state, was obtained and studied in an alkaline medium.

Some communications concerned the latest achievements in the radiochemistry and radiation chemistry of berkelium (the redox potential of the Bk(III)–Bk(IV) pair was measured); a method of selectively extracting Bk by separation from tetravalent cerium, zirconium, and plutonium was developed. Am(IV, VI) was electrochemically obtained in 10–15 M aqueous solutions of phosphoric acid; Am(VI) has greater stability in concentrated and diluted solutions of the acid than Am(IV). A method of applying neptunium and plutonium films on metal substrates from alkaline media has been developed.

The chemistry of melts of actinides was treated in several reports. The published data on the complex formation of actinides in chloride and fluoride salt melts were critically analyzed in relation to the agreement with the theory of the structure of coordination compounds.

The physicochemical properties and the electrochemical behavior of thorium and its compounds in melts of alkaline metal halogenides were studied. Mixed tertiary phosphates of Ce, Zr, Pu, U(VI, IV), and alkali metals were synthesized at 700–800°C in an NaCl–KCl melt.

Papers on the conversion of irradiated materials formed the largest group of reports. Liquid extraction is the dominating process in the practice of modern radiochemistry. Extensive investigations of improvements

in the extraction technology of fuel element regeneration of "warm" atomic electric power stations have been made (details of the components, scheme for heavy incombustible diluents, and experience gathered in the actual testing of a material). Interesting data concerned the overall dynamics to be expected and the optimal unit power of fuel-element regenerating plants.

The extraction technology of a complex scheme of converting exhausted fuel elements of an atomic electric power station with thermal neutron reactors was described (26 months cooling): One of the versions of the complex regeneration with separation of U, Pu, Np and even of Am, Cm, rare-earth elements, and Sr has been worked out in a pilot plant. The uranium, which had been extracted to 99.98%, was purified $5 \cdot 10^5$ times from plutonium and $1.5 \cdot 10^7$ times from fission products. Am, which had been evaporated from the aqueous end solution, Cm, rare-earth elements, and Sr were extracted into D2ÉGFK; after that, the successive selective re-extraction of strontium and of the transplutonium and rare-earth elements was performed; the yields were 95, 92, and 94%, respectively.

The possibilities and chances of using aqueous extraction for the regeneration of hot uranium–plutonium fuel from fast neutron reactors (oxides, carbides, nitrides, and others), but with promising compositions, were critically reviewed. The considerations ranged from the disassembly and stripping of the packages of fuel elements to the winning of fuel forms suitable for the production of new reactor charges. Stressed were the most important problems such as "insoluble rests," criticality in all operations, homogeneity of aqueous and organic solutions, removal of iodine, interprocess stabilization of plutonium and neptunium, trapping of tritium, (self-) evaporation of hot waste, investigations of the macrochemistry of plutonium and the basic fission products, etc.

Conversion by extraction of irradiated ^{241}Am (with three-month cooling time) results in ^{242}Cm. The conversion was made according to the scheme of amine extraction of plutonium and separation of transplutonium and rare-earth elements (separation coefficient $\sim 10^5$) in the system with the aid of the Talspey process (citric acid as buffer agent) and resulted in new, interesting data on the radiolytic stability of the extractant (D2ÉGFK) used in a closed cycle with an aqueous solvent of the activity 2000 Ci/liter and irradiated with a dose of 360 W·h/liter from the radiative oxidation of Pu(IV) and the α radiolysis of the extractant. A ^{242}Cm charge of 95% chemical purity and with a concentration of fission products below 0.1-1 Ci/kg was obtained. Extraction chromatography can be used to convert charges of irradiated Pu, Am, and Cm.

Promising is the method of separating uranium from fission products by dialysis via a liquid extracting membrane (tri-n-butyl phosphate on an inert carrier, e.g., Teflon). It is expected to obtain a coefficient of uranium purification from the γ activity of about 250 per cycle (passage).

Problems related to concentrating solutions of actinides by evaporation and dispersing actinide solutions were considered; the chemism of various versions of the sol–gel process (internal gelation, sol-maintaining coprecipitation, etc.) was also considered. A technique for obtaining monodispersed droplets of a concentrated (colloidal) actinide solution was developed and the conditions for washing the resulting spherical particles from the gel-forming media were also determined.

A new method of determining water-soluble highly inflammable products resulting from the nitration of organic diluents accumulated in the evaporation of the water-tail solution to be concentrated after the extraction of uranium and plutonium from the solution of the fuel elements was described. A reliable method of determining radioactive iodine (from the activity of the separated ^{129}I) in flows from the extraction work in the conversion of VVÉR fuel elements was developed and tested on real material.

Investigations of the radiation-chemical conversions of the purex process in a two-phase system were continued and, specifically, the behavior of radio zirconium and radio iodine were studied; reliable data for the capture mechanism of the radio iodine by the extractant (tri-n-butyl phosphate) were presented.

The report on the pyrochemical methods of nuclear fuel regeneration (Institute of Atomic Energy, Scientific-Research Institute of Atomic Reactions) gave important results of a fluorine-gas test regeneration of the uranium fuel of the fast-neutron BOR-60 reactor (burn-up to 11 at.%; cooling time 3 months). The work was done in a pilot plant.

The unexpected high volatility of cesium and the "nonvolatility" of the gaseous fission products during sweating, the nonfrittability of hot fluorides, i.e., fission products (165,000 Ci/kg, intrinsic temperature 320°C), the "wandering" of xenon (obviously, XeF_6) with uranium, and the volatility of cesium upon fluorination (CsF is nonvolatile) are among the interesting results. By performing sorption–desorption operations with a yield of 99.6%, it was possible to obtain UF_6 with a purification coefficient of 10^7 (10^8 from Ce and Ru; 10^{10} from Cs; and $4 \cdot 10^6$ from Xe). It was established that most of the plutonium left the fluorinating apparatus.

An analysis was made of the thermodynamic stability and the chemical activity of higher volatile fluorides of actinides which are important for the fluoride-gas regeneration of fuel elements, for the utilization of UF_6 in nuclear reactors, and for the plasma chemistry of actinides.

Reports which were concerned with the technology of fast neutron reactors with cooling by dissociating the gas N_2O_4 told of the fuel element corrosion which must be expected, the leaching of various fission products by nitrogen oxide, and the activation of the coolant (formation of ^{16}N, ^{18}F, etc.). Methods of purifying N_2O_4 from fission products, particularly from iodine, are being tested; a purification coefficient of $3.7 \cdot 10^3$ was obtained on a silver-silica gel column at an average gas extraction coefficient of 0.07. The important problem of the chemical forms of individual elements formed in an irradiated solid matrix was considered. More particularly, the form ^{13}N which is formed from carbon as an impurity in metals, fluorides, and oxides was considered.

Many papers reported on theory and practice of ion exchange and the purification of solutions from noxious impurities. Promising results were obtained by the use of natural sorbents (bentonites, zeolites) and polymer sorbents for purifying liquid waste of low activity (^{60}Co, ^{137}Cs). The physicochemical principles of the anion-exchange sorption of uranium from nitric acid were discussed.

Methods of identifying extremely small amounts of radioactive substances in natural objects were considered in relation to environmental shielding (combined preliminary chemical concentrating and increasing the sensitivity of the radiometric monitoring equipment); one must mention a new principle of preliminary concentration, namely the liquid extraction with fixation of the radionuclides in a developing organic solid phase. A potentially economic and promising application of inorganic thin-film sorbents was developed (for sewage, concentrating valuable components, and other purposes); the sorbents were obtained by applying sorbent films to inert granules (glass, sawdust, etc.). These sorbents are characterized by unusually high distribution coefficients, an almost 100% utilization of the volume, and fast sorption; the admissible transmission rates of the solution reach the extremely high values of 200-400 $ml/cm^2 \cdot min$ (!). For example, cesium can be completely extracted from diluted solutions by 1 g of the sorbent, when the solution volume is 1 m^3.

Analytic work in nuclear technology was extensively described. Coulometric methods of determining americium in the form Am(IV) (in the presence of curium and other elements) and a spectrophotometric method based on the Am(IV) band in the ultraviolet have been developed and implemented. A colorimetric analysis method for neptunium (sensitivity $5 \cdot 10^{-6}$ g/liter), new extraction methods for singling out and separating neighboring transplutonium elements, and new analysis methods with instruments (the method of α, γ coincidences allows americium determinations on a curium background up to 0.003% of the α activity of the curium) were developed and implemented. Substoichiometry in radioanalytical chemistry is expanded.

A new method of determining thorium impurities in uranium and plutonium by extraction and spectroscopy has been proposed (sensitivity $1 \cdot 10^{-4}$ mass%). The method of chromatographic concentrating and purifying of metals in combination with nuclear physics measurements using immersed silicon semiconductor α detectors will have many applications in applied radiochemistry.

A series of reports on the subject "The Chemistry of Hot and New Atoms" were presented to the section "Radiochemistry and Nuclear Technology." Problems of the modern chemistry of hot atoms, reactions of hot tritium atoms (including reactions on the surface of solids and in a crystal lattice), the formation of positronium in condensed media, the conditions for charge recombination on a track, the mechanisms of positronium attenuation and of the inhibition of positronium formation, as well as the relation between these mechanisms, the use of muonium in physicochemical research, the chemical aspects of the interaction of negative mesons with matter, the chemical aftereffects of the β decay in molecular systems, and the radiolytic behavior of recoil atoms and ions of actinide elements in aqueous solutions were comprehensively analyzed.

Results closely related to the main subjects of modern nuclear science and technology were reported to the other sections. The reports dealt with the thermodynamics of solid-phase reactions for obtaining heat-resistant compositions; solid solutions (low-temperature synthesis of refractory compounds); glass compositions; cermet compositions for fuel elements; the plasma-chemical synthesis of nitride powders; the production of new semiconductor materials; the cryochemical method of obtaining finely dispersed powders; processes of precipitation (synthesis) of inorganic materials from the gas phase; a new method of obtaining coatings and articles from electrolytically refined tungsten and tantalum; the production of extremely pure alloyed powders of steels and alloys of a given composition with the aid of the hydride-calcium process; the prediction of the properties of compounds and reactions which have not yet been investigated; and the development of new theories of the formation of liquation inhomogeneities.

An analysis of the thermodynamic constants of actinides (ranging from actinium to curium) and their

oxides was used to estimate unavailable data from the periodicity of the properties and the similarity of the properties of lanthanides and actinides. The mechanism of the dissociation of the oxides of all these actinides and their dissociation temperature and boiling points were determined by calculations.

Other data pertained to aerosol technology; laser chemistry; new methods of obtaining extremely pure substances (up to $\geq 10^{-8}$ mass % from nonelectrolytes); the state of radioisotopes in the subsoil water; the mathematical modeling and the physicochemical principles of distillation, crystallization, and osmosis; the mechanism of the chemical destruction of polymers in corrosive media; an automatic information retrieval system for radiochemistry; and the compilation of the corresponding computer dictionary.

In conclusion the 11th Mendeleev Congress summed up the achievements of chemical science and technology and noted on this occasion the accomplishments of the Russian radiochemical industry and the high level of the radiochemistry as a science in our country. The plan prospects within the framework of the 10th Five-Year Plan were outlined for the most important directions which are associated mainly with the development of nuclear power generation, environmental protection, automation of chemical processes, etc.

USE OF RADIOISOTOPE TECHNIQUES AND INSTRUMENTS IN MACHINE CONSTRUCTION

M. L. Gol'din

On Dec. 10-11, 1975 an applied-science conference on the utilization of radioisotope techniques and instruments in machine construction was held in Khar'kov. In addition to representatives of the factories and teaching and scientific research institutions of Khar'kov, engineers and scientists from Moscow, Kiev, Rostov-na-Dony, Riga, Tomsk, Kupyansk, and other cities participated in the conference.

The reports concerned three basic subject fields: utilization of radioisotope instruments for checking various technical processes in machine-building factories; use of labeling atoms in research work; and wear and friction.

The review report "Present State of the Application of Radioisotope Techniques in Industrial Engineering" by M. L. Gol'din dealt mainly with wear measurements. In addition to known methods, the report also told about wear measurements on the basis of the determination of the radiation flux intensity during the operation of a friction pair which had not been initially activated.

Radioisotope checking methods are widely used in the enterprises of farm machinery building (report by B. N. Monzhiev). For example, in the Tula Combiner Plant, the Riga Factory of Farm Machinery Construction, and other factories, radioisotope methods are used to monitor and maintain a given upper level of molten iron in cupola furnaces. Considerable savings in coke were obtained, the efficiency increased, and the entire monitoring system had paid for itself after 6 months. The total savings for four cupola furnaces amounted to 25 thousand rubles. A system for monitoring the total production on conveyor belts is widely used. It provides savings of 5000 rubles per year in one plant of farm machinery construction. Owing to the use of two-position radioisotope instruments, considerable savings in material were obtained in the continuous painting of tractors and other objects. The annual savings which this method of painting provides in the Volgograd Tractor Plant reaches 15,000 rubles. Radioisotope instruments for measuring the thickness of coatings were also used to monitor the plating of radiators and to measure the thickness of varnish-paint coatings.

At the present time potato tubers are sorted by combiners each of which is operated by six persons. The Scientific-Research Institute of Machine-Building Technology of Rostov-na-Dony has developed an experimental model of a radioisotope separator on the basis of ^{241}Am which allows the automation of potato sorting.

V. N. Pozdnikov reported on new γ-ray relaying instruments with digital information processing (GRP-1-1 and GRP-2-1 models). The sensitivity of these instruments was increased 5 times, but the activity of the emitter

Translated from Atomnaya Énergiya, Vol. 40, No. 5, pp. 438-439, May, 1976

was decreased more than 25 times in comparison with previous models. Therefore the discrete monitoring of levels of bulk materials and liquids in vessels with a diameter of up to 10 m became possible without cuts in the refractory lining. This reduced the expenditures for mounting radioisotope devices. The same instruments allow monitoring of the level in small-diameter tubes in the case of low density gradients and the monitoring of the interface of two media with small density differences. High stability and reliability of the parameters were obtained by the transition from an analog recording system to the discrete recording system and the use of a difference-counting technique; the response can be adjusted from $15 \cdot 10^{-4}$ to 1 sec. The instruments have an output with contacts as well as a standard contactless output and can be operated in both positive and negative modes. These instruments replace the previously supplied GR-6 and GR-8 instruments.

Deserving attention is the automatic molding-sand distribution system which has been implemented in the foundry of the Khar'kov Tractor Plant (report by I. Ya. Vidzhe). A γ-ray relay, which monitors the upper and lower levels of the charge in the molding-sand bins is a part of the system. The implementation of this system has considerably increased the quality of the cast production and has precluded long storage of sand in certain bins, which in the past caused partial losses in the properties and a reduction of the sand's moisture content. The runs of the production cycle were improved. The annual saving amounted to about 50 thousand rubles.

Several reports told of the use of γ-ray defectoscopy in combination with ultrasound and magnetic techniques.

Some of the reports were devoted to research on the stability against wear of articles made from iron with a high magnesium concentration; in these investigations, radiometric and autoradiographic analyses were used (reports by G. N. Bakakin, A. P. Lyubchenko, and R. I. Mikhailov); both structure and properties of coating compositions were investigated (reports by A. G. Borzyak and I. Z. Pribysh); the thickness of plated coatings was measured with the albedo of β radiation (report by I. V. Tsarin); and the pressure forming of metal was investigated with the aid of radioactive isotopes (reports by V. K. Lobanov, V. M. Pilipenko, and Yu. S. Uritskii).

The conference has shown that the positive results which were obtained must be put to use in other machine-building factories of our country.

THE ANNUAL CONFERENCE OF THE PLASMA PHYSICS DIVISION OF THE AMERICAN PHYSICAL SOCIETY

A. A. Kalmykov

The 17th Annual Conference of the Plasma Physics Division of the American Physical Society was held Nov. 10-14, 1975 in St. Petersburg (Florida). These conferences are now traditional and attract practically all scientists who actively work in the field of plasma physics in the USA. Usually several delegations of other countries participate in the conferences.

Nine hundred and sixty-three reports were presented to the conference (802 reports in 1974, 715 in 1973, and 619 in 1972). This increase reflects the general development of research programs in the field of plasma physics and controlled thermonuclear fusion in the USA. Papers related to general problems of toroidal plasma confinement and research done on operating tokamaks (157 reports) play the leading role. One hundred and thirty-three reports were concerned with the problems of a laser plasma and laser-controlled thermonuclear fusion. Research on relativistic electron beams, systems with large β, and open traps received much attention. Problems such as the interaction of electron beams with a plasma, nonlinear phenomena in a plasma, waves in plasma, diffusion and transfer of plasmas, and plasma diagnostics were considered separately.

Results of greatest interest were obtained with the Alkator tokamak at the Massachusetts Institute of Technology. A stable plasma with a density $n = 6 \cdot 10^{14}$ cm^{-3} could be obtained with this machine in a strong magnetic field of 75 kOe and a large stability reserve $q \approx 6$; the stable plasma was obtained by injecting a neutral gas into a discharge. It was shown that the effective lifetime increases with increasing density and

Translated from Atomnaya Énergiya, Vol. 40, No. 5, pp. 439-440, May, 1976

reaches 20 msec at the maximum density. This means that the record value $n\tau_E = 10^{13}$ for thermonuclear machines has been reached. Under the conditions resulting in maximum density, $\beta_p = 2.5$-3 and this corresponds to the greatest possible limit values. Furthermore, the concentration of the impurities was under these conditions much lower than under conditions of low density. Great progress was attained in creating methods of additional plasma heating with the aid of injecting beams of neutral particles and with high-frequency plasma heating. When a beam of neutral particles was injected into the Ormak machine, a doubling of the ion temperature was obtained (with $T_i = 1$ keV). The slowing down of the injected particles corresponds to the classical theory. The ATC machine was used for successful experiments of plasma heating with the aid of wave excitation near the lower hybride resonance (the induced power was increased to 200 kW).

The reports which the Livermore Laboratory presented on experiments dealing with the interaction of laser radiation with matter indicated that the laser compression of targets helped to reach values $n\tau \approx 10^{12}$ at $T = 3$ keV and a degree of compression of 100-1000 in the material. An analysis of these experiments has shown that anomalous absorption and transfer, superhot electrons, and self-exciting magnetic fields play a very important role in the interaction processes. In the future execution of the program, new powerful lasers and complex composite targets will be built and the methods of plasma diagnostics will be further developed.

Important results were obtained on open magnetic traps. The 2XIIB machine of the Livermore Laboratory was used for an experiment in which a powerful beam of fast neutral atoms with an energy of 14 keV and an equivalent current of 370 A was injected into a previously generated target plasma. The ion temperature increased from 2 keV to 13 keV, and the electron temperature, from 80 eV to 250 eV. The experiments have shown that drift-cone instability is the main reason for losses. In order to stabilize this instability, it was proposed to inject a quasistationary current of a hot plasma into the plasma. The particles of the current continually fill the cone of the losses and the distribution function becomes isotropic and resembles a Maxwellian distribution. In this manner the main reason for the excitation of the instability would be removed. It was shown in experiments that, when a quasistationary current of a hot plasma is injected along the lines of force of the magnetic field, the drift-cone instability does not arise in the course of the entire time interval within which the current of the hot plasma is present. The plasma confinement time increases sharply and reaches ~ 5 msec with $n\tau = 7 \cdot 10^{10}$ cm^{-3}/sec; the absolute value of $n\tau$ and the similarity law $n\tau \sim T_i^{3/2}$ correspond to the classical confinement time. Conditions characterized by constant density or by a density buildup were obtained dependent upon the intensity of the injected beam of neutral atoms. When the density increased, the maximum β value was 0.35. A new instability, which limits the further increase in density, occurs at $\beta = 0.35$-0.4. Thus, the work which was done in the Livermore Laboratory on the 2XIIB machine has proved the theoretical and experimental possibility of stabilizing the drift-cone instability (one of the most dangerous instabilities of open systems) and reaching plasma parameters, particularly ion temperatures, close to the values of thermonuclear reactions ($T_i = 13 \pm 1$ keV) at classical plasma confinement times. This opens new possibilities of utilizing open systems.

Among the new developments of systems for plasma confinement, one must not forget the systems which in the last few years were developed in the University of California at Los Angeles and which have a surface confinement of the plasma; the main plasma volume in these systems is located in the region without magnetic field and isolated from the walls by a so-called magnetic wall. Such magnetic field configurations can be created by two layers of conductors with oppositely directed currents in the layers (magnetic sheet) and with a system of conductors in which the currents are oppositely directed in neighboring conductors (magnetic net). These systems are characterized by magnetohydrodynamic stability, a confinement time which is directly proportional to the dimensions, the possibility of direct ion injection, large β, and small synchrotron losses. The devices were theoretically and experimentally considered in various geometries, such as plane, cylindrical, and toroidal geometry. The experiments were made under conditions with small and large β in the following range of plasma parameters: $n = 10^8$-10^{13} cm^{-3}, $T_e = 0.5$-10 eV, and $T_i = 0.5$-5 eV. It was shown that the particle losses are appropriately described by classical mechanisms in the entire range of plasma parameters applicable to systems with a magnetic sheet. In the magnetic net, the losses are basically given by the leakage of particles through magnetic slits having the characteristic size $\Delta = 2\sqrt{\rho_e \rho_i}$ (ρ_e and ρ_i denote the cyclotron radius of electrons and ions, respectively) much smaller than the characteristic size of the previously obtained magnetic slits. By creating a space charge inside a system with the magnetic net in analogy to the electromagnetic traps of the Khar'kov Physicotechnical Institute, both the confinement time and the ion temperature could be substantially increased. Preliminary schemes of thermonuclear reactors were presented, in which systems with superficial plasma confinement, among them systems on the basis of an electromagnetic trap, are used. The plans show that this development line is promising for thermonuclear reactors.

In the reports on the research on, and the use of, relativistic electron beams, the results of the develop-

ment and investigation of powerful ion sources were of greatest interest. These sources are the energy sources for relativistic electron beams and are capable of generating ion beams with energies of several megaelectronvolts and currents of dozens or hundreds of kiloamperes. A special section of the conference dealt with research on such ion beams.

Constructions of ion sources and experiments with them were described in the reports presented by Cornell University, the US Navy Research Laboratory, the Sandia Laboratory, the University of Maryland, and others. Several different systems are used to obtain the ions: reflecting triodes, vacuum diodes with magnetic insulation, and converging relativistic electron beams.

At the present time proton beams with a current of up to 6 kA, a current density of 60 A/cm^2, and an energy of 400 keV in a 50-nsec pulse have been obtained in such systems. The results are about the same in reflecting triodes but the current density reaches 100 A/cm^2 in diodes with magnetic insulation; calculations show that currents of up to 60 kA with energies of 1.7 MeV in the case of deuterons exist in systems with pinching of the relativistic electron beam.

High-current ion accelerators provide new possibilities of igniting thermonuclear reactions in solid targets. Several schemes of thermonuclear reactors with ion ignition and spherical or semispherical focusing were considered in the conference. The main advantages of these schemes over relativistic electron beams result from the high stopping power of ions in a material, the absence of bremsstrahlung, the possibility of obtaining high power by time-dependent focusing, etc. Accordingly, the requirements to the ignition power have been reduced 10–100 times specifically in the case of heavy ion beams; these power values can now be reached. One can therefore speak of a new promising direction in the development of pulsed thermonuclear reactors.

The conference took place in 8 parallel sections. A special section was organized; in this section papers were presented in the form of illustrations and the reports were replaced by free discussions with the authors of the papers around the corresponding lectern. This form of holding the individual conference sections deserves attention. The aforementioned results of the various research lines do not originate from all papers presented to the conference (this is evidently impossible).

An idea of all the reports can be obtained from the published abstracts. No transactions of the conference will be published.

IN INSTITUTES AND DESIGN OFFICES

ACCELERATION OF ^{48}Ca IONS AND NEW POSSIBILITIES OF SYNTHESIZING SUPERHEAVY ELEMENTS

A. A. Pleve

Ions of the heavy isotope ^{48}Ca were for the first time in the entire world accelerated and experimentally used in the Laboratory of Nuclear Reactions of the Joint Institute of Nuclear Research.

It is well known that the synthesis of superheavy elements in reactions with heavy ions and research on the properties of superheavy elements are among the most important modern problems of nuclear physics. But in these reactions strongly excited nuclei with a substantial deficit of neutrons are usually obtained. This can have a disastrous influence upon the cross sections of synthesis reactions and the lifetimes of the superheavy nuclei to be synthesized.

The Laboratory of Nuclear Reactions has developed a new method of synthesizing transuranium elements in reactions involving ions with a mass exceeding 40 amu. The method leads to compound nuclei with a relatively low excitation energy and allows the utilization of stable lead and bismuth isotopes as targets. The cross sections of the synthesis reactions increase considerably and there is practically no background when the spontaneous fission of the reaction products is recorded. New isotopes of fermium and kurchatovium and the element with the atomic number 106 were synthesized within a short time in this manner and the properties of

Translated from Atomnaya Énergiya, Vol. 40, No. 5, pp. 440-441, May, 1976.

these isotopes and the element were investigated [Pis'ma v Zh. Éksperim. i Feor. Fiz., 20, 580 (1974)].

The ^{48}Ca ions allow extensive investigations in this direction. The ^{48}Ca nucleus contains 8 neutrons more than the principal double magic ^{40}Ca nucleus. The excitation energy of the compound nucleus is accordingly reduced and the neutron deficit of the final reaction products is reduced to its minimum.

The unique possibilities which ^{48}Ca ions provide for the synthesis have been discussed a long time ago in the scientific literature, but experiments concerning the acceleration of these ions so far have nowhere been made. The reason is that natural calcium contains only small amounts (0.18%) of the ^{48}Ca isotope whose separation is extremely complicated and expensive. Furthermore, as a chemical element calcium does not have suitable gaseous compounds to be used in conventional ion sources.

The Laboratory of Nuclear Reactions has build an ion source in which the active substance is in the solid phase. Recently both the design and the operation of the source were considerably improved so that a maximum ion current could be obtained with a minimum consumption of the active substance in the acceleration of ^{48}Ca ions. In October 1975, sevenfold-charged ^{48}Ca ions were accelerated in the U-300 cyclotron. The beam current amounted to 2 μA ($1.7 \cdot 10^{12}$ particles/sec) and the maximum energy of the ions was 255 MeV.

The isotope ^{252}102 was synthetized for the purpose of experimentally verifying the advantages of the ^{48}Ca ions. Targets from the separated isotopes ^{206}, ^{207}, ^{208}Pb of high purity were irradiated with ^{48}Ca ions. The cross sections of the ^{252}102 isotope formation in reactions with the emission of two, three, or four neutrons were 5, 1.2, and $0.2 \cdot 10^{-31}$ cm^2, respectively. The reaction (^{48}Ca, 2n) dominates. Its cross section exceeds by more than one order of magnitude the reaction cross sections of the conventional synthesis obtained with the aid of light bombarding ^{18}O or ^{22}Ne ions which result in the same product.

Since in most cases only a small number of neutrons are emitted, the fusion reaction (merging) with ^{48}Ca actually leads to the formation of compound nuclei with a low excitation energy.

The synthesis of superheavy nuclei is now being prepared.

THE OPERATOR – STEREOTELEVISION – MANIPULATOR SYSTEM IN NUCLEAR POWER GENERATION

Yu. A. Gerasimov, V. P. Ivanov,
and G. P. Malyuzhonok

Good results are obtained by the use of three-dimensional television for the observation of manipulators and their control in work under conditions dangerous for men; in this manner the alignment of objects in space can be controlled with the necessary accuracy [1].

The design principles of various stereotelevision systems have been described in the literature but data on the accuracy with which objects can be aligned in space with an operator–stereotelevision–manipulator system, i.e., data important for applications, have not been presented.

In the Experimental Design Office of the High-Temperature Institute of the Academy of Sciences of the USSR, experiments on aligning objects in space with the aid of an operator–stereotelevision–manipulator system were made under laboratory conditions and in work in air or water; other experiments were made under direct production conditions. The experimental data were compared with the results of calculations, direct observations, and observations made with television systems rendering a two-dimensional image. The radiation-stable two-channel STU-3 equipment was used in the experiments [2].

The stereographic vision, which is given by the difference of the parallactic angles and which corresponds to the minimum shift of objects in the depth of the field of view [3] is the main parameter characterizing the image quality of a stereotelevision system. However, an observer–operator working with a manipulator is

Translated from Atomnaya Énergiya, Vol. 40, No. 5, pp. 441-443, May, 1976

TABLE 1. Conditions in Executing the Experiments

Curve on Fig. 1a	Medium around the zone of operation	Illumination E (lx) of zone of operations	Type of focus, focal distance F (mm)	Background of zone of operation	Diameter (mm) of objects shifted
1	Water	$E=f(r)$	Zh 49; 22	No bkgd.	Rod, 7— cone, 50
2	»	$E=f(r)$	Zh 51; 50	» »	As above
3	Air	1500	Zh 49; 22	Whatman's paper	» »
4	Water	2300	Zh -51; 50	Aluminum	» »
5	Air	1500	Zh -51; 50	Plywood	Rod, 7— rod, 7
6	»	1500	Zh -51; 50	»	Rod, 7— cone, 50
7	»	1500	Zh 51; 50	»	Cone— cone, 50
8*	»	100	Zh -51; 50	Exptl. hall	Rod, 5— rod, 5

*The tests were made on the ring of the Serpukhov Proton Accelerator.

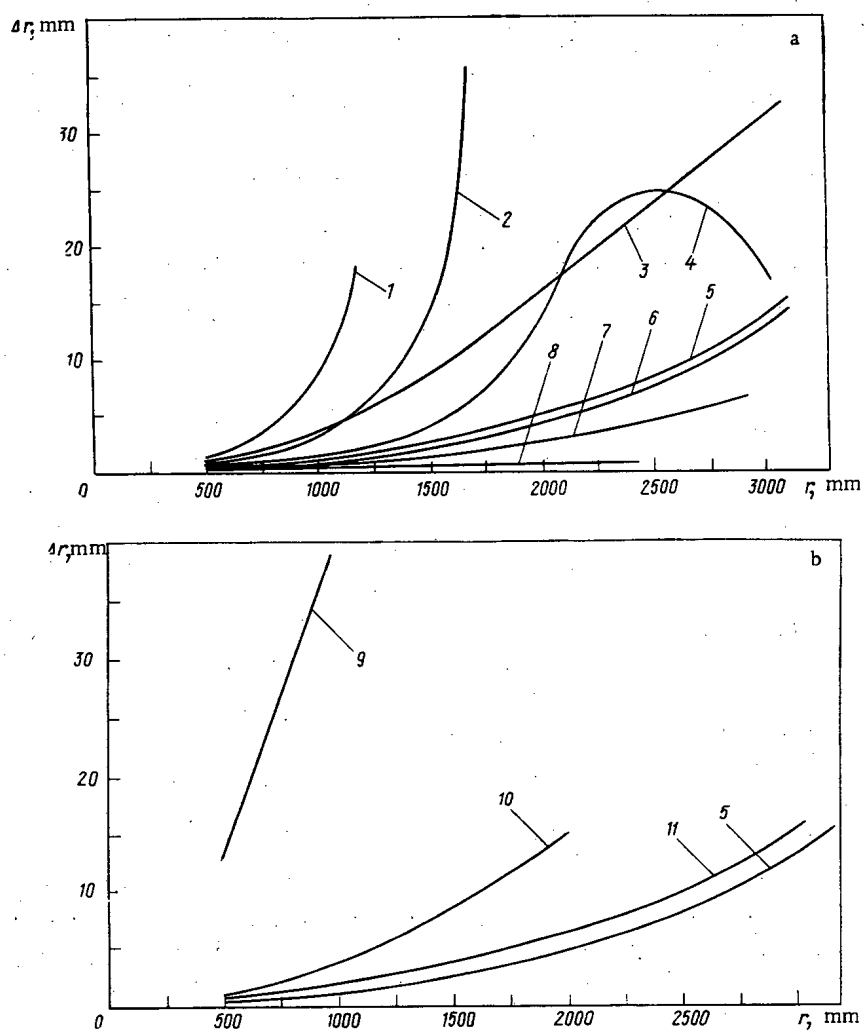

Fig. 1. Dependence of the accuracy Δr with which objects are aligned upon the distance r to the object when the operator—stereotelevision—manipulator system is used: a) under various conditions and b) with possible observation systems.

more interested in the accuracy of the alignment of objects rather than in the smallest noticeable shift of the objects in the depth of the field. Therefore the error Δr made in the alignment of objects in the depth of the field must be considered the important parameter of a stereotelevision system (error obtained when the observer

attempts to align the objects).

All other factors influencing the accuracy of the alignment were kept constant in the investigation.

Measurements in air and water were made in a 4000 × 1500 × 1000-mm tank. The remote-control manipulator was placed on the upper edges of the tank and allowed forward–backward, upward–downward, and right–left motions. Aluminum cones with a diameter of 50 mm and aluminum rods with a diameter of 5 or 7 mm were used as the objects to be observed. One of the objects was affixed to the bottom of the tank; another object was placed on the slave member of the manipulator. The stereo camera was mounted on the outside behind an illuminating system in the wall of the tank.

The observer, who saw before himself only the stereo image of the objects, shifted the one object with the aid of the manipulator and lined it up with the fixed object; each time the error of alignment was determined.

Three observers without practice and experience in the operation participated in the experiments; the observers had a keenness of vision of 1.0-0.9. Their adaptation times were 3-5 min.

Very complicated experimental conditions were selected. The objects to be observed and the centers of the lens systems were placed on the same level. One object was moved in the direction perpendicular to the center of the base of the transfer system. The bases of the objects were beyond the field of view of the observer. The observer made three readings in each experiment; the readings were averaged. The results of experiments in which the alignment error obtained with the operator–stereotelevision–manipulator system was determined in dependence of the distance r to the objects are presented in Fig. 1a; the basic characteristics and the medium in which the experiments were made are listed in Table 1.

In order to obtain a full representation of the efficiency of the stereotelevision system in remotely controlled work with manipulators, Fig. 1b shows for comparison the experimental data on the alignment of objects in space, which data were obtained with various observation methods under otherwise equal conditions. Curve 9 refers to an operator–television–manipulator system in which the television viewing system renders a two-dimensional image of the objects. Curve 10 refers to the calculated values obtained with the formula of [3]:

$$\Delta r = \frac{rl}{2ZB} \frac{S_1 + d/2}{S' + d/2}, \tag{1}$$

where r denotes the distance (mm) between the object and the camera; l denotes the width (mm) of the transmitting scanning pattern; Z denotes the resolution of the television system in horizontal direction (lines; 0249 according to a table); B denotes the base (mm) of the transmission system; $S_1 + d/2$ denotes the distance (mm) between the center of the objective and the object; and $S' + d/2$ denotes the distance (mm) between the center of the objective and the photocathode.

Tentative values can be obtained from calculations based on approximations, i.e., assuming $S_1 + d/2 \approx r$ and $S' + d/2 \approx F$. We obtain

$$\Delta r = \frac{r^2 l}{2ZBF}. \tag{2}$$

Equations (1) and (2) are derived from formulas stated in [1], but the optical parameters of the stereotelevision system were brought into account. After substituting the values F = 50 mm, Z = 500, l = 12.7 mm, and B = 65 mm into Eq. (2), we obtain the Δr values 0.98, 3.9, and 15.6 mm for the distances r = 500, 1000, and 2000 mm, respectively. Curve 11 pertains to an operator–manipulator system in which the observations were made directly by the operator through the illuminating system of the tank; curve 5 refers to the operator–stereotelevision–manipulator system (see Fig. 1a).

When we analyze the graphs, we can draw the following conclusions.

Since very great errors are made in the alignment of the objects when the operator–television–manipulator system is used, the system cannot be recommended for work with manipulators;

the experimental results concerning the alignment which was obtained for objects with the operator–stereotelevision–manipulator system are in good agreement with the calculated values;

the alignment of objects in water is worse than in air, because the light is scattered in the water layer. In this case the water becomes a secondary source of light emission and both contrast and visibility of the object are reduced;

a background behind the object increases the accuracy of the alignment;

the results of observations on the alignment of objects by the operator (with the naked eye) using the operator–manipulator system are in good agreement with the corresponding data obtained in work with the operator–stereotelevision–manipulator system. The system which comprises the stereotelevision renders better results in certain cases, owing to the optical and electronic magnification of the system; and

the accuracy of the alignment is substantially influenced by the operation of the slave mechanism of the manipulator and the manner of recording the results of measurements. For example, during work in the tank, the slave mechanism had a greater overswing than the mechanism used on the Serpukhov proton accelerator; this is evidenced by Fig. 1a.

LITERATURE CITED

1. R. Stevenson, Introduction to Nuclear Technology [Russian translation], Gostekhteorizdat, Moscow (1956).
2. É. M. Afonin et al., At. Énerg., 36, No. 3, 243 (1974).
3. P. V. Shmakov, K. T. Kolin, and V. E. Dzhakoniya, Stereotelevision [in Russian], Cvyaz', Moscow (1968).

EXHIBITIONS

NEW EXHIBITS IN THE HALL "ATOMIC ENERGY" AT THE EXHIBITION OF ACHIEVEMENTS OF THE NATIONAL ECONOMY OF THE USSR

P. A. Sokolov

The exhibits at the hall "Atomic Energy," which was organized by the State Committee for the Use of Atomic Energy of the USSR, familiarizes the visitors of the Exhibition of Achievements of the National Economy of the USSR with the development projects of Russian atomic science and technology within the framework of the Ninth Five-Year Plan and with the outlook in the light of the resolutions of the 25th Congress of the Communist Party of the Soviet Union.

The exhibits in the hall "Nuclear Reactors and Atomic Power Generation" tell the visitor about the construction program of atomic electric power stations in the USSR, about the basic types of Russian atomic reactors, the equipment used in the atomic electric power stations, and new construction materials used in the building of reactors. The central exhibit of the hall is a model of the unique RBMK-1000 channel reactor with an electrical power of 1 million kW, which was erected in the V. I. Lenin Leningrad Atomic Electric Power Station. The uranium–graphite reactors are interesting because they make it possible to obtain any amount of electrical power; typified construction elements and components are used in these reactors, which are reliable in their operation and preclude nuclear overheating of the vapor but allow reloading of fuel without stopping the operation of the reactor.

Water–water power reactors, which were represented by models of the serially produced VVÉR-440 reactor built with the standards of the best examples of atomic technology in the world, and also represented by the serially produced VVÉR-1000 reactor with improved utilization of the volume inside the housing, have increased the specific energy load of the active zone and the parameters of the primary coolant.

Models of the fast reactors BN-600 and BN-350 with water-distilling units represent a third direction in Soviet reactor construction. Owing to the fuel breeding in this type of reactor and to the possibility of using practically any uranium and even thorium, the resources of nuclear fuel have been greatly increased.

Prototypes of VVÉR-440, RBMK-1000, BOR-60, and BN-350 fuel elements, a reactor assembly with a gaseous (CO_2) coolant, and various monitoring, measuring, and auxiliary instruments are also exhibited in the hall. One can become familiar with special aspects of reactor utilization for investigations in nuclear physics and in other fields of science (prototype of an IVV-2 research reactor). Models of the portable atomic electric

Translated from Atomnaya Énergiya, Vol. 40, No. 5, pp. 443-444, May, 1976.

power station Sever-2 and of the Bilinsk Atomic Electric Power Station demonstrate the possibilities of power generation in the USSR by building atomic electric stations of low and medium power, which can be efficiently and economically used to produce electrical and thermal energy in regions in the extreme north without proper roads.

The exhibits in the hall "Thermonuclear Research" inform about investigations of controlled thermonuclear fusion. The final goal of these investigations is to build thermonuclear power stations with an inexhaustable energy source. The success which Soviet scientists have reached in this field is clearly demonstrated by a model of the experimental thermonuclear device Tokamak-10 which was developed by the I. V. Kurchatov Institute of Atomic Energy. Still another step was done to build machines which demonstrate the feasibility of controlled thermonuclear reactions. A model of a hypothetical reactor shows how engineers and scientists imagine the reactor of the future. In the hall one can become acquainted with investigations of the properties of plasmas in magnetic traps provided with probes. A model of the original Soviet Ogra-3 machine is one of the main exhibits in this hall.

A hall for the new subject "Winning and Converting Natural Uranium" was opened for the first time to spectators. The exhibits tell of modern methods of winning low-grade uranium ore by underground leaching and informs about the enrichment of the ore and its hydrometallurgical conversion. The exhibits of the hall comprise a model of equipment for ore enrichment with the SO-2 neutron multiplier; extracting agents for extracting and purifying uranium and the accompanying elements; ion exchange resins and membranes; and equipment for winning, converting, and burying radioactive products; all this was developed in the All-Union Scientific Research Institute of Chemical Engineering and the Sverdlovsk Scientific-Research Institute of Chemical Machinery Construction. In this hall one can also become familiar with one of the new types of chemical equipment, namely a pulsed apparatus built by the All-Union Scientific-Research Institute of Standardization in Machinery and Manufacture. The main advantage of this apparatus is that the zones of operation are completely free of moving parts so that the equipment can be easily and simply sealed and that servicing personnel can be reduced or even completely dispensed with. The method of pulsing can be of interest to specialists in the field of chemistry, petroleum chemistry, metallurgy, medicine, microbiology, the food industry, and other branches of industry.

Products of factories and design offices specialized in the manufacture of nuclear instruments are shown in the hall "Instruments of Nuclear Physics." The exhibition shows a large number of dosimetric and radiometric instruments, of instruments and equipment for research in nuclear physics, biology, and other fields, and instruments of nuclear physics which can be employed in atomic power generation, prospecting, winning, and converting of minerals. All exhibits of this hall are shown in their natural form and in operation. One can see in the hall an RK radiometer which was developed in the All-Union Scientific-Research Institute of Instrument Making; a gas radiometer of the V. G. Khlopin Radium Institute; thermocouples; neutron level indicators; detectors and their qualitative modifications made in recent years; and Mustang and Luk instruments to be used in analytic processes.

A large portion of the exhibition in the hall "Accelerators of Charged Particles" tells of the work of the D. V. Efremov Scientific-Research Institute of Experimental Atomic Physics which has developed acceleration methods of various types and for various purposes. The exhibition comprises models of the LUÉ-10-2D accelerator for defectoscopy which is successfully used in the A. A. Zhadanov Izhorsk Plant; the small-size MGTs cyclotron; the direct high-current accelerators Élektron-3M and Avrona-II which are used as sources of fast electrons in chemistry and the textile industry, the woodworking industry, the radiotechnical industry, the auto industry, and other branches of industry. Accelerators for medical applications were represented by the LUÉ-15 and LUÉ-8-5V models. The exhibition in this hall also shows instruments and apparatus of the S. M. Kirov Scientific-Research Institute of Nuclear Physics of the Tomsk Polytechnical Institute (compact high-current KBS-8-25 betatron), NIIÉI of the same institution (rotational B-32/6 betatron equipment), and of the Scientific-Research Institute of Mechanics and Physics at the Saratov State University (portable IMD-5 microtron for defectoscopy).

The new exhibition in the hall "Atomic Energy" fully and comprehensively tells about the work which the State Committee for the Use of Atomic Energy of the USSR does in the principal subject fields of research; the exhibits are of great interest for specialists of nuclear engineering and of other branches of the national economy.

BOOK REVIEWS

A. A. Glazkov, I. F. Malyshev, and G. L. Saksaganskii

VACUUM SYSTEMS FOR ELECTROPHYSICAL APPARATUS*

Reviewed by A. P. Kukushkin and L. N. Rozanov

The book under review draws upon a wealth of experience gathered in the USSR and elsewhere in the construction of vacuum systems: cyclotrons, synchrocyclotrons, synchrotrons, linear accelerators, storage rings, and thermonuclear reactors.

It presents an interesting historical review of the construction of vacuum systems for charged-particle accelerators from Lawrence and Van de Graaf (1931) to the present day.

The first chapter considers the physical processes occurring in the vacuum chamber of accelerators and thermonuclear reactors, introducing elements of vacuum physics, and indicates the requirements for the limiting pressure, the composition of the residual gas, the constructional materials, and the choice of methods of evacuation. For the basic types of accelerator, an account is given of the theoretical and experimental results obtained on the scattering of accelerated particles on the residual gas, loss of vacuum, multifactorial discharge, activation of the apparatus by scattered particles, stimulated desorption, and for thermonuclear reactors also recharging of plasma ions on impurity atoms.

The second chapter outlines the basic calculation and design of vacuum systems from the point of view of the particular requirements of electrophysical apparatus: the structure of the acceleration chamber or of the equipment for building-up and heating the plasma, the presence of impact gas loads, gases with particular properties, and electromagnetic excitation of the surrounding medium. Typical schemes are developed for a structurally periodic chamber with distributed gas load and for collector evacuation of a small-aperture chamber. Means of optimizing the chamber according to the minimum-cost condition are noted.

The book pays great attention to the choice of constructional materials that retain satisfactory characteristics for doses of particle and electromagnetic radiation of up to 10^4-10^6 Mrad. Very extensive experimental data are given on the desorption characteristics of typical vacuum-device constructional materials, ferrites, adhesive compounds, and heat-absorbing coverings, together with typical designs of various kinds of vacuum system of interest to specialists.

The book synthesizes a great deal of experience of design and engineering work on the creation of nonstandard vacuum equipment and on the construction of chambers for electrophysical apparatus. Particularly noteworthy are new developments of flanged joints, rotating vacuum inlets, and metalloceramic and adhesive compounds.

The extensive factual material allows the reader to become familiar with our native accelerators at Serpukhov, Erevan, Gatchin, etc., and also with the best of the European and American machines.

A shortcoming of this book is the uneven distribution of theoretical material. For example, the scattering of accelerated particles is described in detail, while stimulated desorption and the recharging of ions are adequately summarized (which, it is true, takes up only a small part of the book), but there is a complete lack of material on nonstandard pumping equipment for electrophysical apparatus.

The book is well written and may be read with interest by all who specialize in electrophysical apparatus, and also by engineers, designers, and students specializing in the development of equipment for scientific research.

* Atomizdat, Moscow (1975).

Translated from Atomnaya Énergiya, Vol. 40, No. 5, p. 445, May, 1976.

V. I. Subbotin, M. Kh. Ibragimov, P. A. Ushakov,
V. P. Bobkov, A. V. Zhukov, and Yu. S. Yur'ev

HYDRODYNAMICS AND HEAT EXCHANGE IN ATOMIC-POWER INSTALLATIONS*

Reviewed by V. N. Smolin

The book under review is the result of fundamental research and correlation of research material by the authors. The book gives an idea of the complex processes of hydrodynamics and heat exchange in the active zone of nuclear reactors, and presents calculation-based recommendations for the cooling of single-phase liquids.

In the monograph, some properties of the heat carrier are considered, and descriptions are given of the channels and the construction of the fuel-element assemblies most frequently encountered in practical reactor designs.

The basic equations of hydrodynamics and heat exchange are examined. The kinematic characteristics of the flow are analyzed, using equations of motion in Helmholtz form, and various ways of framing the equations of motion and energy for turbulent flow are evaluated. A physical interpretation is offered for the basic criteria of similarity and the choice of characteristic parameters for simulation is discussed. The principle of approximate simulation of elements of the active zone is illustrated, using the example of fuel elements with a triple casing.

Equations are obtained for the calculation of the relative frictional coefficients for laminar flow in eccentric circular channels. An analytical method is proposed for the calculation of frictional coefficients of laminar flow fluid in a regular array of rods. For channels of arbitrary shape, the authors suggest a division of complex regions into a number of subregions, the problem being solved successively in each subregion.

The formula recommended for the calculation of hydraulic losses and velocity profiles in a turbulent flow of fluid is analyzed for channels of the various geometric forms most often encountered in reactor designs. In a considerable proportion of the authors' investigations, a longitudinally streamline bundle of rods in a turbulent flow of heat carrier is taken as the basis for the determination of the hydrodynamic characteristics. For square and triangular arrays, the tangential stress at the perimeter of the cell and the local velocity at the center are measured. Channels of arbitrary cross section are divided into cells bounded by the flow perimeter, lines of maximum velocity, and normals drawn from characteristic points of the perimeter. These cells are regarded as isolated channels, the hydrodynamic characteristics of which can be calculated by one of the methods described in the monograph.

In the monograph, valuable information is given on methods for hydraulic calculations of bundles of rods with spacing fins and rough channels.

In the chapter dealing with hydrodynamics in a cassette, the problem of determining the hydraulic profile of the reactor is solved using a model of the active zone for dense packing of the fuel elements and cooling by sodium, and the mass transfer in a system of connected channels is considered, taking into account the spacer arrangement and the deviations in the geometrical dimensions of the fuel-element array. It was shown that the introduction of twisting of the heat-carrier flow by means of fuel-element ribs significantly increases the mass transfer in the zone, which leads to equilization of fuel-element temperatures and allows the power output of the reactor to be boosted.

Complex longitudinal–transverse flow around the bundle of rods can be analyzed satisfactorily in terms

*Atomizdat, Moscow (1975).

Translated from Atomnaya Énergiya, Vol. 40, No. 5, pp. 445-446, May, 1976.

of the principles of filtration theory tested in investigations of finely divided bodies.

The effect of input and output conditions on the hydraulic disequilibrium of the flow in the active zone is analyzed. The mechanism of the vibration of individual rods and of bundles of rods is considered.

In the monograph, a review is given of the basic analytical methods of calculating the temperature field of the heat carrier in axisymmetric channels and for longitudinal laminar flow around a regular array of rods. The solution of the problem is also considered for channels with nontwisted flow. Analytical solution of the problem is recommended also for the so-called limiting case of heat exchange, in the longitudinal flow of a liquid-metal heat carrier around a regular fuel-element array.

In calculating the heat exchange and temperature field in the heat carrier for turbulent flow, attention is directed principally toward the cooling of rod assemblies by means of liquid metals. The analysis of the calculated recommendations is based to a considerable extent on experimental data obtained by the authors themselves. One section of particular interest is that which deals with the study of temperature pulsations of fuel elements arising in conditions of steady-state heat exchange. Results are given for measurements of the temperature field in the cassette with different spacings of both smooth and ribbed fuel elements, with and without displacement.

Individual methods of calculating temperature fields in bundles of rods are considered. Methods of calculating random deviations of parameters in the fuel-element temperature field are analyzed, as well as complex hydromechanical phenomena occurring in the active zone when the fuel elements are bent. The effect of ribs on the temperature profile of the fuel elements is examined. A method of calculating a portion of the thermal stabilization is proposed, and formulas for calculating heat exchange for this portion are analyzed. The effect of variations in energy output along the length of the channel on the heat-transfer coefficient are considered. Heat exchange in rough channels is analyzed.

The work provokes the following brief comments. The monograph addresses itself to the problems of hydrodynamics and heat exchange in the flow of single-phase liquids, mainly liquid metals. In it, no consideration is given to problems associated with boiling of the heat carrier, crises of heat exchange, or hydrodynamic stability of the flow rate in the channels. This means that nothing is said regarding the class of boiling reactors and reactors with a high thermal load, in which boiling with underheating occurs, and therefore the monograph should not have been given so general a title.

Since hydrodynamics and heat exchange are interrelated phenomena, it would be expedient to consider these problems together, i.e., Chapters 5, 9, and 10 should be integrated. This would emphasize the interdependence of the phenomena and eliminate certain repetitions that are inevitable when the material is treated separately.

The specific problems considered in the monograph are mainly those for the cooling of fuel elements by liquid metals, i.e., in conditions such that the physical properties of the heat carrier depend comparatively weakly on the temperature and hence the change in temperature of the liquid metal has no significant effect on the heat exchange and drag. However, the monograph claims to apply these methods of calculation also to the cooling of the active zone by nonmetallic trickling liquids and gases. For these cases, the authors should consider in more detail the calculation of the heat exchange and drag for the flow of a liquid with variable physical properties.

The authors of the monograph should devote more attention to the analysis of the recently developed program for determining local parameters of the heat carrier in the thermogenerating assembly, at the same time shortening certain other sections of the book, for example, those describing the construction, and analyzing the operation, of an electromagnetic flow meter, and also those reporting well-known and very fully described findings of similar monographs and the specialist literature.

These comments do not detract from the favorable overall impression of the book, but are simply brought to the authors' attention in anticipation of the preparation of a new edition.

Without doubt, this book will be of value to specialists working in the field of design, to those involved in the construction and design of atomic power stations, and also to scientific workers and researchers investigating the thermophysics of nuclear reactors.

B. V. Lysikov, V. K. Prozorov, V. V. Vasil'ev,
D. N. Popov, L. F. Gromov, and Yu. V. Rybakov

TEMPERATURE MEASUREMENTS IN NUCLEAR REACTORS*

Reviewed by I. S. Kochenov

The book under review discusses problems of the investigation, design, and use of systems for monitoring the temperature of nuclear reactors.

The present monograph is the first on this theme. It consists of three chapters, and contains a large number of tables and illustrations, as well as comprehensive bibliographic material.

The problems that can be solved by means of temperature measurements in the reactor are of many kinds but all contribute to improving the safety and efficiency of the reactor assembly.

The first chapter discusses the specific features of temperature measurements in nuclear reactors caused by the effect of radiation on the characteristics of the sensitive elements, by energy generation in the thermometer material, and by the particular constructional and energy properties of the reactor relevant to temperature monitoring. Up-to-date continuous, discrete, contact, and contactless thermometric methods and devices are analyzed.

A discussion is given of the principles of construction, the structure, and the means of development of a temperature-monitoring system, and also of the problem of the optimum operator representation of the information for reactor control. Unfortunately, some promising methods of temperature measurement (ultrasound, thermosound, etc.) are only briefly dealt with.

The second chapter describes a thermoelectric thermometer (TET) that is widely applicable for reactor control. The advantages of the TET include the small size of its sensor (a thermocouple junction), the capability of measuring the temperature of small objects, the wide temperature range that can be monitored, the acceptable accuracy of the measurements, and the relative stability of the device as regards the action of radiation. The small-scale TET of cable type with mineral insulation and protective shielding (chromium–nickel steel, for example, or alloys) allows an increase in the duration and an expansion of the sphere of application of temperature measurements in the reactor. Practical problems of the production technology for the cable TET are outlined (preliminary operations, preparing the cable, welding the thermoelectrodes and the protective shielding, sealing the inlets for cables of different size and shape when the thermocouple is insulated, and not insulated, from the shielding).

Up-to-date ideas on the errors of temperature measurements using the TET are given, taking into account changes in composition and metallurgical state of the thermoelectrodes and also external physical effects. Methods of investigation of the influence of radiation on the TET characteristics are discussed.

The final chapter considers problems of measuring the temperature of fuel elements, graphite moderators, metallic structures, biological shielding, and heat carriers. Different means of bringing the thermocouple into contact with the fuel elements are described (on the spacing ribs, in a recess, on the surface, in the fuel composition, etc.), and the possibility of damage to the fuel elements associated with disturbance of the thermocouple attachment is considered. Examples of the use of diamond indicators for monitoring the temperature distribution over the radius and height of the fuel element are described. The temperature conditions of operation of the thermometer are considered on the basis of modern concepts, taking into account distortion of the fuel-element temperature field at the points at which the thermocouples are attached. Different designs of a thermometric device for monitoring the temperature state of graphite cladding are described, including multi-

*Atomizdat, Moscow (1975).

Translated from Atomnaya Énergiya, Vol. 40, No. 5, pp. 446-447, May, 1976.

region assemblies of TETs, built on the basis of cable thermometers.

The design of a reactor thermometric device for the measurement of heat-carrier temperature is described, and the basic requirements for its construction are outlined. Regrettably, in the book there occur unclear formulations, certain incorrect references, jargon, and excessive digressions from the basic theme. Some fundamental problems are not considered, for example, the temperature of the heat carrier in the reactor channels (pulsed, time-averaged, mean, and mass flow rate, etc.). In the analysis of systematic errors of temperature measurements in graphite and fuel elements, it is difficult to know when the heat-conduction equation is considered for the thermocouple and when for the medium, the temperature of which is distorted when the thermocouple is inserted.

In addition, inadequate attention was given to temperature measurements in unsteady conditions.

On the whole, the book will undoubtedly be of interest and value to engineers, technicians, and scientific workers involved in the design and use of reactor assemblies.

engineering science

continued from back cover

Title	# of Issues	Subscription Price
Metallurgist *Metallurg*	12	$225.00
Metal Science and Heat Treatment *Metallovedenie i termicheskaya obrabotka metallov*	12	$215.00
Polymer Mechanics *Mekhanika polimerov*	6	$195.00
Problems of Information Transmission *Problemy peredachi informatsii*	4	$175.00
Programming and Computer Softwave *Programmirovanie*	6	$95.00
Protection of Metals *Zashchita metallov*	6	$195.00
Radiophysics and Quantum Electronics (Formerly Soviet Radiophysics) *Izvestiya VUZ. radiofizika*	12	$225.00
Refractories *Ogneupory*	12	$195.00
Soil Mechanics and Foundation Engineering *Osnovaniya, fundamenty i mekhanika gruntov*	6	$195.00
Soviet Applied Mechanics *Prikladnaya mekhanika*	12	$225.00
Soviet Atomic Energy *Atomnaya energiya*	12 (2 vols./yr. 6 issues ea.)	$235.00
Soviet Journal of Glass Physics and Chemistry *Fizika i khimiya stekla*	6	$ 95.00
Soviet Journal of Nondestructive Testing (Formerly Defectoscopy) *Defektoskopiya*	6	$225.00
Soviet Materials Science *Fiziko-khimicheskaya mekhanika materialov*	6	$195.00
Soviet Microelectronics *Mikroélektronika*	6	$135.00
Soviet Mining Science *Fiziko-tekhnicheskie problemy razrabotki poleznykh iskopaemykh*	6	$225.00
Soviet Powder Metallurgy and Metal Ceramics *Poroshkovaya metallurgiya*	12	$245.00
Strength of Materials *Problemy prochnosti*	12	$295.00
Theoretical Foundations of Chemical Engineering *Teoreticheskie osnovy khimicheskoi tekhnologii*	6	$195.00
Water Resources *Vodnye Resursy*	6	$190.00

Back volumes are available. For further information, please contact the Publishers.

SEND FOR YOUR FREE EXAMINATION COPIES

Plenum Publishing Corporation

Plenum Press • Consultants Bureau • IFI/Plenum Data Corporation

227 WEST 17th STREET
NEW YORK, N. Y. 10011

United Kingdom: Black Arrow House
2 Chandos Road, London NW10 6NR England

breaking the language barrier

WITH COVER-TO-COVER
ENGLISH TRANSLATIONS
OF SOVIET JOURNALS

in engineering science

Title	# of Issues	Subscription Price
Automation and Remote Control *Avtomatika i telemekhanika*	24	$260.00
Biomedical Engineering *Meditsinskaya tekhnika*	6	$195.00
Chemical and Petroleum Engineering *Khimicheskoe i neftyanoe mashinostroenie*	12	$275.00
Chemistry and Technology of Fuels and Oils *Khimiya i tekhnologiya topliv i masel*	12	$275.00
Combustion, Explosion, and Shock Waves *Fizika goreniya i vzryva*	6	$195.00
Cosmic Research (Formerly Artificial Earth Satellites) *Kosmicheskie issledovaniya*	6	$215.00
Cybernetics *Kibernetika*	6	$195.00
Doklady Chemical Technology *Doklady Akademii Nauk SSSR*	2	$65.00
Fibre Chemistry *Khimicheskie volokna*	6	$175.00
Fluid Dynamics *Izvestiya Akademii Nauk SSSR mekhanika zhidkosti i gaza*	6	$225.00
Functional Analysis and Its Applications *Funktsional'nyi analiz i ego prilozheniya*	4	$150.00
Glass and Ceramics *Steklo i keramika*	12	$245.00
High Temperature *Teplofizika vysokikh temperatur*	6	$195.00
Industrial Laboratory *Zavodskaya laboratoriya*	12	$215.00
Inorganic Materials *Izvestiya Akademii Nauk SSSR, Seriya neorganicheskie materialy*	12	$275.00
Instruments and Experimental Techniques *Pribory i tekhnika eksperimenta*	12	$265.00
Journal of Applied Mechanics and Technical Physics *Zhurnal prikladnoi mekhaniki i tekhnicheskoi fiziki*	6	$225.00
Journal of Engineering Physics *Inzhenerno-fizicheskii zhurnal*	12 (2 vols./yr. 6 issues ea.)	$225.00
Magnetohydrodynamics *Magnitnaya gidrodinamika*	4	$175.00
Measurement Techniques *Izmeritel'naya tekhnika*	12	$195.00

SEND FOR YOUR FREE EXAMINATION COPIES

Back volumes are available.
For further information, please contact the Publishers.

continued on inside back cover